

# CCSR Ocean Component Model (COCO)

Version 4.0

April 16, 2007

**Hiroyasu Hasumi**

Center for Climate System Research,  
The University of Tokyo

Documentation for CCSR Ocean Component Model (COCO) Version 4.0,  
as of April 16, 2007

Corresponding to:  
Hiroyasu Hasumi  
Center for Climate System Research, The University of Tokyo  
5-1-5 Kashiwanoha, Kashiwa, Chiba 277-8568, Japan  
[hasumi@ccsr.u-tokyo.ac.jp](mailto:hasumi@ccsr.u-tokyo.ac.jp)

# Preface

This is a documentation for the version 4.0 of COCO (CCSR Ocean Component Model), an ocean general circulation model (OGCM) developed at Center for Climate System Research. The current version of COCO is based on the primitive equations under the hydrostatic and Boussinesq approximations with explicit free surface, and is formulated on the generalized curvilinear horizontal coordinate and (basically) the geopotential height vertical coordinate. COCO also constitutes an ocean component of MIROC, a coupled general circulation model developed at CCSR.

The author takes full responsibility for formulation, discretization, and coding of the current version, although its development owes a great deal to current and former members of the CCSR ocean modeling group. Special thanks are due to Nobuo Sugimoto (current director of Institute of Observational Research for Global Change, Japan Agency for Marine-Earth Science and Technology), who led the CCSR ocean modeling group in 1990's and had started developing a prototype of COCO in 1970's; Yasuhiro Yamanaka (currently at Hokkaido University), who established a basis for discretization and coding strategy of COCO and also established a basis for World Ocean simulation in the CCSR ocean modeling group; and Hideyuki Nakano (currently at Meteorological Research Institute of Japan Meteorological Agency), who devised the bottom boundary layer parameterization used in COCO and significantly contributed to develop a code for distributed memory systems using MPI (Message-Passing Interface). Two of the current members, Akira Oka and Yoshiki Komuro, kindly spared time to proofread the manuscript, and their efforts in the model development over several years are also appreciated. The model development is also supported by collaborating partners outside CCSR, and the contribution made by Tatsuo Suzuki (Frontier Research Center for Global Change, Japan Agency for Marine-Earth Science and Technology) is outstanding in adapting the model to eddy-resolving resolution and coupled modeling.

Some of the description herein may seem verbose to some readers, but such verbosity is mostly intentional. COCO is developed at a university, which means that it is not only a research tool but also intended to be an educational tool for students, even of undergraduate level. I hope this documentation to serve as good learning material for those who are inexperienced in numerical modeling of the ocean.

Hiro Hasumi



# Contents

<b>Preface</b>	<b>i</b>
<b>1 Model Formulation</b>	<b>1</b>
1.1 Basic Equations . . . . .	1
1.2 Diffusion and Viscosity Terms . . . . .	4
1.2.1 Diffusion . . . . .	4
1.2.2 Viscosity . . . . .	4
1.3 Boundary Conditions . . . . .	5
1.4 Mode Split for Horizontal Velocity . . . . .	6
1.4.1 External Mode Equations . . . . .	6
1.4.2 Internal Mode Equations . . . . .	9
1.4.3 Mode Combination . . . . .	10
<b>2 Horizontal Coordinate and Grid</b>	<b>11</b>
2.1 Polar Stereographic Projection . . . . .	11
2.2 Conformal Mapping on Complex Plane . . . . .	12
2.3 Transformed Coordinate and Grid System . . . . .	13
2.4 Defining a Suitable Linear Fractional Transformation . . . . .	14
2.5 Metrics of Transformed Coordinate . . . . .	16
2.6 Transformation of Vector . . . . .	16
2.7 Mercator Grid . . . . .	17
2.8 Coordinate/Grid System Examples . . . . .	18
<b>3 Discretization of Baseline Model</b>	<b>21</b>
3.1 Arrangement of Discretized Variables and Their Labeling . . . . .	21
3.1.1 Discretization in Time . . . . .	21
3.1.2 Horizontal Grid . . . . .	21
3.1.3 Vertical Grid . . . . .	22
3.1.4 Flux . . . . .	23
3.2 Time Differencing . . . . .	24
3.2.1 Internal Mode Equations . . . . .	24
3.2.2 External Mode Equations . . . . .	25
3.2.3 Tracer Equations . . . . .	25
3.2.4 Implicit Treatment for Vertical Diffusion . . . . .	28
3.2.5 Accelerating Model's Approach Toward a Steady State . . . . .	29

3.3	Spatial Differencing . . . . .	30
3.3.1	Grid Spacing and Metrics . . . . .	30
3.3.2	Continuity Equation and T-Point Vertical Velocity . . . . .	31
3.3.3	Tracer Equations . . . . .	32
3.3.4	Internal Mode Equations . . . . .	34
3.3.5	External Mode Equations . . . . .	39
3.4	Treatment of Boundary . . . . .	40
3.4.1	Cyclic Boundary Condition . . . . .	40
3.4.2	Masking Array and Boundary Condition . . . . .	41
<b>4</b>	<b>Numerical Algorithm and Physical Parameterization in Standard Use</b>	<b>43</b>
4.1	Tracer Advection . . . . .	43
4.1.1	QUICKEST . . . . .	43
4.1.2	Flux Limiter for One-Dimensional Advection . . . . .	46
4.1.3	Two-Dimensional UTOPIA . . . . .	47
4.1.4	Flux Limiter for Two-Dimensional Advection . . . . .	51
4.2	Momentum Advection . . . . .	53
4.2.1	Up/Down-Slope Momentum Advection . . . . .	53
4.2.2	Preservation of Enstrophy . . . . .	54
4.3	Horizontal Friction . . . . .	55
4.3.1	Two-coefficient horizontal viscosity . . . . .	55
4.3.2	Shear-dependent viscosity coefficient . . . . .	56
4.4	Convection . . . . .	56
4.5	Surface Mixed Layer . . . . .	57
4.6	Background Vertical Diffusivity . . . . .	59
4.7	Bottom Boundary Layer . . . . .	60
4.8	Isopycnal Diffusion . . . . .	62
4.9	Isopycnal Layer Thickness Diffusion . . . . .	63

## Appendices

<b>A</b>	<b>Sea Surface Forcing</b>	<b>65</b>
A.1	Heat Flux . . . . .	65
A.1.1	Sea Surface Temperature Restore . . . . .	65
A.1.2	Using Surface Air Properties and Bulk Formulae . . . . .	66
A.1.3	Bulk Formula-Based Sea Surface Temperature Restore . . . . .	67
A.2	Freshwater Flux . . . . .	67
A.2.1	Sea Surface Salinity Restore . . . . .	67
A.2.2	Drive Directly by Freshwater Flux . . . . .	68
A.3	Momentum Flux . . . . .	68
<b>B</b>	<b>Coupling to Sea Ice Model</b>	<b>71</b>
B.1	Thermodynamics . . . . .	71
B.1.1	Heat Flux and Growth Rate . . . . .	71

B.1.2	Sublimation of Sea Ice . . . . .	73
B.1.3	Dynamical Redistribution . . . . .	74
B.1.4	Growth and Melting . . . . .	74
B.1.5	Heat and Freshwater Fluxes Passed to the Ocean . . . . .	76
B.1.6	Empirical Parameterization . . . . .	77
B.2	Dynamics . . . . .	77
B.2.1	Horizontal Ice Transport . . . . .	77
B.2.2	Momentum Equation . . . . .	78
<b>C</b>	<b>The Equation of State for Seawater</b>	<b>81</b>
C.1	International Equation of State for Seawater . . . . .	81
C.1.1	IES80 Formula . . . . .	81
C.1.2	Relationship Between Temperature and Potential Temperature . . . . .	82
C.1.3	Polynomial Approximation of the Equation of State . . . . .	82
C.2	Simpler Expressions for the Equation of State . . . . .	83
C.2.1	Mellor [1991] . . . . .	83
C.2.2	McDougall et al., [2003] . . . . .	83
<b>D</b>	<b>Basics of Tensor Analysis and Its Physical Application</b>	<b>85</b>
D.1	Definition of Tensor . . . . .	85
D.1.1	Coordinate Transformation . . . . .	85
D.1.2	Tensor . . . . .	85
D.1.3	Relative Tensor and Levi-Civita Symbols . . . . .	86
D.2	Riemannian Geometry . . . . .	87
D.2.1	Riemannian Metric . . . . .	87
D.2.2	Christoffel Symbols and Covariant Differentiation . . . . .	87
D.2.3	Descartes Coordinate System . . . . .	88
D.3	Orthogonal Curvilinear Coordinate System . . . . .	89
D.4	Tensoric Representation of Physical Quantities . . . . .	91
D.4.1	How should physical quantities be defined as tensors? . . . . .	91
D.4.2	External Product and Curl Operation . . . . .	92
D.4.3	Tensoric Representation of Viscosity . . . . .	93
D.4.4	Anisotropic viscosity for three-dimensional fluid . . . . .	95
D.5	Three-Dimensional Polar Coordinate Example . . . . .	96
D.6	Application to COCO . . . . .	97
	<b>References</b>	<b>101</b>



# Chapter 1

## Model Formulation

### 1.1 Basic Equations

The basic equations for COCO are the primitive equations for the ocean on a sphere, where the Boussinesq and hydrostatic approximations are applied. Several more approximations are employed for usual general circulation models of the ocean and atmosphere. See, for example, *Peixoto [1991]* for detail. The equations are formulated on the generalized curvilinear coordinate in horizontal, and on a hybrid of the geopotential height and normalized geopotential height in vertical. The normalized vertical coordinate is employed to avoid outcropping of surface layers, and used between the free surface and a fixed geopotential depth in the upper ocean ( $\sim 50$  m in most applications).

The coordinates are denoted by  $t$  for time,  $x$  and  $y$  for the two horizontal directions,  $z$  for the geopotential height (measured upward from the mean sea level), and  $\sigma$  for the normalized geopotential height (1 for the free surface and 0 for a fixed depth above which this coordinate system is applied). With  $u$ ,  $v$ , and  $w$  for  $x$ ,  $y$ , and  $z$  direction velocity components, respectively,  $P$  for pressure,  $T$  for potential temperature,  $S$  for salinity, and  $\rho$  for density, the equations under the  $z$  vertical coordinate are written as:

$$\frac{\partial u}{\partial t} + \frac{1}{h_x h_y} \left[ \frac{\partial}{\partial x}(h_y u u) + \frac{\partial}{\partial y}(h_x v u) \right] + \frac{\partial}{\partial z}(w u) + h_{xy} u v - h_{yx} v v - f v = -\frac{1}{\rho_0 h_x} \frac{\partial P}{\partial x} + \mathcal{V}_u, \quad (1.1)$$

$$\frac{\partial v}{\partial t} + \frac{1}{h_x h_y} \left[ \frac{\partial}{\partial x}(h_y u v) + \frac{\partial}{\partial y}(h_x v v) \right] + \frac{\partial}{\partial z}(w v) + h_{yx} u v - h_{xy} u u + f u = -\frac{1}{\rho_0 h_y} \frac{\partial P}{\partial y} + \mathcal{V}_v, \quad (1.2)$$

$$0 = -\frac{\partial P}{\partial z} - \rho g, \quad (1.3)$$

$$\frac{1}{h_x h_y} \left[ \frac{\partial}{\partial x}(h_y u) + \frac{\partial}{\partial y}(h_x v) \right] + \frac{\partial w}{\partial z} = 0, \quad (1.4)$$

$$\frac{\partial T}{\partial t} + \frac{1}{h_x h_y} \left[ \frac{\partial}{\partial x}(h_y u T) + \frac{\partial}{\partial y}(h_x v T) \right] + \frac{\partial}{\partial z}(w T) = \mathcal{D}_T, \quad (1.5)$$

$$\frac{\partial S}{\partial t} + \frac{1}{h_x h_y} \left[ \frac{\partial}{\partial x}(h_y u S) + \frac{\partial}{\partial y}(h_x v S) \right] + \frac{\partial}{\partial z}(w S) = \mathcal{D}_S, \quad (1.6)$$

$$\rho = \rho(T, S, P), \quad (1.7)$$

where  $f$  is the Coriolis parameter ( $= 2\Omega \sin \varphi$ , where  $\Omega$  is the angular velocity of the earth's rotation and  $\varphi$  is latitude),  $g$  is the gravitational acceleration, and  $\rho_0$  is a fixed reference density value. The coefficients  $h_x$  and  $h_y$  are the metrics for the  $x$  and  $y$  coordinates, respectively, and

$$h_{xy} = \frac{1}{h_x h_y} \frac{\partial h_x}{\partial y}, \quad h_{yx} = \frac{1}{h_x h_y} \frac{\partial h_y}{\partial x}. \quad (1.8)$$

The way to obtain metrics for a selected horizontal coordinate system is described in chapter 2, and see appendix D for the basis of representing the equations under the generalized curvilinear coordinate system.  $\mathcal{V}$  and  $\mathcal{D}$  represent viscosity and diffusion terms, respectively, and their formulation will be described later. The equation of state (1.7) used in this model is a polynomial approximation of the IES80 formula [UNESCO, 1981]. It is described in appendix C. The model can also deal with passive tracers (tracers which do not affect density of seawater), and their equations are formally identical to (1.5) and (1.6).

There's no explicit mechanism to remove vertically unstable density stratification in these basic equations, due to the hydrostatic approximation (1.3). The effect of vertical convection is parameterized by convective adjustment, which is artificial, instantaneous vertical homogenization of unstable water columns, or by some other methods. The convective adjustment is described in chapter 4.

Equations under the  $\sigma$  vertical coordinate are derived now. The mean sea level is set to  $z = 0$ , and sea surface height is represented by  $z = \eta(x, y, t)$ . By prescribing a fixed depth  $z = z_B (< 0)$ , the normalized vertical coordinate  $\sigma$  is defined as

$$\sigma = \frac{z - z_B}{\eta - z_B}. \quad (1.9)$$

Hereafter, the coordinate systems with the  $z$  and  $\sigma$  vertical coordinates are called  $z$  and  $\sigma$  coordinate systems, respectively, and the independent variables for the  $z$  coordinate system are temporarily described by  $(x^*, y^*, z^*, t^*)$ , while those for the  $\sigma$  coordinate system are described by  $(x, y, \sigma, t)$ . The transformation between the two coordinate systems is described by

$$x = x^*, \quad y = y^*, \quad \sigma = \frac{z^* - z_B}{\eta - z_B}, \quad t = t^*. \quad (1.10)$$

When a physical quantity  $\Psi$  is functionally represented as  $\Psi = \psi^*(x^*, y^*, z^*, t^*)$  in the  $z$  coordinate system and as  $\Psi = \psi(x, y, \sigma, t)$  in the  $\sigma$  coordinate system, its derivatives are transformed as

$$\begin{aligned} \frac{\partial \psi^*}{\partial x^*} &= \frac{\partial \psi}{\partial x} \frac{\partial x}{\partial x^*} + \frac{\partial \psi}{\partial y} \frac{\partial y}{\partial x^*} + \frac{\partial \psi}{\partial \sigma} \frac{\partial \sigma}{\partial x^*} + \frac{\partial \psi}{\partial t} \frac{\partial t}{\partial x^*} \\ &= \frac{\partial \psi}{\partial x} - \frac{\sigma}{\eta - z_B} \frac{\partial \eta}{\partial x} \frac{\partial \psi}{\partial \sigma}, \end{aligned} \quad (1.11)$$

$$\frac{\partial \psi^*}{\partial y^*} = \frac{\partial \psi}{\partial y} - \frac{\sigma}{\eta - z_B} \frac{\partial \eta}{\partial y} \frac{\partial \psi}{\partial \sigma}, \quad (1.12)$$

$$\frac{\partial \psi^*}{\partial z^*} = \frac{1}{\eta - z_B} \frac{\partial \psi}{\partial \sigma}, \quad (1.13)$$

$$\frac{\partial \psi^*}{\partial t^*} = \frac{\partial \psi}{\partial t} - \frac{\sigma}{\eta - z_B} \frac{\partial \eta}{\partial t} \frac{\partial \psi}{\partial \sigma}. \quad (1.14)$$

Lagrangian differential of  $\Psi$  is transformed as

$$\begin{aligned} \frac{d\psi^*}{dt^*} &\equiv \frac{\partial \psi^*}{\partial t^*} + \frac{u}{h_x} \frac{\partial \psi^*}{\partial x^*} + \frac{v}{h_y} \frac{\partial \psi^*}{\partial y^*} + w \frac{\partial \psi^*}{\partial z^*} \\ &= \frac{\partial \psi}{\partial t} + \frac{u}{h_x} \frac{\partial \psi}{\partial x} + \frac{v}{h_y} \frac{\partial \psi}{\partial y} + \frac{w}{\eta - z_B} \frac{\partial \psi}{\partial \sigma} - \frac{\sigma}{\eta - z_B} \frac{\partial \psi}{\partial \sigma} \left( \frac{\partial \eta}{\partial t} + \frac{u}{h_x} \frac{\partial \eta}{\partial x} + \frac{v}{h_y} \frac{\partial \eta}{\partial y} \right), \end{aligned} \quad (1.15)$$

where the velocity components are assumed to represent the same quantities in the both coordinate systems. Vertical velocity in the  $\sigma$  coordinate system,  $\omega$ , is defined by

$$\omega \equiv \frac{d\sigma}{dt^*} = \frac{w}{\eta - z_B} - \frac{\sigma}{\eta - z_B} \left( \frac{\partial \eta}{\partial t} + \frac{u}{h_x} \frac{\partial \eta}{\partial x} + \frac{v}{h_y} \frac{\partial \eta}{\partial y} \right), \quad (1.16)$$

and thus (1.15) is rewritten as

$$\frac{d\psi^*}{dt^*} = \frac{\partial \psi}{\partial t} + \frac{u}{h_x} \frac{\partial \psi}{\partial x} + \frac{v}{h_y} \frac{\partial \psi}{\partial y} + \omega \frac{\partial \psi}{\partial \sigma} \equiv \frac{d\psi}{dt}. \quad (1.17)$$

Using these relationships, (1.1)–(1.6) are transformed as

$$\frac{du}{dt} + h_{xy}uv - h_{yx}vv - fv = -\frac{1}{\rho_0 h_x} \left( \frac{\partial P}{\partial x} + \sigma \rho g \frac{\partial \eta}{\partial x} \right) + \mathcal{V}_u, \quad (1.18)$$

$$\frac{dv}{dt} + h_{yx}uv - h_{xy}uu + fu = -\frac{1}{\rho_0 h_y} \left( \frac{\partial P}{\partial y} + \sigma \rho g \frac{\partial \eta}{\partial y} \right) + \mathcal{V}_v, \quad (1.19)$$

$$0 = -\frac{1}{\eta - z_B} \frac{\partial P}{\partial \sigma} - \rho g, \quad (1.20)$$

$$\begin{aligned} \frac{\partial \eta}{\partial t} + \frac{1}{h_x h_y} \left\{ \frac{\partial}{\partial x} [h_y u (\eta - z_B)] + \frac{\partial}{\partial y} [h_x v (\eta - z_B)] \right\} + (\eta - z_B) \frac{\partial \omega}{\partial \sigma} \\ = 0, \end{aligned} \quad (1.21)$$

$$\begin{aligned} \frac{\partial}{\partial t} [T(\eta - z_B)] + \frac{1}{h_x h_y} \left\{ \frac{\partial}{\partial x} [h_y u T(\eta - z_B)] + \frac{\partial}{\partial y} [h_x v T(\eta - z_B)] \right\} + \frac{\partial}{\partial \sigma} [\omega T(\eta - z_B)] \\ = (\eta - z_B) D_T, \end{aligned} \quad (1.22)$$

$$\begin{aligned} \frac{\partial}{\partial t} [S(\eta - z_B)] + \frac{1}{h_x h_y} \left\{ \frac{\partial}{\partial x} [h_y u S(\eta - z_B)] + \frac{\partial}{\partial y} [h_x v S(\eta - z_B)] \right\} + \frac{\partial}{\partial \sigma} [\omega S(\eta - z_B)] \\ = (\eta - z_B) D_S, \end{aligned} \quad (1.23)$$

where the diffusion terms in (1.22) and (1.23) are assumed to be expressed with the same dimension as in (1.5) and (1.6). Here, the advection terms in the momentum equations are represented by the advective form, while those in the tracer equations are by the flux form. These expressions are coordinated with the actual discretization of COCO, which will be described in chapter 3.

The prognostic equation for sea surface height is obtained by vertically integrating (1.4) from bottom to top. By expressing the depth of the ocean floor by  $z = -H(x, y)$ , vertical integration of the continuity equation yields

$$\frac{1}{h_x h_y} \int_{-H}^{\eta} \frac{\partial}{\partial x} (h_y u) dz + \frac{1}{h_x h_y} \int_{-H}^{\eta} \frac{\partial}{\partial y} (h_x v) dz + w|_{z=\eta} - w|_{z=-H} = 0. \quad (1.24)$$

Applying the relationships

$$\int_{-H}^{\eta} \frac{\partial}{\partial x} (h_y u) dz = \frac{\partial}{\partial x} \left( h_y \int_{-H}^{\eta} u dz \right) - u|_{z=\eta} h_y \frac{\partial \eta}{\partial x} - u|_{z=-H} h_y \frac{\partial H}{\partial x}, \quad (1.25)$$

$$\int_{-H}^{\eta} \frac{\partial}{\partial y} (h_x v) dz = \frac{\partial}{\partial y} \left( h_x \int_{-H}^{\eta} v dz \right) - v|_{z=\eta} h_x \frac{\partial \eta}{\partial y} - v|_{z=-H} h_x \frac{\partial H}{\partial y}, \quad (1.26)$$

and the later described boundary conditions for  $w$ , (1.52) and (1.53),

$$\frac{\partial \eta}{\partial t} + \frac{1}{h_x h_y} \left[ \frac{\partial}{\partial x} (h_y U) + \frac{\partial}{\partial y} (h_x V) \right] = 0 \quad (1.27)$$

is obtained, where  $U$  and  $V$  indicate the vertically integrated horizontal velocity components

$$U = \int_{-H}^{\eta} u dz = (\eta - z_B) \int_0^1 u d\sigma + \int_{-H}^{z_B} u dz, \quad (1.28)$$

$$V = \int_{-H}^{\eta} v dz = (\eta - z_B) \int_0^1 v d\sigma + \int_{-H}^{z_B} v dz. \quad (1.29)$$

When sea surface pressure  $P_\eta$  is given, pressure in the ocean is calculated by vertically integrating (1.3) and (1.20) from the sea surface. It is expressed as

$$P = P_\eta + g(\eta - z_B) \int_\sigma^1 \rho d\sigma' \quad \text{for } z_B < z < \eta \quad (0 < \sigma < 1), \quad (1.30)$$

$$= P_\eta + g(\eta - z_B) \int_0^1 \rho d\sigma + g \int_z^{z_B} \rho dz' \quad \text{for } z < z_B. \quad (1.31)$$

## 1.2 Diffusion and Viscosity Terms

### 1.2.1 Diffusion

The case considered here is that:

1. Diffusive flux of tracer follows the Fick's law.
2. Diffusion coefficient tensor is diagonal, and its two horizontal components are identical.

It corresponds to a classical case of Laplacian diffusion, with anisotropy between the horizontal and vertical directions. Other cases, such as isopycnal diffusion, will be described later in corresponding sections. Only the expression for  $\mathcal{D}_T$  is presented here, as that for  $\mathcal{D}_S$  is obvious once  $\mathcal{D}_T$  is known.

When the horizontal and vertical diffusion coefficients are described by  $K_H$  and  $K_V$ , respectively, the components of the diffusive tracer flux vector are represented by

$$x : \frac{K_H}{h_x} \frac{\partial T}{\partial x}, \quad y : \frac{K_H}{h_y} \frac{\partial T}{\partial y}, \quad z : K_V \frac{\partial T}{\partial z}. \quad (1.32)$$

The diffusion term is the divergence of this vector, thus

$$\mathcal{D}_T = \frac{1}{h_x h_y} \left[ \frac{\partial}{\partial x} \left( K_H \frac{h_y}{h_x} \frac{\partial T}{\partial x} \right) + \frac{\partial}{\partial y} \left( K_H \frac{h_x}{h_y} \frac{\partial T}{\partial y} \right) \right] + \frac{\partial}{\partial z} \left( K_V \frac{\partial T}{\partial z} \right). \quad (1.33)$$

### 1.2.2 Viscosity

Under the shallowness and hydrostatic approximations, the viscosity terms are represented by

$$\mathcal{V}_u = \frac{1}{h_x h_y} \left[ \frac{1}{h_y} \frac{\partial}{\partial x} \left( \frac{h_y^2 \tau_{xx} - \tau_{yy}}{2} \right) + \frac{1}{h_x} \frac{\partial}{\partial y} (h_x^2 \tau_{xy}) \right] + \frac{\partial \tau_{xz}}{\partial z} + \frac{\tau_{xz}}{a}, \quad (1.34)$$

$$\mathcal{V}_v = \frac{1}{h_x h_y} \left[ \frac{1}{h_y} \frac{\partial}{\partial x} (h_y^2 \tau_{xy}) + \frac{1}{h_x} \frac{\partial}{\partial y} \left( \frac{h_x^2 \tau_{yy} - \tau_{xx}}{2} \right) \right] + \frac{\partial \tau_{yz}}{\partial z} + \frac{\tau_{yz}}{a}, \quad (1.35)$$

where  $\tau$  is stress tensor. A constitutive equation linearly relates components of the stress tensor with components of strain rate tensor  $\varepsilon$ . For the classical case of Laplacian viscosity with horizontal-vertical transverse anisotropy, the constitutive equation is

$$\tau_{xx} - \tau_{yy} = 2A_H(\varepsilon_{xx} - \varepsilon_{yy}), \quad (1.36)$$

$$\tau_{xy} = 2A_H \varepsilon_{xy}, \quad (1.37)$$

$$\tau_{xz} = 2A_V \varepsilon_{xz}, \quad (1.38)$$

$$\tau_{yz} = 2A_V \varepsilon_{yz}, \quad (1.39)$$

and components of the strain rate tensor are represented by

$$\varepsilon_{xx} - \varepsilon_{yy} = \frac{1}{h_x} \frac{\partial u}{\partial x} + h_{xy} v - \frac{1}{h_y} \frac{\partial v}{\partial y} - h_{yx} u, \quad (1.40)$$

$$\varepsilon_{xy} = \frac{1}{2} \left[ \frac{h_x}{h_y} \frac{\partial}{\partial y} \left( \frac{u}{h_x} \right) + \frac{h_y}{h_x} \frac{\partial}{\partial x} \left( \frac{v}{h_y} \right) \right], \quad (1.41)$$

$$\varepsilon_{xz} = \frac{1}{2} \left( \frac{\partial u}{\partial z} - \frac{u}{a} \right), \quad (1.42)$$

$$\varepsilon_{yz} = \frac{1}{2} \left( \frac{\partial v}{\partial z} - \frac{v}{a} \right). \quad (1.43)$$

$A_H$  and  $A_V$  are horizontal and vertical, respectively, viscosity coefficients. This formulation is well-defined for the case of spatially varying viscosity coefficients. See appendix D.6 for detail.

### 1.3 Boundary Conditions

A no-slip condition is imposed on the momentum equations (1.1)/(1.18) and (1.2)/(1.19) on lateral boundaries:

$$u|_{\text{lateral}} = 0, \quad (1.44)$$

$$v|_{\text{lateral}} = 0. \quad (1.45)$$

At the bottom, vertical momentum flux is assumed to follow a simple quadratic drag formula, and the bottom boundary condition is expressed as

$$A_V \frac{\partial u}{\partial z} \Big|_{\text{bottom}} = C_b \sqrt{u^2 + v^2} \times u, \quad (1.46)$$

$$A_V \frac{\partial v}{\partial z} \Big|_{\text{bottom}} = C_b \sqrt{u^2 + v^2} \times v, \quad (1.47)$$

where  $C_b$  is a drag coefficient (nondimensional). Since the vertical resolution is not fine enough to resolve the bottom Ekman layer in most applications, the flow direction of the model's bottom level is expected to be significantly different from that at the ocean floor. In order to take it into account, the bottom stress is often formulated by

$$A_V \frac{\partial u}{\partial z} \Big|_{\text{bottom}} = C_b \sqrt{u^2 + v^2} (u \cos \theta + v \sin \theta), \quad (1.48)$$

$$A_V \frac{\partial v}{\partial z} \Big|_{\text{bottom}} = C_b \sqrt{u^2 + v^2} (v \cos \theta - u \sin \theta) \quad (1.49)$$

with nonzero turning angle  $\theta$ , although it is fixed at zero in the default setup of COCO. At the sea surface, the condition is

$$A_V \frac{\partial u}{\partial z} \Big|_{\text{surface}} = \frac{\tau_x}{\rho_0}, \quad (1.50)$$

$$A_V \frac{\partial v}{\partial z} \Big|_{\text{surface}} = \frac{\tau_y}{\rho_0}, \quad (1.51)$$

where  $\tau_x$  and  $\tau_y$  are  $x$  and  $y$  components, respectively, of surface wind stress.

Continuity of fluid requires a boundary condition for  $w$  at the ocean floor:

$$w|_{\text{bottom}} = - \left( \frac{u|_{\text{bottom}}}{h_x} \frac{\partial H}{\partial x} + \frac{v|_{\text{bottom}}}{h_y} \frac{\partial H}{\partial y} \right). \quad (1.52)$$

On the other hand,  $w$  at the sea surface is defined by

$$\begin{aligned} w|_{\text{surface}} &= \frac{d\eta}{dt} \\ &= \frac{\partial \eta}{\partial t} + \frac{u|_{z=\eta}}{h_x} \frac{\partial \eta}{\partial x} + \frac{v|_{z=\eta}}{h_y} \frac{\partial \eta}{\partial y}. \end{aligned} \quad (1.53)$$

By definition, boundary conditions for  $\omega$  are:

$$\omega|_{\sigma=0} = \frac{w|_{z=z_B}}{\eta - z_B}, \quad (1.54)$$

$$\omega|_{\sigma=1} = \frac{w|_{z=\eta}}{\eta - z_B} - \frac{1}{\eta - z_B} \left( \frac{\partial \eta}{\partial t} + \frac{u|_{z=\eta}}{h_x} \frac{\partial \eta}{\partial x} + \frac{v|_{z=\eta}}{h_y} \frac{\partial \eta}{\partial y} \right) = 0. \quad (1.55)$$

For the tracer equations (1.5)/(1.22) and (1.6)/(1.23), a no-flux condition is applied on solid boundaries:

$$\left. \frac{\partial T}{\partial n} \right|_{\text{solid}} = 0, \quad (1.56)$$

$$\left. \frac{\partial S}{\partial n} \right|_{\text{solid}} = 0, \quad (1.57)$$

where  $\partial/\partial n$  represents partial differentiation in the direction normal to the boundary. Sea surface boundary condition for the temperature equation is

$$K_V \left. \frac{\partial T}{\partial z} \right|_{\text{surface}} = -\frac{F_H}{\rho_0 C_p}, \quad (1.58)$$

where  $F_H$  is heat flux at the sea surface (positive upward) and  $C_p$  is the heat capacity of seawater. The surface boundary condition for the salinity equation is generally represented by

$$\left. \frac{\partial S}{\partial z} \right|_{\text{surface}} = -F_S, \quad (1.59)$$

where  $F_S$  is salt flux at the sea surface (positive upward, i.e., it is positive when salt is extracted from seawater). Nonzero salt flux occurs mostly where sea ice forms or melts<sup>1</sup>. Note, however, that freshwater flux at the sea surface,  $F_W$ , dilutes or concentrates seawater and thus affects sea surface salinity even if  $F_S = 0$ . Note also that addition or subtraction of freshwater by nonzero  $F_W$  makes it necessary to take account of the heat (temperature) of added or subtracted water. Treatment for such effects of  $F_W$  on salinity and temperature is described in section 3.2.3.

Sea surface boundary conditions are the principal driving force for the ocean circulation, and the methods used in COCO to specify them are described in appendix A. The sea surface fluxes are significantly affected by existence of sea ice, and its treatment is described in appendix B.

## 1.4 Mode Split for Horizontal Velocity

COCO version 4.0 explicitly predicts changes of the free surface, so external gravity waves are represented in the model, whose phase speed is significantly larger than that of other waves or advection velocity. In order to reduce the computational cost arising from a severe CFL condition for external gravity waves, their governing equations are separately solved with a short time step. This separation is realized by splitting the horizontal velocity components into their vertical mean (external mode) and deviation from it (internal mode). The basic idea for mode separation is taken from *Killworth et al. [1991]*, though it is re-formulated from scratch to adapt to COCO.

### 1.4.1 External Mode Equations

The advection terms of the  $\sigma$  coordinate momentum equations (1.18) and (1.19) are expressed by

$$\frac{u}{h_x} \frac{\partial \alpha}{\partial x} + \frac{v}{h_y} \frac{\partial \alpha}{\partial y} + \omega \frac{\partial \alpha}{\partial \sigma}, \quad (1.60)$$

where  $\alpha$  stands for  $u$  or  $v$ . Its flux form is obtained by applying the continuity equation (1.21) as

$$\frac{1}{\eta - z_B} \left\{ \frac{1}{h_x h_y} \frac{\partial}{\partial x} [h_y u \alpha (\eta - z_B)] + \frac{1}{h_x h_y} \frac{\partial}{\partial y} [h_x v \alpha (\eta - z_B)] + (\eta - z_B) \frac{\partial}{\partial \sigma} (\omega \alpha) + \alpha \frac{\partial \eta}{\partial t} \right\}. \quad (1.61)$$

<sup>1</sup>There also is extraction of salt by generation of sea-salt aerosols, which is induced by seawater splashes, and their precipitation leads to addition of salt. Such factors are negligible.

Therefore, vertical integration of the advection terms of the  $\sigma$  coordinate momentum equations yields

$$\begin{aligned}
& (\eta - z_B) \int_0^1 \left( \frac{u}{h_x} \frac{\partial \alpha}{\partial x} + \frac{v}{h_y} \frac{\partial \alpha}{\partial y} + \omega \frac{\partial \alpha}{\partial \sigma} \right) d\sigma \\
&= \frac{1}{h_x h_y} \frac{\partial}{\partial x} \left[ h_y (\eta - z_B) \int_0^1 u \alpha d\sigma \right] + \frac{1}{h_x h_y} \frac{\partial}{\partial y} \left[ h_x (\eta - z_B) \int_0^1 v \alpha d\sigma \right] \\
&\quad - (\eta - z_B) (\omega \alpha)|_{\sigma=0} + \frac{\partial \eta}{\partial t} \int_0^1 \alpha d\sigma.
\end{aligned} \tag{1.62}$$

Since

$$(\eta - z_B) \int_0^1 \frac{\partial \alpha}{\partial t} d\sigma = \frac{\partial}{\partial t} \left[ (\eta - z_B) \int_0^1 \alpha d\sigma \right] - \frac{\partial \eta}{\partial t} \int_0^1 \alpha d\sigma, \tag{1.63}$$

vertical integration of  $d\alpha/dt$  becomes

$$\begin{aligned}
(\eta - z_B) \int_0^1 \frac{d\alpha}{dt} d\sigma &= \frac{\partial}{\partial t} \left[ (\eta - z_B) \int_0^1 \alpha d\sigma \right] + \frac{1}{h_x h_y} \frac{\partial}{\partial x} \left[ h_y (\eta - z_B) \int_0^1 u \alpha d\sigma \right] \\
&\quad + \frac{1}{h_x h_y} \frac{\partial}{\partial y} \left[ h_x (\eta - z_B) \int_0^1 v \alpha d\sigma \right] - (\eta - z_B) (\omega \alpha)|_{\sigma=0}.
\end{aligned} \tag{1.64}$$

For  $z < z_B$

$$\begin{aligned}
\int_{-H}^{z_B} \frac{d\alpha}{dt} dz &= \int_{-H}^{z_B} \frac{\partial \alpha}{\partial t} dz + \int_{-H}^{z_B} \left\{ \frac{1}{h_x h_y} \left[ \frac{\partial}{\partial x} (h_y u \alpha) + \frac{\partial}{\partial y} (h_x v \alpha) \right] + \frac{\partial}{\partial z} (w \alpha) \right\} dz \\
&= \frac{\partial}{\partial t} \int_{-H}^{z_B} \alpha dz + \frac{1}{h_x h_y} \left[ \int_{-H}^{z_B} \frac{\partial}{\partial x} (h_y u \alpha) dz + \int_{-H}^{z_B} \frac{\partial}{\partial y} (h_x v \alpha) dz \right] \\
&\quad + (w \alpha)|_{z=z_B} - (w \alpha)|_{z=-H} \\
&= \frac{\partial}{\partial t} \int_{-H}^{z_B} \alpha dz + \frac{1}{h_x h_y} \left[ \frac{\partial}{\partial x} \int_{-H}^{z_B} h_y u \alpha dz - h_y (u \alpha)|_{z=-H} \frac{\partial H}{\partial x} \right] \\
&\quad + \frac{1}{h_x h_y} \left[ \frac{\partial}{\partial y} \int_{-H}^{z_B} h_x v \alpha dz - h_x (v \alpha)|_{z=-H} \frac{\partial H}{\partial y} \right] \\
&\quad + (w \alpha)|_{z=z_B} - \alpha|_{z=-H} \left( -\frac{u|_{z=-H}}{h_x} \frac{\partial H}{\partial x} - \frac{v|_{z=-H}}{h_y} \frac{\partial H}{\partial y} \right) \\
&= \frac{\partial}{\partial t} \int_{-H}^{z_B} \alpha dz + \frac{1}{h_x h_y} \left[ \frac{\partial}{\partial x} \left( h_y \int_{-H}^{z_B} u \alpha dz \right) + \frac{\partial}{\partial y} \left( h_x \int_{-H}^{z_B} v \alpha dz \right) \right] + (w \alpha)|_{z=z_B}. \tag{1.65}
\end{aligned}$$

Therefore, vertical integration of  $d\alpha/dt$  over a full water column is

$$\begin{aligned}
& (\eta - z_B) \int_0^1 \frac{d\alpha}{dt} d\sigma + \int_{-H}^{z_B} \frac{d\alpha}{dt} dz \\
&= \frac{\partial}{\partial t} \left[ (\eta - z_B) \int_0^1 \alpha d\sigma \right] + \frac{\partial}{\partial t} \int_{-H}^{z_B} \alpha dz \\
&\quad + \frac{1}{h_x h_y} \frac{\partial}{\partial x} \left[ h_y (\eta - z_B) \int_0^1 u \alpha d\sigma \right] + \frac{1}{h_x h_y} \frac{\partial}{\partial x} \left( h_y \int_{-H}^{z_B} u \alpha dz \right) \\
&\quad + \frac{1}{h_x h_y} \frac{\partial}{\partial y} \left[ h_x (\eta - z_B) \int_0^1 v \alpha d\sigma \right] + \frac{1}{h_x h_y} \frac{\partial}{\partial y} \left( h_x \int_{-H}^{z_B} v \alpha dz \right).
\end{aligned} \tag{1.66}$$

The pressure gradient term in the  $\sigma$  coordinate is represented by

$$\frac{\partial P}{\partial x} + \sigma \rho g \frac{\partial \eta}{\partial x} = \frac{\partial P_\eta}{\partial x} + \left( \sigma \rho + \int_\sigma^1 \rho d\sigma' \right) g \frac{\partial \eta}{\partial x} + g (\eta - z_B) \int_\sigma^1 \frac{\partial \rho}{\partial x} d\sigma' \tag{1.67}$$

for the  $x$  direction, for example. The parenthesized quantity of the second term in the right hand side becomes sea surface density for  $\sigma = 1$ , becomes averaged density over  $0 \leq \sigma \leq 1$

$$\bar{\rho}^\sigma \equiv \int_0^1 \rho d\sigma \quad (1.68)$$

for  $\sigma = 0$ , and monotonically decrease with  $\sigma$  in between (as  $\rho$  is a monotonically decreasing function of  $\sigma$ ). As described later, the dependence of this quantity on  $\sigma$  makes the mode separation difficult. Assuming that density variation over  $0 \leq \sigma \leq 1$  is small, therefore, this quantity is approximated by  $\bar{\rho}^\sigma$ , which means that the pressure gradient terms in (1.18) and (1.19) are replaced by

$$\frac{\partial P}{\partial x} + \sigma \rho g \frac{\partial \eta}{\partial x} \rightarrow \frac{\partial P_\eta}{\partial x} + \bar{\rho}^\sigma g \frac{\partial \eta}{\partial x} + g(\eta - z_B) \int_\sigma^1 \frac{\partial \rho}{\partial x} d\sigma', \quad (1.69)$$

$$\frac{\partial P}{\partial y} + \sigma \rho g \frac{\partial \eta}{\partial y} \rightarrow \frac{\partial P_\eta}{\partial y} + \bar{\rho}^\sigma g \frac{\partial \eta}{\partial y} + g(\eta - z_B) \int_\sigma^1 \frac{\partial \rho}{\partial y} d\sigma'. \quad (1.70)$$

Since horizontal derivative of (1.31) is

$$\frac{\partial P}{\partial x} = \frac{\partial P_\eta}{\partial x} + \bar{\rho}^\sigma g \frac{\partial \eta}{\partial x} + g(\eta - z_B) \int_0^1 \frac{\partial \rho}{\partial x} d\sigma + g \int_z^{z_B} \frac{\partial \rho}{\partial x} dz', \quad (1.71)$$

this treatment does not violate continuity of pressure at  $z = z_B$ , at least.

Using the above, vertical integration of the momentum equations (1.1)/(1.18) and (1.2)/(1.19) results in

$$\begin{aligned} \frac{\partial U}{\partial t} - fV &= -\frac{1}{h_x h_y} \frac{\partial}{\partial x} \left[ h_y (\eta - z_B) \int_0^1 u^2 d\sigma \right] - \frac{1}{h_x h_y} \frac{\partial}{\partial x} \left( h_y \int_{-H}^{z_B} u^2 dz \right) \\ &\quad - \frac{1}{h_x h_y} \frac{\partial}{\partial y} \left[ h_x (\eta - z_B) \int_0^1 uv d\sigma \right] - \frac{1}{h_x h_y} \frac{\partial}{\partial y} \left( h_x \int_{-H}^{z_B} uv dz \right) \\ &\quad - h_{xy} \left[ (\eta - z_B) \int_0^1 uv d\sigma + \int_{-H}^{z_B} uv dz \right] + h_{yx} \left[ (\eta - z_B) \int_0^1 v^2 d\sigma + \int_{-H}^{z_B} v^2 dz \right] \\ &\quad + (\eta - z_B) \int_0^1 \mathcal{V}_u d\sigma + \int_{-H}^{z_B} \mathcal{V}_u dz \\ &\quad - \frac{\bar{\rho}^\sigma g (\eta + H)}{\rho_0 h_x} \frac{\partial \eta}{\partial x} - \frac{\eta + H}{\rho_0 h_x} \frac{\partial P_\eta}{\partial x} - \frac{g(\eta - z_B)(z_B + H)}{\rho h_x} \frac{\partial \bar{\rho}^\sigma}{\partial x} \\ &\quad - \frac{g(\eta - z_B)^2}{\rho_0 h_x} \int_0^1 d\sigma \int_\sigma^1 d\sigma' \frac{\partial \rho}{\partial x} - \frac{g}{\rho_0 h_x} \int_{-H}^{z_B} dz \int_z^{z_B} dz' \frac{\partial \rho}{\partial x}, \end{aligned} \quad (1.72)$$

$$\begin{aligned} \frac{\partial V}{\partial t} + fU &= -\frac{1}{h_x h_y} \frac{\partial}{\partial x} \left[ h_y (\eta - z_B) \int_0^1 uv d\sigma \right] - \frac{1}{h_x h_y} \frac{\partial}{\partial x} \left( h_y \int_{-H}^{z_B} uv dz \right) \\ &\quad - \frac{1}{h_x h_y} \frac{\partial}{\partial y} \left[ h_x (\eta - z_B) \int_0^1 v^2 d\sigma \right] - \frac{1}{h_x h_y} \frac{\partial}{\partial y} \left( h_x \int_{-H}^{z_B} v^2 dz \right) \\ &\quad - h_{yx} \left[ (\eta - z_B) \int_0^1 uv d\sigma + \int_{-H}^{z_B} uv dz \right] + h_{xy} \left[ (\eta - z_B) \int_0^1 u^2 d\sigma + \int_{-H}^{z_B} u^2 dz \right] \\ &\quad + (\eta - z_B) \int_0^1 \mathcal{V}_v d\sigma + \int_{-H}^{z_B} \mathcal{V}_v dz \\ &\quad - \frac{\bar{\rho}^\sigma g (\eta + H)}{\rho_0 h_y} \frac{\partial \eta}{\partial y} - \frac{\eta + H}{\rho_0 h_y} \frac{\partial P_\eta}{\partial y} - \frac{g(\eta - z_B)(z_B + H)}{\rho h_y} \frac{\partial \bar{\rho}^\sigma}{\partial y} \\ &\quad - \frac{g(\eta - z_B)^2}{\rho_0 h_y} \int_0^1 d\sigma \int_\sigma^1 d\sigma' \frac{\partial \rho}{\partial y} - \frac{g}{\rho_0 h_y} \int_{-H}^{z_B} dz \int_z^{z_B} dz' \frac{\partial \rho}{\partial y}. \end{aligned} \quad (1.73)$$

Here, we rewrite these equations symbolically as

$$\frac{\partial U}{\partial t} - fV = -\frac{\bar{\rho}^\sigma g(\eta + H)}{\rho_0 h_x} \frac{\partial \eta}{\partial x} - \frac{(\eta + H)}{\rho_0 h_x} \frac{\partial P_\eta}{\partial x} + X, \quad (1.74)$$

$$\frac{\partial V}{\partial t} + fU = -\frac{\bar{\rho}^\sigma g(\eta + H)}{\rho_0 h_y} \frac{\partial \eta}{\partial y} - \frac{(\eta + H)}{\rho_0 h_y} \frac{\partial P_\eta}{\partial y} + Y. \quad (1.75)$$

These are further modified to

$$\frac{\partial U}{\partial t} - fV = -\frac{\bar{\rho}^\sigma g(\eta + H)}{\rho_0 h_x} \frac{\partial \eta}{\partial x} - \frac{(\eta + H)}{\rho_0 h_x} \frac{\partial P_\eta}{\partial x} + X' + \mathcal{V}_U, \quad (1.76)$$

$$\frac{\partial V}{\partial t} + fU = -\frac{\bar{\rho}^\sigma g(\eta + H)}{\rho_0 h_y} \frac{\partial \eta}{\partial y} - \frac{(\eta + H)}{\rho_0 h_y} \frac{\partial P_\eta}{\partial y} + Y' + \mathcal{V}_V, \quad (1.77)$$

where

$$X' = X - \mathcal{V}_U, \quad (1.78)$$

$$Y' = Y - \mathcal{V}_V, \quad (1.79)$$

and  $\mathcal{V}_U$  ( $\mathcal{V}_V$ ) is calculated by replacing  $u$  ( $v$ ) by  $U$  ( $V$ ) in  $\mathcal{V}_u$  ( $\mathcal{V}_v$ ). This treatment is for the sake of numerical stability. These equations are approximated by

$$\frac{\partial U}{\partial t} - fV = -\frac{gH}{h_x} \frac{\partial \eta}{\partial x} - \frac{H}{\rho_0 h_x} \frac{\partial P_\eta}{\partial x} + X' + \mathcal{V}_U, \quad (1.80)$$

$$\frac{\partial V}{\partial t} + fU = -\frac{gH}{h_y} \frac{\partial \eta}{\partial y} - \frac{H}{\rho_0 h_y} \frac{\partial P_\eta}{\partial y} + Y' + \mathcal{V}_V, \quad (1.81)$$

The equations (1.27), (1.80) and (1.81) construct the governing equations for the external mode. One time interval of integration for the internal mode equations is split into a number of shorter time intervals, and integration of the external mode equations proceeds incrementally by using that shorter time step. During an interval of internal mode integration,  $X'$  and  $Y'$  are estimated once initially and don't vary, while  $\mathcal{V}_U$  and  $\mathcal{V}_V$  change according to changing  $U$  and  $V$ .

### 1.4.2 Internal Mode Equations

The momentum equations (1.1)/(1.18) and (1.2)/(1.19) can be expressed in the form of

$$\frac{\partial u}{\partial t} - fv = -\frac{\bar{\rho}^\sigma g}{\rho_0 h_x} \frac{\partial \eta}{\partial x} - \frac{1}{\rho_0 h_x} \frac{\partial P_\eta}{\partial x} + G_X, \quad (1.82)$$

$$\frac{\partial v}{\partial t} + fu = -\frac{\bar{\rho}^\sigma g}{\rho_0 h_y} \frac{\partial \eta}{\partial y} - \frac{1}{\rho_0 h_y} \frac{\partial P_\eta}{\partial y} + G_Y. \quad (1.83)$$

These formal expressions are identical between the  $z$  and  $\sigma$  coordinate systems. Here, an average of a quantity  $\alpha$  in the form of

$$\tilde{\alpha} = \frac{1}{H} \left[ (-z_B) \int_0^1 \alpha d\sigma + \int_{-H}^{z_B} \alpha dz \right] \quad (1.84)$$

is considered. Since its upper and lower limits are independent of time, identities

$$\frac{\partial \tilde{u}}{\partial t} + f\tilde{v} = -\frac{\bar{\rho}^\sigma g}{\rho_0 h_x} \frac{\partial \eta}{\partial x} - \frac{1}{\rho_0 h_x} \frac{\partial P_\eta}{\partial x} + \tilde{G}_X, \quad (1.85)$$

$$\frac{\partial \tilde{v}}{\partial t} - f\tilde{u} = -\frac{\bar{\rho}^\sigma g}{\rho_0 h_y} \frac{\partial \eta}{\partial y} - \frac{1}{\rho_0 h_y} \frac{\partial P_\eta}{\partial y} + \tilde{G}_Y \quad (1.86)$$

hold. On the other hand, when quantities  $\hat{u}$  and  $\hat{v}$  which follow

$$\frac{\partial \hat{u}}{\partial t} - f\hat{v} = G_X, \quad (1.87)$$

$$\frac{\partial \hat{v}}{\partial t} + f\hat{u} = G_Y \quad (1.88)$$

are considered, equations

$$\frac{\partial(\hat{u} - \tilde{u})}{\partial t} - f(\hat{v} - \tilde{v}) = \frac{\partial(u - \tilde{u})}{\partial t} - f(v - \tilde{v}), \quad (1.89)$$

$$\frac{\partial(\hat{v} - \tilde{v})}{\partial t} + f(\hat{u} - \tilde{u}) = \frac{\partial(v - \tilde{v})}{\partial t} + f(u - \tilde{u}) \quad (1.90)$$

hold, as the approximation (1.69) and (1.70) are applied. Therefore, deviation of velocity components from their average of the form of (1.84)

$$u' = u - \tilde{u}, \quad v' = v - \tilde{v} \quad (1.91)$$

is obtained by solving (1.87) and (1.88). This deviation is here defined as the internal mode of horizontal velocity.

### 1.4.3 Mode Combination

When the external ( $U$  and  $V$ ) and internal ( $u'$  and  $v'$ ) modes are given, actual horizontal velocity components  $u$  and  $v$  are calculated by

$$u = \frac{U}{H} + u' - \frac{\eta}{H} \int_0^1 u d\sigma, \quad (1.92)$$

$$v = \frac{V}{H} + v' - \frac{\eta}{H} \int_0^1 v d\sigma. \quad (1.93)$$

It is impossible to analytically solve these integral equations. Nor is it easy to obtain their numerical solutions under their discretized expressions. In addition, their dependence on  $\eta$  complicates tracer conservation under discretized form. Therefore, the last terms of (1.92) and (1.93) are neglected.

## Chapter 2

# Horizontal Coordinate and Grid

In COCO version 4.0, the model horizontal coordinate/grid is generated by transforming the spherical (longitude-latitude) coordinate system and its coordinate lines (meridians and latitude circles) using the polar stereographic projection and conformal mapping. The basic concept of the transformation follows the method proposed by *Bentsen et al. [1999]*.

### 2.1 Polar Stereographic Projection

Consider the spherical coordinate system on a sphere of radius  $1/2$ , and represent its longitude by  $\lambda$  and latitude by  $\varphi$ . Assume the extended complex plane<sup>1</sup> tangential to this sphere, which contact with the sphere at  $\varphi = \pi/2$  (the North Pole) and whose real axis is in the direction of  $\lambda = 0$ . The polar stereographic projection of a point  $(\lambda, \varphi)$  on the sphere onto a value (point)  $z$  of the complex plane is given by

$$z = \tan\left(\frac{\pi}{4} - \frac{\varphi}{2}\right) e^{i\lambda}. \quad (2.1)$$

This mapping is a bijection, and its inverse is given by

$$\lambda = \arg z, \quad (2.2)$$

$$\varphi = \frac{\pi}{2} - 2 \arctan |z|. \quad (2.3)$$

This projection is obtained as an intersecting point of the complex plane and a line connecting the given point and the South Pole of the sphere (Figure 2.1).

This polar stereographic projection has the following characteristics:

1. The North Pole, the South Pole, and the equator of the sphere are transformed into the coordinate origin (zero), the point at infinity, and a circle of unit radius centered at the origin, respectively, of the complex plane.
2. Meridians and latitude circles on the sphere are transformed into straight lines starting from the origin and circles centered at the origin, respectively.
3. A circle on the sphere (a plane section of the sphere) is transformed into a circle on the complex plane. Note that a circle passing through the South Pole of the sphere is transformed into a straight line (a circle of infinite radius) on the complex plane.

---

<sup>1</sup>The point at infinity is added to the complex plane.

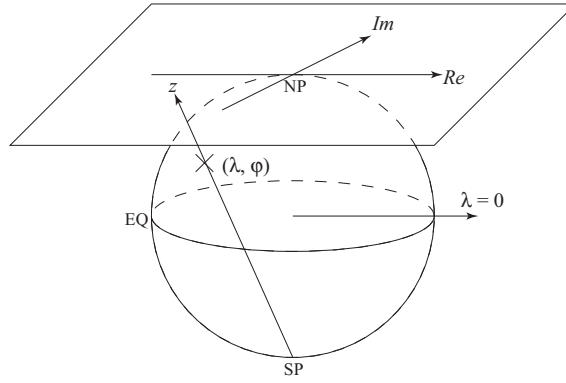


Figure 2.1: Polar stereographic projection.

4. Angle of any two intersecting curves is preserved by the mapping.
5. Shape of an infinitesimal figure on the sphere is preserved by the mapping.

The last item means that an infinitesimal figure on the sphere is isotropically enlarged or shrunk by this projection, and its scaling factor is represented by

$$\frac{2}{1 + \sin \varphi} \quad \text{or} \quad 1 + |z|^2. \quad (2.4)$$

## 2.2 Conformal Mapping on Complex Plane

A mapping  $f$  defined in a region of the complex plane is called conformal mapping if it is analytic and its derivatives are nonzero in the considered region. A conformal mapping  $f$  has the following characteristics:

1. A line tangential to any curve at  $z_0$  is rotated by an angle of  $\arg f'(z_0)$ . Therefore, an angle of two intersecting curves is preserved by a conformal mapping.
2. An infinitesimal figure at  $z_0$  is (isotropically) enlarged with a scaling factor of  $|f'(z_0)|$ .

A transformation on the complex plane (a bijection of the complex plane onto itself) expressed by the form of

$$f : z \mapsto w; \quad w = \frac{az + b}{cz + d} \quad (ad - bc \neq 0), \quad (2.5)$$

where  $a$ ,  $b$ ,  $c$  and  $d$  denote fixed complex numbers, is called a linear fractional transformation. A linear fractional transformation is regular and  $f' \neq 0$  except for  $z = -d/c$ . This singular point is mapped onto infinity. Including infinity, therefore, a linear fractional transformation is a conformal mapping on the extended complex plane. A linear fractional transformation is uniquely determined by designating transformation of three points. When the points  $z_1$ ,  $z_2$  and  $z_3$  are transformed into  $w_1$ ,  $w_2$  and  $w_3$ , the linear fractional transformation is determined as

$$\frac{(w - w_1)(w_3 - w_2)}{(w - w_2)(w_3 - w_1)} = \frac{(z - z_1)(z_3 - z_2)}{(z - z_2)(z_3 - z_1)}. \quad (2.6)$$

A linear fractional transformation maps a circle on the complex plane onto a circle (a straight line is regarded as a circle of infinite radius).

### 2.3 Transformed Coordinate and Grid System

The spherical coordinate system is defined by a set of (infinite) meridians (lines with constant longitudes) and a set of (infinite) latitude circles (lines with constant latitudes). This coordinate system defined by geographical longitudes and latitudes is hereafter referred to as the geographical coordinate system. A finite subset of these meridians and latitude circles constructs a grid system for the geographical coordinate. The following procedure generates a new coordinate/grid system on the sphere:

1. Project the meridians and latitude circles onto the complex plane by the polar stereographic projection.
2. Transform the projected lines by a linear fractional transformation on the complex plane.
3. Project the transformed lines back onto the sphere by the inverse of the polar stereographic projection.

Since the polar stereographic projection (and its inverse) and the linear fractional transformation preserve an angle of any two intersecting curves, the new coordinate lines on the sphere meet at right angles at every intersecting point. Therefore, the new coordinate lines define an orthogonal curvilinear coordinate/grid system. Grid lines of the geographical coordinate system are naturally transformed into those of the transformed coordinate system, and thus define a grid system on the transformed coordinate system. Note that any conformal mapping, not restricted to linear fractional transformations, is allowed in the second step to obtain an orthogonal curvilinear coordinate/grid system, but we limit our discussion to the case of linear fractional transformations for practical applications.

Let  $x$  and  $y$  denote horizontal coordinates of the transformed coordinate system on the sphere, and let  $x$  be transformed from “longitude” and  $y$  from “latitude.” Then, the ranges for these coordinates are:

$$0 \leq x \leq 2\pi, \quad -\frac{\pi}{2} \leq y \leq \frac{\pi}{2}. \quad (2.7)$$

Consider a point  $P$  on the sphere, whose geographical coordinate is denoted by  $(\lambda_P, \varphi_P)$  and transformed coordinate by  $(x_P, y_P)$ . Its projection onto the complex plane is

$$z_P = \tan\left(\frac{\pi}{4} - \frac{\varphi_P}{2}\right) e^{i\lambda_P}. \quad (2.8)$$

Let  $f$  be the linear fractional transformation used to obtain the transformed coordinate system currently under consideration. Since the coordinate system is transformed by  $f$ , a coordinate value of a point is transformed by its inverse  $f^{-1}$ . Then, consider a point  $Q$  defined by

$$z_Q = f^{-1}(z_P) \quad \text{or} \quad z_P = f(z_Q). \quad (2.9)$$

Since the transformed coordinate of  $P$  takes the same value as the geographical coordinate of  $Q$  (transformation is so made), the *geographical* coordinate of  $Q$  is represented by  $(x_P, y_P)$ , and its projection onto the complex plane is

$$z_Q = \tan\left(\frac{\pi}{4} - \frac{y_P}{2}\right) e^{ix_P}. \quad (2.10)$$

Given the transformed coordinate of  $P$ , therefore, the geographical coordinate of  $P$  is determined as

$$\lambda_P = \arg f(z_Q), \quad (2.11)$$

$$\varphi_P = \frac{\pi}{2} - 2 \arctan |f(z_Q)| \quad (2.12)$$

(see Figure 2.2).

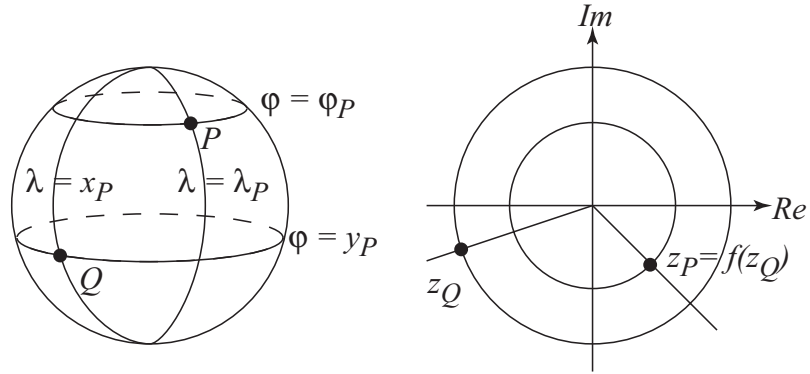


Figure 2.2: Transformation of coordinate values.

## 2.4 Defining a Suitable Linear Fractional Transformation

If we know the *transformed* coordinate of the *geographical* North and South Poles, i.e., if we know the transformed coordinate  $(x_{NP}, y_{NP})$  of the geographical North Pole ( $\lambda_{NP} = 0, \varphi_{NP} = \pi/2$ ) and the transformed coordinate  $(x_{SP}, y_{SP})$  of the geographical South Pole ( $\lambda_{SP} = 0, \varphi_{SP} = -\pi/2$ ), it indicates that the linear fractional transformation  $f$  yields

$$z_{NP} = f(z_{NQ}), \quad z_{SP} = f(z_{SQ}), \quad (2.13)$$

where

$$z_{NP} = 0, \quad z_{SP} = \infty, \quad (2.14)$$

and

$$z_{NQ} = \tan\left(\frac{\pi}{4} - \frac{y_{NP}}{2}\right) e^{ix_{NP}}, \quad (2.15)$$

$$z_{SQ} = \tan\left(\frac{\pi}{4} - \frac{y_{SP}}{2}\right) e^{ix_{SP}}. \quad (2.16)$$

This means that we can set  $z_1, z_2, w_1$  and  $w_2$  of (2.6) as

$$z_1 = z_{NQ}, \quad z_2 = z_{SQ}, \quad w_1 = 0, \quad w_2 = \infty. \quad (2.17)$$

Thus, the current linear fractional transformation is written as

$$w = f(z) = \frac{w_3(z - z_{NQ})(z_3 - z_{SQ})}{(z - z_{SQ})(z_3 - z_{NQ})}. \quad (2.18)$$

When the transformed coordinate  $(x_3, y_3)$  of another point is given with its geographical coordinate known, the current linear fractional transformation is uniquely determined.

In most cases, however, we want to obtain a transformed coordinate system by designating the *geographical* coordinate to which the two coordinate singularities (the North and South Poles of the geographical coordinate system) are moved. For example, when we want to move one of the coordinate singularities to Greenland, it is straightforward to designate the *geographical* coordinate of the singularity of the *transformed* coordinate system, whereas it is not easy to know the *transformed* coordinate of the singularity of the *geographical* coordinate system. In this case, the inverse expression of (2.18) is applicable:

$$w = f(z) = \frac{-z_2(z_3 - z_1)z/w_3 + z_1(z_3 - z_2)}{-(z_3 - z_1)z/w_3 + z_3 - z_2}, \quad (2.19)$$

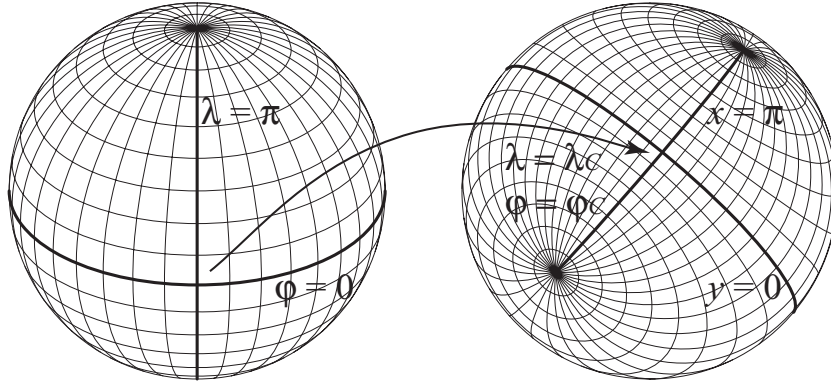


Figure 2.3: Designation of the third point. Under this choice, the coordinate lines  $\lambda = \pi$  and  $\varphi = 0$  (left) are transformed into great circles (right), and the geographical coordinate of their intersecting point is  $(\lambda_C, \varphi_C)$ .

where

$$z_1 = \tan\left(\frac{\pi}{4} - \frac{\varphi_N}{2}\right) e^{i\lambda_N}, \quad (2.20)$$

$$z_2 = \tan\left(\frac{\pi}{4} - \frac{\varphi_S}{2}\right) e^{i\lambda_S}, \quad (2.21)$$

and  $(\lambda_N, \varphi_N)$  and  $(\lambda_S, \varphi_S)$  indicate the geographical coordinates of the singularities (the original North Pole and South Pole, respectively) for the transformed coordinate system. The third point can be, of course, arbitrarily chosen. It is convenient in most cases to set

$$w_3 = -1, \quad z_3 = \tan\left(\frac{\pi}{4} - \frac{\varphi_C}{2}\right) e^{i\lambda_C}, \quad (2.22)$$

i.e., to designate the geographical coordinate  $(\lambda_C, \varphi_C)$  to which the intersecting point of the equator and the date line of the original geographical coordinate system is moved. Furthermore, it is convenient in most cases to select  $(\lambda_C, \varphi_C)$  as the midpoint of the great circle connecting the two (moved) singularities (Figure 2.3). In the Descartes coordinate with its origin at the center of the sphere, the points  $(\lambda_N, \varphi_N)$  and  $(\lambda_S, \varphi_S)$  are represented by  $(\cos \varphi_N \cos \lambda_N, \cos \varphi_N \sin \lambda_N, \sin \varphi_N)$  and  $(\cos \varphi_S \cos \lambda_S, \cos \varphi_S \sin \lambda_S, \sin \varphi_S)$ , respectively. The Descartes coordinate  $(\xi, \eta, \zeta)$  of the point  $(\lambda_C, \varphi_C)$  is then given by

$$2\xi = \cos \varphi_N \cos \lambda_N + \cos \varphi_S \cos \lambda_S, \quad (2.23)$$

$$2\eta = \cos \varphi_N \sin \lambda_N + \cos \varphi_S \sin \lambda_S, \quad (2.24)$$

$$2\zeta = \sin \varphi_N + \sin \varphi_S, \quad (2.25)$$

and thus

$$(\lambda_C, \varphi_C) = \left( \arctan \frac{\eta}{\xi}, \arctan \frac{\zeta}{\sqrt{\xi^2 + \eta^2}} \right). \quad (2.26)$$

Note that the above method of automatically determine the third point is not applicable to the case of  $\lambda_S = \lambda_N + \pi$  and  $\varphi_S = -\varphi_N$ , which corresponds to simple rotation of the spherical coordinate system, as it results in  $\xi = \eta = \zeta = 0$ . In this case, the third point should be selected as  $(\lambda_N, 0)$  of the original geographical coordinate system. The geographical coordinate to which this point is moved is

$$\begin{cases} (\lambda_N, \varphi_N - \pi/2) & \text{when } 0 < \varphi_N < \pi/2 \\ (\lambda_N + \pi, -\varphi_N - \pi/2) & \text{when } -\pi/2 < \varphi_N < 0 \end{cases}. \quad (2.27)$$

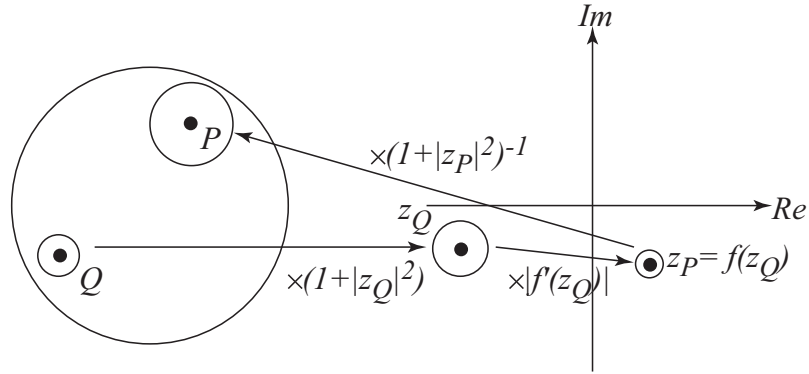


Figure 2.4: Transformation of metrics.

## 2.5 Metrics of Transformed Coordinate

Components of the metric tensor of the transformed coordinate system are derived from those of the geographical coordinate system ( $a \cos \varphi$  for  $\lambda$  and  $a$  for  $\varphi$ , where  $a$  is the radius of the sphere). Since the current coordinate transformation converts an orthogonal coordinate to another orthogonal coordinate, it suffices to take account of scaling factors for the two coordinate directions. The scaling factors for the two coordinate directions at a given point are the same, as the polar stereographic projection (and its inverse) and conformal mapping isotropically magnifies any infinitesimal figure.

An infinitesimal circle centered at the point  $Q$  on the sphere is projected onto the complex plane as a circle centered at  $z_Q$  with a scaling factor of  $1 + |z_Q|^2$ . This projected infinitesimal circle is transformed into a circle centered at  $z_P$  with a scaling factor of  $|f'(z_Q)|$ , which is then projected back to a circle on the sphere centered at the point  $P$  with a scaling factor of  $(1 + |z_P|^2)^{-1}$ . As a whole, an infinitesimal circle centered at  $Q$  on the sphere is mapped to a circle centered at  $P$  by the above procedure, and its scaling factor is

$$\frac{1 + |z_Q|^2}{1 + |z_P|^2} |f'(z_Q)| \quad (2.28)$$

(see Figure 2.4). Coordinate lines are magnified (or shrunk) with this scaling factor, so metrics should also be scaled by the same factor. Therefore, the metrics of the transformed coordinate at the point  $P$  are given by

$$h_x(x_P, y_P) = \frac{1 + |z_Q|^2}{1 + |z_P|^2} |f'(z_Q)| \cdot a \cos y_P, \quad (2.29)$$

$$h_y(x_P, y_P) = \frac{1 + |z_Q|^2}{1 + |z_P|^2} |f'(z_Q)| \cdot a. \quad (2.30)$$

The derivative of (2.19) is

$$f'(z) = \frac{(z_3 - z_1)(z_3 - z_2)(z_1 - z_2)}{w_3 [z_3 - z_2 - (z_3 - z_1)z/w_3]^2}. \quad (2.31)$$

## 2.6 Transformation of Vector

When local Descartes coordinate (see appendix D for its definition) representation is adopted to quantify components of vectors for both the geographical and transformed coordinate systems (it is an usual choice), components of a vector on the transformed coordinate system are obtained by simply taking account of

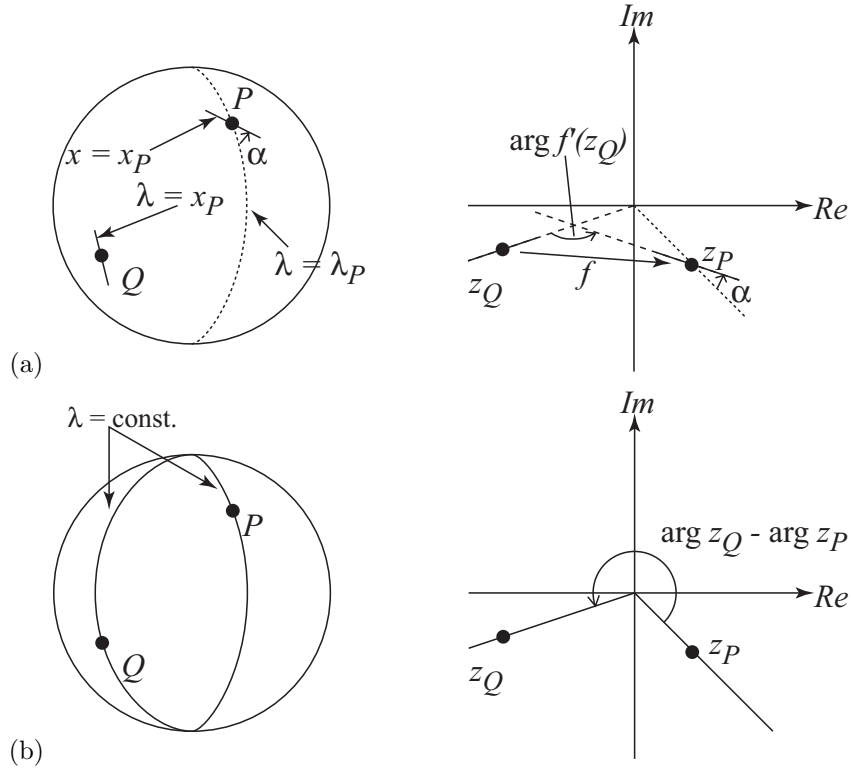


Figure 2.5: Rotation of coordinate lines.

relative rotation of the two local Descartes coordinate systems. In order to know that angle of rotation at a point  $P$ , it suffices to know the angle between a line of constant  $\lambda$  (or constant  $\varphi$ ) passing through a point  $P$  and a line of constant  $x$  (or constant  $y$ ) passing through the same point. Assume that the line of constant  $x$  is inclined by an angle of  $\alpha$  against the line of constant  $\lambda$ , the components of a vector for the transformed coordinate system is determined by calculating rotation of the components of that vector for the geographical coordinate system by the angle of  $-\alpha$ .

The polar stereographic projection of the line of constant  $\lambda$  passing through the point  $Q$  is transformed into the polar stereographic projection of the line of constant  $x$ , and the latter is inclined by the angle of  $\arg f'(z_Q)$  against the former (Figure 2.5a). On the other hand, the former is inclined by the angle of  $\arg z_Q - \arg z_P$  against the polar stereographic projection of the line of constant  $\lambda$  passing through the point  $P$  (Figure 2.5b). Therefore, the angle  $\alpha$  is the sum of the two, namely,

$$\alpha = \arg z_Q - \arg z_P + \arg f'(z_Q). \quad (2.32)$$

## 2.7 Mercator Grid

If a grid system of the geographical coordinate system is defined by a set of constant-interval meridians and latitude circles, i.e., if both the longitudinal grid interval  $\Delta\lambda$  and the latitudinal grid interval  $\Delta\varphi$  are constant, the actual shape of grids on the sphere varies with latitude (more latitudinally elongated rectangles at higher latitudes). If one wish to define a grid system of the geographical coordinate system where shapes

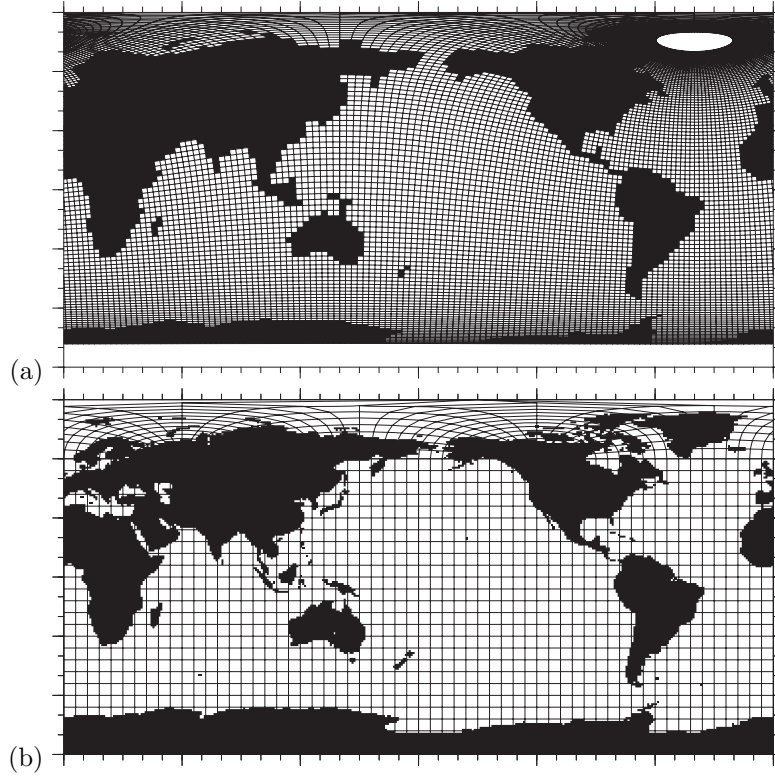


Figure 2.6: Grid system examples.

of the grids on the sphere are similar to one another, latitudinal grid interval should be varied with latitude. For such a purpose, the Mercator projection is useful.

The Mercator projection of spherical surface onto a plane is defined by

$$X = \lambda, \quad (2.33)$$

$$Y = \ln \left[ \tan \left( \frac{\varphi}{2} + \frac{\pi}{4} \right) \right], \quad (2.34)$$

where  $X$  and  $Y$  denote the projected coordinates. The Mercator projection maps an infinitesimal figure on the sphere onto a plane with preserving its shape. Therefore, when a grid system is defined on the Mercator coordinate system by lines of constant  $X$  and  $Y$  with constant grid intervals ( $\Delta X$  and  $\Delta Y$  are constant), its inverse projection onto the sphere forms grids of similar shapes on the geographical coordinate system. Note that one must select upper and lower limits for  $Y$  (or equivalent geographical latitudes) in constructing such a Mercator grid system, as the range of possible  $Y$  is unbounded ( $-\infty < Y < \infty$ ).

Since the coordinate transformation considered hereabove preserves shape of figures, a Mercator grid on the geographical coordinate system also defines a system of similar-shaped grids on the transformed coordinate system.

## 2.8 Coordinate/Grid System Examples

Two examples for grid systems generated by the above mentioned procedure are shown in Figure 2.6. In Figure 2.6a, there are 128 and 120 grids in the  $x$  and  $y$  directions, respectively. The base grid system on the geographical coordinate system is a Mercator grid system defined between  $\varphi = 78^\circ\text{S}$  and  $\varphi = 85^\circ\text{N}$ . The

geographical North Pole is moved to  $\lambda = 40^\circ\text{W}$ ,  $\varphi = 75^\circ\text{N}$  on Greenland, and the geographical South Pole is kept unchanged. This grid system is actually used at CCSR as one of the standard model configurations.

Figure 2.6b exemplifies a so-called tripolar grid system. The regular geographical coordinate/grid system is applied to the south of  $\varphi = 60^\circ\text{N}$ . The grid system to the north of this latitude, on the other hand, is generated by a linear fractional transformation, whose poles are located at  $\lambda = 60^\circ\text{E}$ ,  $\varphi = 60^\circ\text{N}$  and  $\lambda = 120^\circ\text{W}$ ,  $\varphi = 60^\circ\text{N}$ . The grid interval in the  $y$  direction is constant, and the number of grids in the  $y$  direction is chosen to match that of longitudinal grids of the geographical grid system defined to the south of  $\varphi = 60^\circ\text{N}$  (a half of longitudinal grids). The grid interval and the number of grids in the  $x$  direction is arbitrarily selected. This method guarantees smooth (differentiable) connection of the two coordinate systems.



## Chapter 3

# Discretization of Baseline Model

The mathematical model formulated in chapter 1 is discretized by use of the finite difference (or finite volume) method. In the baseline model, very simple and primitive algorithms are adopted for finite differencing the model equations. Some of those primitive schemes are replaced by much more sophisticated ones in most applications. For the purpose of grasping the gross structure of the model, however, it is very useful to start with the simple ones. More sophisticated numerical algorithms and physical parameterizations currently included in the COCO package are described in chapter 4.

### 3.1 Arrangement of Discretized Variables and Their Labeling

Before going into the description of the finite differenced expressions of the equations, some general rules are described first with regard to the arrangement of the variables on the grid system and the labeling of grids. The rule defined here is utilized throughout this document.

#### 3.1.1 Discretization in Time

The model is numerically integrated by using a fixed time interval  $\Delta t$ . When there is a need to specify the time level, it is indicated by a superscript. For example, the value of the variable  $T$  at the  $n$ -th time level is represented by  $T^n$ .

#### 3.1.2 Horizontal Grid

The domain is horizontally divided into a number of “boxes” by lines of constant  $x$  and  $y$ . Grid spacing in the  $x$  direction  $\Delta x$  is assumed to be constant, while that in the  $y$  direction  $\Delta y$  is allowed to vary ( $\Delta y$  is a function of  $y$ ). In the following description, the terms “east,” “west,” “north,” and “south” are used to indicate horizontal directions. The direction of increasing  $x$  is referred to as “east,” and that of increasing  $y$  is referred to as “north.”

The variables are arranged at grid points. The Arakawa B-grid system [*Mesinger and Arakawa, 1976*] is used, where the horizontal velocity components are defined at the vertices of the grid boxes and the tracer quantities (temperature and salinity), density, and sea surface height are defined at the centers of the grid boxes. Hereafter in this document, the vertices of the grid boxes are called “velocity points” or “V-points,” and the centers are called “tracer points” or “T-points.” As for the vertical velocity component, two sets of grid-point values are defined: one defined at the vertices of the grid boxes and the other at the center. In the horizontal view, these points for the vertical velocity coincide with either of V-points or T-points. However,

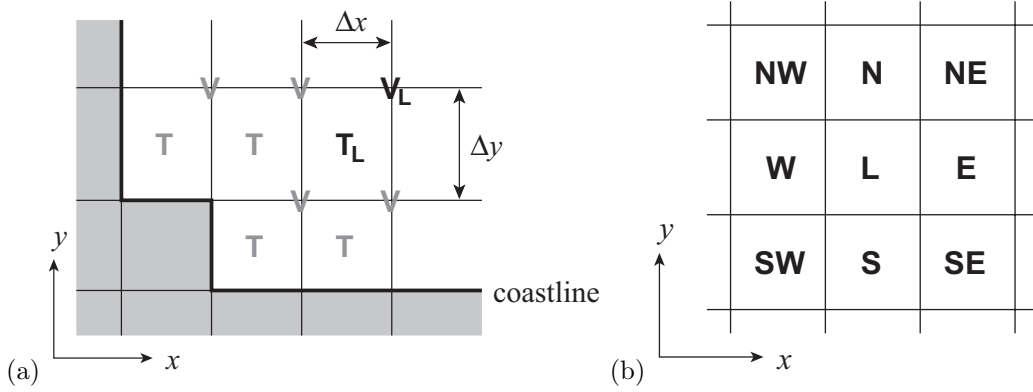


Figure 3.1: (a) Horizontal arrangement of the variables. Symbol  $V$  is placed only where the V-point variables could take nonzero values. (b) Labeling of the grid boxes in the horizontal direction relative to the centered box denoted by  $L$ .

as described in the next subsection, the vertical velocity and the other variables are defined at different levels in the vertical. When it is intended to draw a distinction, the terms “WV-points” and “WT-points” are used. Coastlines are defined by grid lines connecting V-points.

Grid points are identified by subscripts attached to the variables. For example,  $T_L$  indicates the value of the variable  $T$  at the grid point labeled by  $L$ . The V-point labeled by  $L$  is located at the northeastern vertex of the grid box containing  $T_L$ . When there is a need to refer to the grid points adjacent to the point labeled by  $L$ , the labels  $E$ ,  $W$ ,  $N$ ,  $S$ ,  $NE$ ,  $SE$ ,  $NW$ , and  $SW$  are used for subscripts, which denote the adjacent grid point to the east, west, north, south, northeast, southeast, northwest, and southwest, respectively. The horizontal arrangement of the variables and the labeling of the horizontal grids are illustrated in Figure 3.1.

### 3.1.3 Vertical Grid

In the  $z$  coordinate region, the domain is vertically divided into “levels” by horizontal planes. Spacing of the horizontal planes  $\Delta z$  is allowed to vary with depth. In the  $\sigma$  coordinate region, the domain is vertically divided by lines of constant  $\sigma$ , whose spacing  $\Delta\sigma$  is also allowed to vary in vertical. At each horizontal grid box, bottom of the water column must be located at  $z = z_B$  or deeper. The partial step representation [Adcroft *et al.*, 1997] is adopted for bottom topography, where bottom of water columns does not have to coincide with the vertical grid boundaries, so  $\Delta z$  could horizontally vary.

The WT-point labeled by  $L$  is located at the center of the top face of the grid box containing  $T_L$ . The same is true for WV-points. When there is a need to refer to the grid points vertically adjacent to the point labeled by  $L$ , the labels  $U$  and  $D$  are used for subscript, which denote the grid points just above and below, respectively. The vertical arrangement of the variables and the labeling of the vertical grids are illustrated in Figure 3.2.

Depths of water columns  $H$  are given at T-points. It is now denoted by  $H^T$ . The depths at V-points  $H^V$  are defined by the minimum of the four surrounding T-point depths, namely

$$H_L^V = \min(H_L^T, H_E^T, H_N^T, H_{NE}^T). \quad (3.1)$$

Only  $H_L^V$  appears in the finite differenced expressions described below.

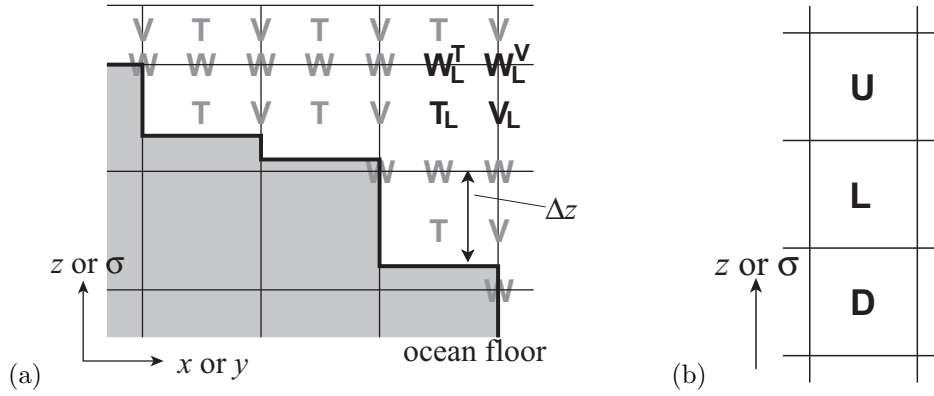


Figure 3.2: (a) Vertical arrangement of the variables. Symbols  $V$  and  $W$  are placed only where the variables could take nonzero values. (b) Labeling of the grid boxes in the vertical direction relative to the centered box denoted by  $L$ .

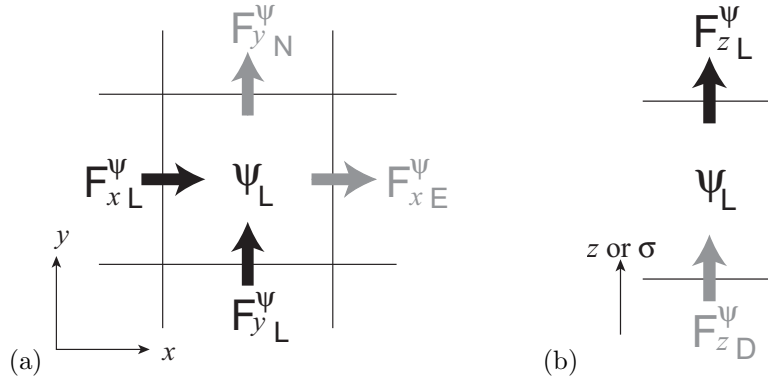


Figure 3.3: (a) Horizontal view for the arrangement of fluxes. (b) Vertical view for the arrangement of fluxes.

### 3.1.4 Flux

The equations (1.1), (1.2), (1.5), and (1.6) are written in the flux-form, i.e., the advection term (and the diffusion term in most cases) is represented by divergence of relevant flux. Adopting a flux-form representation also in finite differenced expressions facilitates to preserve the conservative nature of the equations.

Let us consider a flux-form time-evolving equation for a quantity  $\psi$ :

$$\frac{\partial \psi}{\partial t} = \frac{1}{h_x h_y} \left[ \frac{\partial}{\partial x} (h_y F_x^\psi) + \frac{\partial}{\partial y} (h_x F_y^\psi) \right] + \frac{\partial F_z^\psi}{\partial z}, \quad (3.2)$$

where the subscripted  $F^\psi$  is the flux of  $\psi$  in the direction indicated by the subscript. The variable  $\psi$  is a conservative quantity, in the sense that the volume integral of  $\psi$  does not change in time if there is no flux across the boundaries enclosing the domain of the volume integral. For finite differencing this flux-form equation, it is convenient to define the fluxes on the boundaries of the grid boxes. For the grid box containing  $\psi_L$  inside, the fluxes labeled by  $L$  are defined at the western, southern, and upper boundaries, respectively, of the box (Figure 3.3). The flux  $F_{xL}^\psi$ , for example, is the flux on the western boundary of the grid box  $L$ , and at the same time it is the flux on the eastern boundary of the grid box  $W$ . Sharing the same flux between the adjacent grids, the conservative nature is easily preserved in the finite differenced equation. The discussion is applicable to any of the variables defined at T-points, V-points, WT-points, or WV-points.

## 3.2 Time Differencing

Consider here the case of calculating values of the prognostic variables at the  $(n+1)$ -th time level when those at the  $n$ -th and  $(n-1)$ -th time levels are known. There are three sets of prognostic equations, namely, the internal mode equations (1.87) and (1.88); the external mode equations (1.27), (1.80) and (1.81); and the tracer equations (1.5)/(1.22) and (1.6)/(1.23). They are solved in this order, and each step of this procedure is described below.

### 3.2.1 Internal Mode Equations

Since the equations to be solved, (1.87) and (1.88), include the Coriolis term, numerical time integration of the equations require  $\Delta t$  be less than the inertial period when the Coriolis term is explicitly (forward-in-time) integrated in time. This restriction for  $\Delta t$  is somewhat relaxed by introducing the semi-implicit time stepping for the Coriolis term.

In estimating the Coriolis terms at the time level  $n$ , weighted average of velocity at the time levels  $n+1$  and  $n-1$  is used:

$$(f\mathbf{v})^n = f[\alpha\mathbf{v}^{n+1} + (1-\alpha)\mathbf{v}^{n-1}], \quad (3.3)$$

where  $\mathbf{v}$  is the two-dimensional vector whose components are  $u$  and  $v$ , and  $\alpha$  is the semi-implicit parameter which takes a value between zero and unity. The parameter value is adjustable in COCO, and its usual choice is  $1/2$ . By defining

$$\Delta\mathbf{v}^n = \mathbf{v}^{n+1} - \mathbf{v}^{n-1} = (u^{n+1} - u^{n-1}, v^{n+1} - v^{n-1}) = (\Delta u^n, \Delta v^n), \quad (3.4)$$

the time differenced expressions for the momentum equations (1.87) and (1.88) become

$$\frac{\Delta\hat{u}^n}{2\Delta t} - \alpha f \Delta\hat{v}^n = F_X^n, \quad (3.5)$$

$$\frac{\Delta\hat{v}^n}{2\Delta t} + \alpha f \Delta\hat{u}^n = F_Y^n, \quad (3.6)$$

where

$$F_X^n = G_X^n + f\hat{v}^{n-1}, \quad (3.7)$$

$$F_Y^n = G_Y^n - f\hat{u}^{n-1}. \quad (3.8)$$

Given  $F_X^n$  and  $F_Y^n$ , therefore,  $\hat{u}$  and  $\hat{v}$  are solved as

$$\Delta\hat{u}^n = \frac{2\Delta t}{1 + (2\Delta t\alpha f)^2} (F_X^n + 2\Delta t\alpha f F_Y^n), \quad (3.9)$$

$$\Delta\hat{v}^n = \frac{2\Delta t}{1 + (2\Delta t\alpha f)^2} (F_Y^n - 2\Delta t\alpha f F_X^n). \quad (3.10)$$

The advection and pressure gradient terms in  $G_X$  and  $G_Y$  are integrated by the leap-frog time stepping, i.e.,  $G_X^n$  and  $G_Y^n$  are estimated by using  $u^n$ ,  $v^n$  and  $\rho^n$ . Density at the  $n$ -th time level is obtained by substituting  $T^n$  and  $S^n$  into (1.7). The viscosity term, on the other hand, is integrated by the forward-in-time method, so  $u^{n-1}$  and  $v^{n-1}$  are used in estimating  $G_X^n$  and  $G_Y^n$ .

For the sake of computational stability, the Euler-backward scheme (also called the Matsuno scheme) is periodically applied, which is known to reduce high frequency variations induced by mode splitting nature of the leap-frog scheme [Mesinger and Arakawa, 1976]. In the standard configuration of COCO, nine

Euler-backward steps and one forward step are carried out after every ninety leap-frog steps. When the Euler-backward scheme is used, the variables at the  $(n - 1)$ -th time level are replaced by those at the  $n$ -th time level for the predictor step, and are replaced by those estimated by the predictor step for the corrector step. The  $2\Delta t$  is replaced by  $\Delta t$ , and  $\Delta \mathbf{v}^n$  is defined by  $\mathbf{v}^{n+1} - \mathbf{v}^n$ , as well.

### 3.2.2 External Mode Equations

The prognostic variables in the external mode equations ( $U$ ,  $V$  and  $\eta$ ) are numerically integrated from the  $(n - 1)$ -th time level to the  $(n + 1)$ -th time level. In so doing, the time interval  $2\Delta t$  is divided into  $N$  subintervals, and the Euler-backward time stepping are repeated by  $N$  times.

The number of repetition of the Euler-backward time stepping is indicated by a superscript  $i$ . In the predictor step, temporal estimates  $U'$ ,  $V'$  and  $\eta'$  are calculated by

$$\frac{\eta' - \eta^i}{2\Delta t/N} = -\frac{1}{h_x h_y} \left[ \frac{\partial}{\partial x} (h_y U^i) + \frac{\partial}{\partial y} (h_x V^i) \right], \quad (3.11)$$

$$\frac{U' - U^i}{2\Delta t/N} - f \frac{V' + V^i}{2} = -\frac{gH}{h_x} \frac{\partial \eta^i}{\partial x} - \frac{H}{\rho_0 h_x} \frac{\partial P_\eta}{\partial x} + X' + \mathcal{V}_{U^i}, \quad (3.12)$$

$$\frac{V' - V^i}{2\Delta t/N} + f \frac{U' + U^i}{2} = -\frac{gH}{h_y} \frac{\partial \eta^i}{\partial y} - \frac{H}{\rho_0 h_y} \frac{\partial P_\eta}{\partial y} + Y' + \mathcal{V}_{V^i}. \quad (3.13)$$

Then, the corrector step gives  $(i + 1)$ -th step values:

$$\frac{\eta^{i+1} - \eta^i}{2\Delta t/N} = -\frac{1}{h_x h_y} \left[ \frac{\partial}{\partial x} (h_y U') + \frac{\partial}{\partial y} (h_x V') \right], \quad (3.14)$$

$$\frac{U^{i+1} - U^i}{2\Delta t/N} - f \frac{V^{i+1} + V'}{2} = -\frac{gH}{h_x} \frac{\partial \eta'}{\partial x} - \frac{H}{\rho_0 h_x} \frac{\partial P_\eta}{\partial x} + X' + \mathcal{V}_{U'}, \quad (3.15)$$

$$\frac{V^{i+1} - V^i}{2\Delta t/N} + f \frac{U^{i+1} + U'}{2} = -\frac{gH}{h_y} \frac{\partial \eta'}{\partial y} - \frac{H}{\rho_0 h_y} \frac{\partial P_\eta}{\partial y} + Y' + \mathcal{V}_{V'}. \quad (3.16)$$

Here, the Coriolis term is semi-implicitly differenced, as in the case of the internal mode equations. The semi-implicit parameter is fixed at  $1/2$ .

For later use, quantities  $\bar{U}$  and  $\bar{V}$  which satisfy

$$\frac{\eta^{n+1} - \eta^{n-1}}{2\Delta t} = -\frac{1}{h_x h_y} \left[ \frac{\partial}{\partial x} (h_y \bar{U}) + \frac{\partial}{\partial y} (h_x \bar{V}) \right] \quad (3.17)$$

need to be calculated. They are obtained by averaging  $U'$  and  $V'$ , as the sum of the left hand side of (3.14) results in

$$\sum_{i=1}^N \frac{\eta^{i+1} - \eta^i}{2\Delta t/N} = N \frac{\eta^{n+1} - \eta^{n-1}}{2\Delta t}. \quad (3.18)$$

### 3.2.3 Tracer Equations

Only the prognostic equation for salinity is described here, as the procedure for the temperature equation is identical. Horizontal velocity components used in the advection terms of the tracer equations are defined here by

$$u^t = \frac{\bar{U}}{H} + u^n, \quad (3.19)$$

$$v^t = \frac{\bar{V}}{H} + v^n, \quad (3.20)$$

where the mode combination equations (1.92) and (1.93) are applied under the condition of  $\eta = 0$ , and  $u'$  and  $v'$  are defined by (1.91). Advection velocity so defined satisfies

$$\begin{aligned} \frac{\eta^{n+1} - \eta^{n-1}}{2\Delta t} &= -\frac{1}{h_x h_y} \frac{\partial}{\partial x} \left[ (-z_B) h_y \int_0^1 u^t d\sigma + h_y \int_{-H}^{z_B} u^t dz \right] \\ &\quad - \frac{1}{h_x h_y} \frac{\partial}{\partial y} \left[ (-z_B) h_x \int_0^1 v^t d\sigma + h_x \int_{-H}^{z_B} v^t dz \right] \end{aligned} \quad (3.21)$$

To be consistent with the approximation made in the mode combination, the  $\sigma$  coordinate tracer equations must be modified (tracers are not conserved otherwise). It requires that  $\eta$  should be set to zero in the horizontal advection terms of (1.23):

$$\frac{\partial}{\partial t} [S(\eta - z_B)] + \frac{-z_B}{h_x h_y} \left[ \frac{\partial}{\partial x} (h_y u S) + \frac{\partial}{\partial y} (h_x v S) \right] + (\eta - z_B) \frac{\partial}{\partial \sigma} (\omega S) = (\eta - z_B) D_S, \quad (3.22)$$

where  $(\eta - z_B)$  in the right hand side should also be replaced by  $-z_B$  for horizontal diffusion (not for vertical diffusion). The vertical component of the advection velocity is estimated by vertically integrating the continuity equation (1.4)/(1.21) from the bottom, with its value at the bottom taken to be zero. The  $\sigma$  coordinate continuity equation must also be modified as

$$\frac{\partial \eta}{\partial t} + \frac{-z_B}{h_x h_y} \left[ \frac{\partial}{\partial x} (h_y u) + \frac{\partial}{\partial y} (h_x v) \right] + (\eta - z_B) \frac{\partial \omega}{\partial \sigma} = 0. \quad (3.23)$$

The time-differenced equation for (3.23) is represented by

$$\frac{\eta^{n+1} - \eta^{n-1}}{2\Delta t} = -\frac{-z_B}{h_x h_y} \left[ \frac{\partial}{\partial x} (h_y u^t) + \frac{\partial}{\partial y} (h_x v^t) \right] - (\eta^{n-1} - z_B) \frac{\partial \omega}{\partial \sigma}, \quad (3.24)$$

where  $\eta^{n+1}$  is already known. The time-differenced equation for (3.22) is represented by

$$\frac{S^{n+1}(\eta^{n+1} - z_B) - S^{n-1}(\eta^{n-1} - z_B)}{2\Delta t} = \frac{-z_B}{h_x h_y} \left[ \frac{\partial F_x^S}{\partial x} + \frac{\partial F_y^S}{\partial y} \right] + (\eta^{n-1} - z_B) \frac{\partial F_\sigma^S}{\partial \sigma}, \quad (3.25)$$

where  $F^S$  indicates flux of salinity, whose physical dimension is the product of salinity and velocity, due to advection and diffusion in the direction of its subscript. Note that the time level of  $\eta$  in the last term of the right hand side must coincide with that used for the last term of (3.24). The adequate time level for  $S$  used in estimating the flux  $F^S$  depends on what kind of time differencing scheme is used. The default time differencing scheme of COCO version 4.0 is the forward-in-time method for both of advection and diffusion, i.e.,  $S^{n-1}$  is used for flux estimation. Changes of salinity due to addition and/or subtraction of freshwater through the sea surface are not calculated here but separately treated afterward. When actually solving the equation (3.25), an alternative form

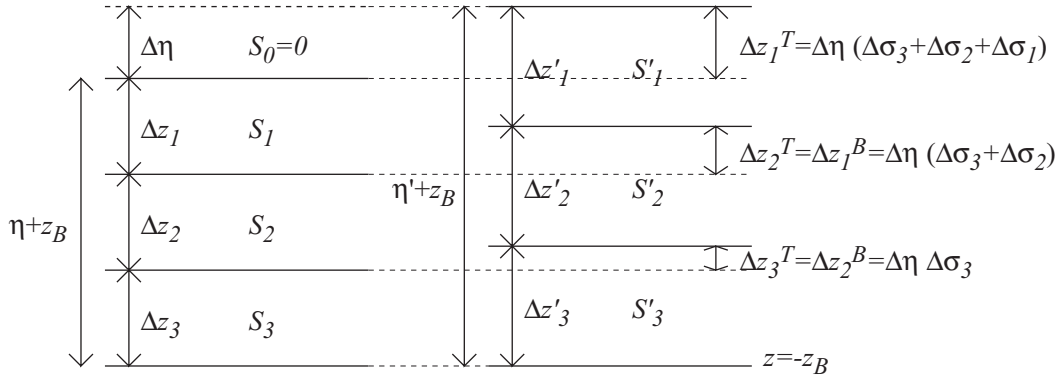
$$\frac{S^{n+1} - S^{n-1}}{2\Delta t} \frac{\eta^{n+1} - z_B}{-z_B} + \frac{\eta^{n+1} - \eta^{n-1}}{2\Delta t} \frac{S^{n-1}}{-z_B} = \frac{1}{h_x h_y} \left[ \frac{\partial F_x^S}{\partial x} + \frac{\partial F_y^S}{\partial y} \right] + \frac{\eta^{n-1} - z_B}{-z_B} \frac{\partial F_\sigma^S}{\partial \sigma} \quad (3.26)$$

is used, as its right hand side takes an almost identical form<sup>1</sup> to that of the time differenced salinity equation in the  $z$  coordinate (1.6):

$$\frac{S^{n+1} - S^{n-1}}{2\Delta t} = \frac{1}{h_x h_y} \left[ \frac{\partial F_x^S}{\partial x} + \frac{\partial F_y^S}{\partial y} \right] + \frac{\partial F_z^S}{\partial z}, \quad (3.27)$$

which makes it possible to merge the vertical direction loops for the  $\sigma$  and  $z$  coordinates in programming.

<sup>1</sup>It actually becomes identical when  $-z_B \Delta \sigma$  and  $(\eta^{n-1} - z_B) \omega$  are regarded as  $\Delta z$  and  $w$ , respectively.


 Figure 3.4: Redistribution of tracer for  $\sigma$  levels due to freshwater addition.

After solving advective/diffusive changes of tracers, the effect of heat and freshwater fluxes at the sea surface is taken into account. Since the height of water column contained in the  $\sigma$  coordinate region changes with the freshwater flux, tracers at each  $\sigma$  level should be re-estimated. Let  $K$  be the number of total  $\sigma$  levels, and let the first level represent the top (surface). When surface freshwater flux  $F_W$  (positive upward, i.e., sea level is lowered when  $F_W > 0$ ) is imposed, the sea level becomes

$$\eta^{n+1} = \eta^{n+1} + \Delta\eta \quad (3.28)$$

after taking the effect of  $F_W$  into account, where

$$\Delta\eta = -2\Delta t F_W. \quad (3.29)$$

When  $\Delta\eta > 0$ , the bottom of the  $k$ -th  $\sigma$  level in the  $z$  coordinate is raised by

$$\Delta z_k^B = \left(1 - \sum_{l=1}^k \Delta\sigma_l\right) \Delta\eta, \quad (3.30)$$

where  $\Delta\sigma_l$  is the vertical grid interval for the  $l$ -th level, and its top is raised by

$$\Delta z_k^T = \left(1 - \sum_{l=1}^{k-1} \Delta\sigma_l\right) \Delta\eta, \quad (3.31)$$

where

$$\Delta z_k^T = \Delta z_{k-1}^B \quad (3.32)$$

holds. Therefore, salinity of the  $k$ -th  $\sigma$  level becomes

$$S_k^{n+1} = \frac{S_k^{n+1}(\eta^{n+1} - z_B) - S_k^{n+1} \Delta z_k^B + S_{k-1}^{n+1} \Delta z_k^T}{\eta^{n+1} - z_B}, \quad (3.33)$$

where  $\Delta\eta \ll -z_B \Delta\sigma_k$  is assumed, which means that there is no need to take account of contribution from  $S_{k-2}^{n+1}$  in this expression. For its application to the top level ( $k = 1$ ),  $S_0$ , which represents salinity of the incoming freshwater, is taken to be zero<sup>2</sup>. See Figure 3.4 for its illustration. When  $\Delta\eta < 0$ , on the other

<sup>2</sup>Separate consideration is required when addition or subtraction of saline water is dealt with, as in the case of sea ice formation or melting. See appendix B for it.

hand, the bottom of the  $k$ -th  $\sigma$  level is lowered by  $|\Delta z_k^B|$ , and its top is lowered by  $|\Delta z_k^T|$ . In this case, tracer of the  $K$ -th level is not affected. For  $1 \leq k \leq K-1$ ,

$$S_k^{n+1} = \frac{S_k^{n+1}(\eta^{n+1} - z_B) - S_{k+1}^{n+1}\Delta z_k^B + S_k^{n+1}\Delta z_k^T}{\eta^{n+1} - z_B}. \quad (3.34)$$

When (3.33) is applied to the temperature equation,  $T_0$  is regarded as temperature of precipitating water. To be more precise, the effects of freshwater input due to precipitation and freshwater extraction due to evaporation should separately be treated, where (3.33) is applied to the former and (3.34) is applied to the latter. The effect of heat flux  $F_H$  (positive upward, i.e., sea surface is cooled when  $F_H > 0$ ) is represented by subtracting  $2\Delta t F_H / \rho_0 C_p$  from the numerator of (3.33) or (3.34) for  $k = 1$ .

### 3.2.4 Implicit Treatment for Vertical Diffusion

Consider the case that vertical diffusion is represented by the form of the last term of (1.33) and it is implicitly (backward-in-time) integrated. This is the standard choice of COCO version 4.0.

Let us now express (3.26) by

$$\frac{S_k^{n+1} - S_k^{n-1}}{2\Delta t} \frac{\eta^{n+1} - z_B}{-z_B} + \frac{\eta^{n+1} - \eta^{n-1}}{2\Delta t} \frac{S_k^{n-1}}{-z_B} = \mathcal{F}_k^{n-1} \quad (3.35)$$

when whole of the diffusion term is time differenced by the explicit (forward-in-time) method, which means that  $S^{n-1}$  is used in  $\mathcal{D}_S$ . The subscript  $k$  indicates vertical level, and this expression is applied to  $1 \leq k \leq K$ . For the levels  $k \geq K+1$ , (3.27) is written as

$$\frac{S_k^{n+1} - S_k^{n-1}}{2\Delta t} = \mathcal{F}_k^{n-1}. \quad (3.36)$$

When the vertical diffusion term is implicitly solved, the corresponding equation for  $1 \leq k \leq K$  becomes

$$\begin{aligned} & \frac{S_k^{n+1} - S_k^{n-1}}{2\Delta t} \frac{\eta^{n+1} - z_B}{-z_B} + \frac{\eta^{n+1} - \eta^{n-1}}{2\Delta t} \frac{S_k^{n-1}}{-z_B} \\ &= \mathcal{F}_k^{n-1} + \frac{1}{-z_B \Delta \sigma_k} \left( K_{V_k} \frac{S_{k-1}^{n+1} - S_k^{n+1}}{(\eta^{n-1} - z_B) \Delta \sigma'_k} - K_{V_{k+1}} \frac{S_k^{n+1} - S_{k+1}^{n+1}}{(\eta^{n-1} - z_B) \Delta \sigma'_{k+1}} \right) \\ & \quad - \frac{1}{-z_B \Delta \sigma_k} \left( K_{V_k} \frac{S_{k-1}^{n-1} - S_k^{n-1}}{(\eta^{n-1} - z_B) \Delta \sigma'_k} - K_{V_{k+1}} \frac{S_k^{n-1} - S_{k+1}^{n-1}}{(\eta^{n-1} - z_B) \Delta \sigma'_{k+1}} \right) \end{aligned} \quad (3.37)$$

and that for  $k \geq K+1$  becomes

$$\begin{aligned} \frac{S_k^{n+1} - S_k^{n-1}}{2\Delta t} = \mathcal{F}_k^{n-1} & + \frac{1}{\Delta z_k} \left( K_{V_k} \frac{S_{k-1}^{n+1} - S_k^{n+1}}{\Delta z'_k} - K_{V_{k+1}} \frac{S_k^{n+1} - S_{k+1}^{n+1}}{\Delta z'_{k+1}} \right) \\ & - \frac{1}{\Delta z_k} \left( K_{V_k} \frac{S_{k-1}^{n-1} - S_k^{n-1}}{\Delta z'_k} - K_{V_{k+1}} \frac{S_k^{n-1} - S_{k+1}^{n-1}}{\Delta z'_{k+1}} \right). \end{aligned} \quad (3.38)$$

Note that  $S_{k-1} - S_k$  is regarded as zero for  $k = 1$ , and  $S_k - S_{k+1}$  is regarded as zero when the level  $k+1$  is below the ocean floor (no-flux condition). Note also that  $(\eta^{n-1} - z_B) \Delta \sigma'_{K+1}$  is taken to be  $\Delta z'_{K+1}$ . See the later description for the definition of  $\Delta \sigma'$  and  $\Delta z'$ . By defining

$$\Delta S_k = S_k^{n+1} - S_k^{n-1}, \quad (3.39)$$

$$\eta_t = \frac{\eta^{n+1} - \eta^{n-1}}{2\Delta t}, \quad (3.40)$$

$$\Delta z_k = (-z_B) \Delta \sigma_k \quad \text{for } 1 \leq k \leq K, \quad (3.41)$$

$$\Delta z'_k = (\eta^{n-1} - z_B) \Delta \sigma'_k \quad \text{for } 1 \leq k \leq K, \quad (3.42)$$

the previous expressions are rewritten as

$$\frac{\Delta S_k}{2\Delta t} \frac{\eta^{n+1} - z_B}{-z_B} + \eta_t \frac{S_k^{n-1}}{-z_B} = \mathcal{F}_k^{n-1} + \frac{1}{\Delta z_k} \left( K_{V_k} \frac{\Delta S_{k-1} - \Delta S_k}{\Delta z'_k} - K_{V_{k+1}} \frac{\Delta S_k - \Delta S_{k+1}}{\Delta z'_{k+1}} \right) \quad (3.43)$$

for  $1 \leq k \leq K$  and

$$\frac{\Delta S_k}{2\Delta t} = \mathcal{F}_k^{n-1} + \frac{1}{\Delta z_k} \left( K_{V_k} \frac{\Delta S_{k-1} - \Delta S_k}{\Delta z'_k} - K_{V_{k+1}} \frac{\Delta S_k - \Delta S_{k+1}}{\Delta z'_{k+1}} \right) \quad (3.44)$$

for  $k \geq K+1$ . These are further rewritten as

$$-\alpha_k \Delta S_{k-1} + \beta_k \Delta S_k - \gamma_k \Delta S_{k+1} = F_k^{n-1} - \eta_t \frac{S_k^{n-1}}{-z_B} \quad (1 \leq k \leq K), \quad (3.45)$$

$$-\alpha_k \Delta S_{k-1} + \beta_k \Delta S_k - \gamma_k \Delta S_{k+1} = F_k^{n-1} \quad (k \geq K+1), \quad (3.46)$$

where

$$\alpha_k = \frac{K_{V_k}}{\Delta z_k \Delta z'_k}, \quad (3.47)$$

$$\gamma_k = \frac{K_{V_{k+1}}}{\Delta z_k \Delta z'_{k+1}}, \quad (3.48)$$

$$\beta_k = \frac{\eta^{n+1} - z_B}{2\Delta t(-z_B)} + \alpha_k + \gamma_k \quad \text{for } 1 \leq k \leq K, \quad (3.49)$$

$$= \frac{1}{2\Delta t} + \alpha_k + \gamma_k \quad \text{for } k \geq K+1. \quad (3.50)$$

Therefore,  $\Delta S_k$  is obtained by solving the linear equations expressed by a tridiagonal matrix:

$$\begin{pmatrix} \beta_1 & -\gamma_1 & 0 & \cdots & & & & & \\ -\alpha_2 & \beta_2 & -\gamma_2 & 0 & \cdots & & & & \\ \vdots & \ddots & \ddots & \ddots & & & & & \\ \vdots & 0 & -\alpha_K & \beta_K & -\gamma_K & 0 & \cdots & & \\ \vdots & 0 & 0 & -\alpha_{K+1} & \beta_{K+1} & -\gamma_{K+1} & 0 & \cdots & \\ \vdots & \vdots & \vdots & \vdots & \ddots & \ddots & \ddots & & \end{pmatrix} \begin{pmatrix} \Delta S_1 \\ \Delta S_2 \\ \vdots \\ \Delta S_K \\ \Delta S_{K+1} \\ \vdots \end{pmatrix} = \begin{pmatrix} \mathcal{F}_1^{n-1} - \frac{\eta_t S_1^{n-1}}{-z_B} \\ \mathcal{F}_2^{n-1} - \frac{\eta_t S_2^{n-1}}{-z_B} \\ \vdots \\ \mathcal{F}_K^{n-1} - \frac{\eta_t S_K^{n-1}}{-z_B} \\ \mathcal{F}_{K+1}^{n-1} \\ \vdots \end{pmatrix}. \quad (3.51)$$

### 3.2.5 Accelerating Model's Approach Toward a Steady State

When the surface boundary conditions are fixed in time, it is expected that the state realized in the model approaches to a steady state after long enough time integration. The asymptotic time evolution toward a steady state is accelerated by introducing ‘‘acceleration parameters’’  $\alpha_c$  and  $\gamma_c$  into the momentum and the tracer equations [Bryan, 1984], where the time derivative terms of the momentum equations (1.1)/(1.18) and (1.2)/(1.19) are multiplied by the factor  $\alpha_c$ , while the time derivative terms of the tracer equations (1.5)/(1.22) and (1.6)/(1.23) are multiplied by the factor  $\gamma_c$ . As obvious from these equations, a steady solution, where  $\partial/\partial t = 0$ , is not influenced by the choice of these parameters.

The  $\alpha_c$  larger than unity slows down the propagation speed of waves in the ocean, making it possible to use a larger value for  $\Delta t$ ; while the  $\gamma_c$  smaller than unity lessens the volume of the ocean, making the approach toward a steady state faster. The parameters may vary in space. Especially, it is sometimes useful to take smaller values for  $\gamma_c$  in the deeper levels, where thickness of the levels tends to be taken large.

It is very easy to implement this acceleration technique into the model: just divide  $\Delta t$  by  $\alpha_c$  for the momentum equations (for both internal and external modes), and by  $\gamma_c$  for the tracer equations. If vertically variable  $\gamma_c$  is introduced, however, care must be taken when convective adjustment is used. Since the parameter affects effective volume of grid boxes, conservation of heat and salt is violated unless its contribution is taken into account.

It is also technically possible to set different values for  $\alpha_c$  between the external mode momentum equations and the internal mode equations (a much larger value for the former). This treatment effectively reduces the speed of fast external waves, so helps reduce the computational cost in solving the external mode equations. This treatment is justified under the condition (assumption) that external waves do not play a significant role in forming a long-term (much longer than the time scale of external wave propagation) mean state of the ocean.

### 3.3 Spatial Differencing

#### 3.3.1 Grid Spacing and Metrics

Since grid intervals in the  $y$  and vertical directions are variable, they are expressed by adding subscripts denoting their position, such as  $\Delta y_L$ ,  $\Delta z_L$  and  $\Delta\sigma_L$ .  $\Delta y_L$  is the  $y$  direction width of the grid box with the T-point labeled by  $L$  at its center, and  $\Delta z_L$  ( $\Delta\sigma_L$ ) is the  $z$  direction ( $\sigma$  direction) thickness of the grid box with the T-point labeled by  $L$  at its center. Since  $\Delta z$  can vary also in horizontal (when the partial step bottom representation is applied), vertical grid spacing at V-points is defined separately from that at T-points. The vertical grid spacing of the grid box with the V-point labeled by  $L$  at its center is defined by the minimum of  $\Delta z$  of the four surrounding T-points:

$$\Delta z_L^V = \min(\Delta z_L, \Delta z_E, \Delta z_N, \Delta z_{NE}). \quad (3.52)$$

There also is a need to introduce grid spacing defined by

$$\Delta y'_L = \frac{\Delta y_L + \Delta y_N}{2}, \quad (3.53)$$

$$\Delta z'_L = \frac{\Delta z_L + \Delta z_U}{2}, \quad (3.54)$$

$$\Delta\sigma'_L = \frac{\Delta\sigma_L + \Delta\sigma_U}{2}. \quad (3.55)$$

$\Delta y'_L$  is the  $y$  direction distance between the T-points labeled by  $L$  and  $N$ , and  $\Delta z'_L$  ( $\Delta\sigma'_L$ ) is the vertical distance between the T-points labeled by  $L$  and  $U$ . From another point of view,  $\Delta y'_L$  is the  $y$  direction width of the grid box containing the V-point labeled by  $L$ , while  $\Delta z'_L$  ( $\Delta\sigma'_L$ ) is the vertical thickness of the grid box containing the WT-point labeled by  $L$ . Position (coordinate value) itself is also indicated by subscript and superscript. The  $y$  coordinate of the T-point (V-point) labeled by  $L$  is indicated by  $y_L$  ( $y_L^V$ ), and the  $z$  coordinate of the T- or V-point (WT- or WV-point) labeled by  $L$  is indicated by  $z_L$  ( $z_L^V$ ). Labeling of the  $\sigma$  coordinate is the same as that of the  $z$  coordinate. The definition of these grid variables are illustrated in Figure 3.5.

The metrics  $h_x$  and  $h_y$  are also horizontally variable, so their position is denoted by their subscript. There also is a need to distinguish T-point and V-point values, and it is denoted by superscript, as in the case of grid interval. In the following description, values of the metrics are assumed to be defined only at grid points (T- and V-points).

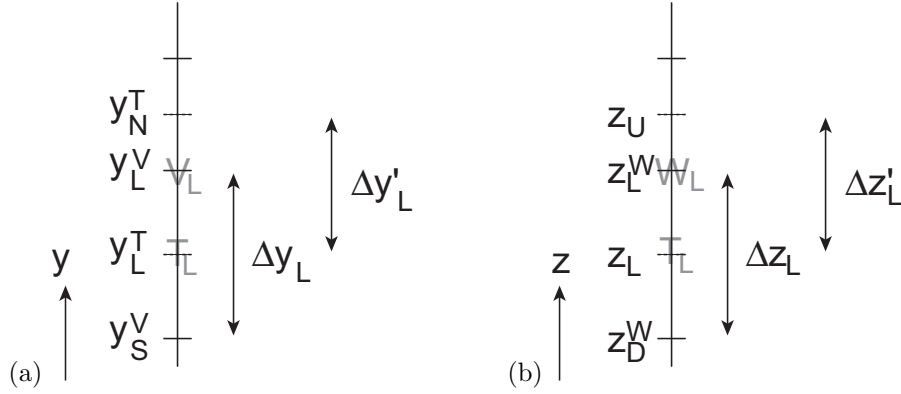


Figure 3.5: (a) Grid spacing in  $y$  direction. (b) Grid spacing in  $z$  direction.

### 3.3.2 Continuity Equation and T-Point Vertical Velocity

The continuity equation represents conservation of fluid volume, so its discretization should be based on the method of finite volume. For this purpose, the continuity equation is volume-integrated over a grid box.

Vertical integration of (1.4) from  $z = z_1$  to  $z = z_2$  yields

$$\begin{aligned} \frac{\partial}{\partial x} \int_{z_1}^{z_2} h_y u dz + \frac{\partial}{\partial y} \int_{z_1}^{z_2} h_x v dz + h_x h_y (w|_{z=z_2} - w|_{z=z_1}) \\ - \left[ \frac{\partial z_2}{\partial x} h_y u|_{z=z_2} + \frac{\partial z_2}{\partial y} h_x v|_{z=z_2} \right] + \left[ \frac{\partial z_1}{\partial x} h_y u|_{z=z_1} + \frac{\partial z_1}{\partial y} h_x v|_{z=z_1} \right] = 0, \end{aligned} \quad (3.56)$$

where  $z_2$  is the depth of grid top, thus it is independent of  $x$  and  $y$  ( $\partial z_2/\partial x = \partial z_2/\partial y = 0$ ). On the other hand,  $z_1$  is taken to be the depth of the ocean floor if the considered vertical interval hits the ocean floor. Otherwise,  $z_1$  is the depth of grid bottom, and  $\partial z_1/\partial x = \partial z_1/\partial y = 0$ . Since a depth of the ocean floor does not necessarily coincide with vertical grid boundaries,  $z_1$  is a function of  $x$  and  $y$  in the former case. In this case, the condition (1.52) applies with  $z_1 = -H$ , so

$$\left[ \frac{\partial z_1}{\partial x} h_y u|_{z=z_1} + \frac{\partial z_1}{\partial y} h_x v|_{z=z_1} \right] - h_x h_y w|_{z=z_1} = 0. \quad (3.57)$$

Therefore, the vertically integrated continuity equation is represented by

$$\frac{\partial}{\partial x} \int_{z_1}^{z_2} h_y u dz + \frac{\partial}{\partial y} \int_{z_1}^{z_2} h_x v dz + h_x h_y (w|_{z=z_2} - w|_{z=z_1}) = 0, \quad (3.58)$$

with a condition that  $w|_{z=z_1}$  is taken to be zero when  $z_1$  represents a depth of the ocean floor.

Horizontal integration of (3.58) over a grid box, whose area is defined by  $x_1 \leq x \leq x_2$  and  $y_1 \leq y \leq y_2$ , is represented by

$$\int_{x_1}^{x_2} \frac{\partial F_x^V}{\partial x} dx + \int_{y_1}^{y_2} \frac{\partial F_y^V}{\partial y} dy + \int_{z_1}^{z_2} \frac{\partial F_z^V}{\partial z} dz = 0, \quad (3.59)$$

where  $F^V$  is fluid volume flux defined by

$$F_x^V = \int_{y_1}^{y_2} dy \int_{z_1}^{z_2} dz h_y u, \quad (3.60)$$

$$F_y^V = \int_{x_1}^{x_2} dx \int_{z_1}^{z_2} dz h_x v, \quad (3.61)$$

$$F_z^V = \int_{x_1}^{x_2} dx \int_{y_1}^{y_2} dy h_x h_y w. \quad (3.62)$$

Note that the limits of integration for  $x$  and  $y$  are all constant values.

The discretized representation of the  $z$  coordinate continuity equation is obtained from (3.59) as

$$(F_{xE}^V - F_{xL}^V) + (F_{yN}^V - F_{yL}^V) + (F_{zL}^V - F_{zD}^V) = 0, \quad (3.63)$$

where the discretized form of fluid volume flux is obtained from (3.60)–(3.62) with applying  $u^t$  and  $v^t$  defined in (3.19) and (3.20):

$$F_{xL}^V = \frac{\Delta y_L}{2} (h_{yW}^V u_W^t \Delta z_W^V + h_{ySW}^V u_{SW}^t \Delta z_{SW}^V), \quad (3.64)$$

$$F_{yL}^V = \frac{\Delta x}{2} (h_{xS}^V v_S^t \Delta z_S^V + h_{xSW}^V v_{SW}^t \Delta z_{SW}^V), \quad (3.65)$$

$$F_{zL}^V = h_{xL}^T h_{yL}^T w_L^t \Delta x \Delta y_L, \quad (3.66)$$

where  $w^t$  is T-point vertical velocity used for tracer advection, and is obtained by solving (3.63).

The above consideration implicitly defines volume of a T-point-centered grid box. The volume  $\Delta V_L^T$  of the grid box containing  $T_L$  is given by

$$\Delta V_L^T = \int_{x_1}^{x_2} dx \int_{y_1}^{y_2} dy \int_{z_1}^{z_2} dz h_x h_y = h_{xL}^T h_{yL}^T \Delta x \Delta y_L \Delta z_L. \quad (3.67)$$

Then, for instance, volume integral of a T-point variable  $S$  is (must be) calculated by

$$\sum_L S_L \Delta V_L^T. \quad (3.68)$$

The discretized representation of the  $\sigma$  coordinate continuity equation (3.23) is almost identical to the above. The only fundamental difference is the  $\partial\eta/\partial t$  term, and the way to include it is obvious. By regarding  $-z_B \Delta\sigma$  as  $\Delta z$  and  $(\eta - z_B)\omega$  as  $w$ , expressions for the other terms becomes actually identical to the  $z$  coordinate case.

### 3.3.3 Tracer Equations

Only the prognostic equation for salinity is described here, again. Discretization of the tracer equations are formulated in a consistent way with that of the continuity equation. Otherwise, conservation of tracer is not guaranteed. Volume integral of the  $z$  coordinate salinity equation over a grid box is achieved by a procedure similar to the case of the continuity equation, and it results in

$$\frac{\partial S_L}{\partial t} \Delta V_L^T = \int_{x_1}^{x_2} \frac{\partial F_x^S}{\partial x} dx + \int_{y_1}^{y_2} \frac{\partial F_y^S}{\partial y} dy + \int_{z_1}^{z_2} \frac{\partial F_z^S}{\partial z} dz. \quad (3.69)$$

Note that the current definition of  $F^S$  is different from that in (3.27), and that the sign is reversed compared with usual definition of fluxes. The salinity flux  $F^S$  is decomposed into an advection part  $F^{Sa}$  and a diffusion part  $F^{Sd}$ , and the advection part is expressed by

$$F_x^{Sa} = - \int_{y_1}^{y_2} dy \int_{z_1}^{z_2} dz h_y u S, \quad (3.70)$$

$$F_y^{Sa} = - \int_{x_1}^{x_2} dx \int_{z_1}^{z_2} dz h_x v S, \quad (3.71)$$

$$F_z^{Sa} = - \int_{x_1}^{x_2} dx \int_{y_1}^{y_2} dy h_x h_y w S. \quad (3.72)$$

Expression for the diffusion part depends on its formulation. When it takes the form of the simplest Laplacian diffusion (1.33),

$$F_x^{Sd} = \int_{y_1}^{y_2} dy \int_{z_1}^{z_2} dz K_H \frac{h_y}{h_x} \frac{\partial S}{\partial x}, \quad (3.73)$$

$$F_y^{Sd} = \int_{x_1}^{x_2} dx \int_{z_1}^{z_2} dz K_H \frac{h_x}{h_y} \frac{\partial S}{\partial y}, \quad (3.74)$$

$$F_z^{Sd} = \int_{x_1}^{x_2} dx \int_{y_1}^{y_2} dy h_x h_y K_V \frac{\partial S}{\partial z}. \quad (3.75)$$

The discretized advective flux is represented by the product of the volume flux and the value of tracer at the point where the flux is defined (on the corresponding face of the considered grid box). Using (3.64)–(3.66),

$$F_{xL}^{Sa} = -F_{xL}^V S_w, \quad F_{yL}^{Sa} = -F_{yL}^V S_s, \quad F_{zL}^{Sa} = -F_{zL}^V S_u, \quad (3.76)$$

where the subscripts  $w$ ,  $s$  and  $u$  denote the positions where the value of  $S$  is estimated: western, southern and upper face, respectively, of the grid box containing  $S_L$ . These values of  $S$  at grid faces must, of course, be represented by grid point values of  $S$ . The simplest and lowest-order way of representing these grid-face values is the upstream differencing method, which means

$$F_{xL}^V S_w = \frac{F_{xL}^V + |F_{xL}^V|}{2} S_W + \frac{F_{xL}^V - |F_{xL}^V|}{2} S_L, \quad (3.77)$$

$$F_{yL}^V S_s = \frac{F_{yL}^V + |F_{yL}^V|}{2} S_S + \frac{F_{yL}^V - |F_{yL}^V|}{2} S_L, \quad (3.78)$$

$$F_{zL}^V S_u = \frac{F_{zL}^V + |F_{zL}^V|}{2} S_L + \frac{F_{zL}^V - |F_{zL}^V|}{2} S_U, \quad (3.79)$$

In usual application of COCO, a higher-order representation is adopted, which will be described in chapter 4.

Let  $\Delta A_w^T$ ,  $\Delta A_s^T$  and  $\Delta A_u^T$  denote the effective area of the western, southern and upper, respectively, faces of the grid box containing  $S_L$ . The components of fluxes of T-point variables labeled by  $L$  are defined on these faces. The term “effective” means that the area below the ocean floor is excluded, so they are defined by

$$\Delta A_w^T = \frac{h_{yW}^V + h_{ySW}^V}{2} \Delta y_L \times \min(\Delta z_L, \Delta z_W), \quad (3.80)$$

$$\Delta A_s^T = \frac{h_{xS}^V + h_{ySW}^V}{2} \Delta x \times \min(\Delta z_L, \Delta z_S), \quad (3.81)$$

$$\Delta A_u^T = h_{xL}^T h_{yL}^T \Delta x \Delta y_L. \quad (3.82)$$

The discretized diffusive flux for the case of the Laplacian diffusion is represented by the product of the grid-face area and the tracer gradient estimated on the face. By adopting the simplest, still second-order precision, way of representing the tracer gradient, the diffusive flux is expressed as

$$F_x^{Sd} = \Delta A_w^T K_H \frac{2}{h_{xL}^T + h_{xW}^T} \frac{S_L - S_W}{\Delta x}, \quad (3.83)$$

$$F_y^{Sd} = \Delta A_s^T K_H \frac{2}{h_{yL}^T + h_{yS}^T} \frac{S_L - S_S}{\Delta y'_S}, \quad (3.84)$$

$$F_z^{Sd} = \Delta A_u^T K_V \frac{S_U - S_L}{\Delta z'_L}. \quad (3.85)$$

Note that the diffusion coefficients are allowed to spatially vary. In this case, their values are defined at the same points as the tracer flux.

The final expression for the spatially discretized tracer equation is

$$\frac{\partial S_L}{\partial t} = \frac{(F_{xE}^S - F_{xL}^S) + (F_{yN}^S - F_{yL}^S) + (F_{zL}^S - F_{zD}^S)}{\Delta V_L^T}. \quad (3.86)$$

As in the case of the continuity equation, the spatial discretization of the tracer equations in the  $\sigma$  coordinate (3.26) is identical to that in the  $z$  coordinate when  $-z_B \Delta \sigma$  is regarded as  $\Delta z$  and  $(\eta - z_B)\omega$  as  $w$ .

### 3.3.4 Internal Mode Equations

In the discretized representation of the tracer equations, the tracer quantities are advected by ‘‘tracer advection velocity,’’ whose components are represented by  $u^t$ ,  $v^t$  and  $w^t$  ( $\omega^t$ ). Since the tracer advection velocity is defined such that it is perfectly consistent with the continuity equation, its application to the tracer equations guarantees conservation of the tracer quantities under the advection process. The same concept is introduced to the discretized representation of the momentum equations. Its basic idea is suggested by *Webb [1995]*.

Consider a grid box which contains the V-point labeled by  $L$  at its center. Its vertices are the eight surrounding WT-points. ‘‘Momentum advection velocity,’’ whose components are represented by  $u^a$ ,  $v^a$  and  $w^a$ , is defined on each face of the grid box, where momentum flux is also defined. To retain consistency with the continuity equation, definition of the momentum advection velocity should be based on area weighted average of fluid volume transport for T-point-centered boxes. In addition, its horizontal components are multiplied by the grid thickness for the convenience of later use. Its exact representation in the  $z$  coordinate region is

$$u_L^a = \frac{(u_L^t h_{yL}^V \Delta z_L^V + u_W^t h_{yW}^V \Delta z_W^V + u_N^t h_{yN}^V \Delta z_N^V + u_{NW}^t h_{yNW}^V \Delta z_{NW}^V) \Delta y_N + (u_L^t h_{yL}^V \Delta z_L^V + u_W^t h_{yW}^V \Delta z_W^V + u_S^t h_{yS}^V \Delta z_S^V + u_{SW}^t h_{ySW}^V \Delta z_{SW}^V) \Delta y_L}{(h_{yL}^V + h_{yW}^V + h_{yN}^V + h_{yNW}^V) \Delta y_N + (h_{yL}^V + h_{yW}^V + h_{yS}^V + h_{ySW}^V) \Delta y_L}, \quad (3.87)$$

$$v_L^a = \frac{2v_L^t h_{xL}^V \Delta z_L^V + 2v_S^t h_{xS}^V \Delta z_S^V + v_E^t h_{xE}^V \Delta z_E^V + v_{SE}^t h_{xSE}^V \Delta z_{SE}^V + v_W^t h_{xW}^V \Delta z_W^V + v_{SW}^t h_{xSW}^V \Delta z_{SW}^V}{2h_{xL}^V + 2h_{xS}^V + h_{xE}^V + h_{xSE}^V + h_{xW}^V + h_{xSW}^V}, \quad (3.88)$$

$$w_L^a = \frac{(w_L^t h_{xL}^T h_{yL}^T + w_E^t h_{xE}^T h_{yE}^T) \Delta y_L + (w_N^t h_{xN}^T h_{yN}^T + w_{NE}^t h_{xNE}^T h_{yNE}^T) \Delta y_N}{(h_{xL}^T h_{yL}^T + h_{xE}^T h_{yE}^T) \Delta y_L + (h_{xN}^T h_{yN}^T + h_{xNE}^T h_{yNE}^T) \Delta y_N}. \quad (3.89)$$

In the actual application, they are approximated by

$$u_L^a = \frac{(u_L^t \Delta z_L^V + u_W^t \Delta z_W^V + u_N^t \Delta z_N^V + u_{NW}^t \Delta z_{NW}^V) \Delta y_N + (u_L^t \Delta z_L^V + u_W^t \Delta z_W^V + u_S^t \Delta z_S^V + u_{SW}^t \Delta z_{SW}^V) \Delta y_L}{8 \Delta y_L'}, \quad (3.90)$$

$$v_L^a = \frac{2v_L^t \Delta z_L^V + 2v_S^t \Delta z_S^V + v_E^t \Delta z_E^V + v_{SE}^t \Delta z_{SE}^V + v_W^t \Delta z_W^V + v_{SW}^t \Delta z_{SW}^V}{8}, \quad (3.91)$$

$$w_L^a = \frac{(w_L^t + w_E^t) \Delta y_L + (w_N^t + w_{NE}^t) \Delta y_N}{4 \Delta y_L'}, \quad (3.92)$$

assuming that difference of the metrics between adjacent grids is small.

Let us first consider only the flux convergence part of the momentum equation (1.1):

$$\frac{\partial u}{\partial t} = -\frac{1}{h_x h_y} \left[ \frac{\partial}{\partial x} (h_y u u) + \frac{\partial}{\partial y} (h_x v u) \right] - \frac{\partial}{\partial z} (w u). \quad (3.93)$$

Similarly to the case of the tracer equations, its volume integral yields

$$\frac{\partial u_L}{\partial t} \Delta V_L^V = \int_{x_1}^{x_2} \frac{\partial F_x^u}{\partial x} dx + \int_{y_1}^{y_2} \frac{\partial F_y^u}{\partial y} dy + \int_{z_1}^{z_2} \frac{\partial F_z^u}{\partial z} dz, \quad (3.94)$$

where

$$F_x^u = - \int_{y_1}^{y_2} dy \int_{z_1}^{z_2} dz h_y u u, \quad (3.95)$$

$$F_y^u = - \int_{x_1}^{x_2} dx \int_{z_1}^{z_2} dz h_x v u, \quad (3.96)$$

$$F_z^u = - \int_{x_1}^{x_2} dx \int_{y_1}^{y_2} dy h_x h_y w u, \quad (3.97)$$

$$\Delta V_L^V = h_{xL}^V h_{yL}^V \Delta x \Delta y_L^V \Delta z_L^V. \quad (3.98)$$

Note that the limits of integration are for the boundaries of the grid box centered at the V-point labeled by  $L$ . Grid point values of the flux  $F^u$  are represented by

$$F_{xL}^u = -\Delta y_L^V u_L^a (h_y u)_w, \quad (3.99)$$

$$F_{yL}^u = -\Delta x v_L^a (h_x u)_s, \quad (3.100)$$

$$F_{zL}^u = -h_{xL}^V h_{yL}^V \Delta x \Delta y_L^V w_L^a u_u, \quad (3.101)$$

where the subscripts  $w$ ,  $s$  and  $u$  denote the position of the western, southern and upper, respectively, faces of the considered grid box. These grid-face values are simply represented by the average of the two nearest grid point values on the both sides of the face:

$$(h_y u)_w = \frac{h_{yL}^V u_L + h_{yW}^V u_W}{2}, \quad (3.102)$$

$$(h_x u)_s = \frac{h_{xL}^V u_L + h_{xS}^V u_S}{2}, \quad (3.103)$$

$$u_u = \frac{u_L + u_U}{2}. \quad (3.104)$$

When the grid spacing is invariable, these expressions give the second-order precision (centered-in-space differencing scheme). Note that it is more relevant to couple the metrics with the momentum advection velocity rather than with the ‘‘advected’’ velocity, as in the case of the tracer advection velocity. In that case, the momentum advection velocity multiplied by the corresponding coordinate metric (i.e.,  $(h_y u)_L^a$ ,  $(h_x v)_L^a$  and  $(h_x h_y w)_L^a$ ) should be defined by (3.87)–(3.89) with replacing metrics in the denominators by unity. In the current expression, coding simplicity (and reduction of calculation) is preferred at the cost of relevance (and exactness). The final discretized representation of (3.93) is

$$\frac{\partial u_L}{\partial t} = \frac{(F_{xE}^u - F_{xL}^u) + (F_{yN}^u - F_{yL}^u) + (F_{zL}^u - F_{zD}^u)}{\Delta V_L^V}. \quad (3.105)$$

An identical procedure is applicable to spatially discretizing (1.2). The discretized representation of

$$\frac{\partial v}{\partial t} = -\frac{1}{h_x h_y} \left[ \frac{\partial}{\partial x} (h_y v) + \frac{\partial}{\partial y} (h_x v) \right] - \frac{\partial}{\partial z} (wv) \quad (3.106)$$

becomes

$$\frac{\partial v_L}{\partial t} = \frac{(F_{xE}^v - F_{xL}^v) + (F_{yN}^v - F_{yL}^v) + (F_{zL}^v - F_{zD}^v)}{\Delta V_L^V}, \quad (3.107)$$

where

$$F_{xL}^v = -\Delta y'_L u_L^a (h_y v)_w, \quad (3.108)$$

$$F_{yL}^v = -\Delta x v_L^a (h_x v)_s, \quad (3.109)$$

$$F_{zL}^v = -h_{xL}^V h_{yL}^V \Delta x \Delta y'_L w_L^a v_u, \quad (3.110)$$

and

$$(h_y v)_w = \frac{h_{yL}^V v_L + h_{yW}^V v_W}{2}, \quad (3.111)$$

$$(h_x v)_s = \frac{h_{xL}^V v_L + h_{xS}^V v_S}{2}, \quad (3.112)$$

$$v_u = \frac{v_L + v_U}{2}. \quad (3.113)$$

Other terms of (1.1) and (1.2) are restored now. The metric and Coriolis terms are estimated simply by using  $u_L$  and  $v_L$ . Pressure is a T-point variable, and it is determined from sea level pressure  $P_\eta$ , sea level  $\eta$ , and density  $\rho$ , all of which are T-point variables. Horizontal gradient of a T-point variable  $\psi$  at the V-point labeled by  $L$  is estimated by using the four surrounding grid point values of  $\psi$  as

$$\left( \frac{1}{h_x} \frac{\partial \psi}{\partial x} \right)_L = \frac{\psi_{NE} + \psi_E - \psi_N - \psi_L}{2h_{xL}^V \Delta x}, \quad (3.114)$$

$$\left( \frac{1}{h_y} \frac{\partial \psi}{\partial y} \right)_L = \frac{\psi_{NE} + \psi_N - \psi_E - \psi_L}{2h_{yL}^V \Delta y'_L}. \quad (3.115)$$

Vertical integration of horizontal density gradient needs to be calculated. For the  $\sigma$  coordinate region,

$$\begin{aligned} & \left[ (\eta - z_B) \int_\sigma^1 \frac{\partial \rho}{\partial x} d\sigma' \right]_L \\ &= \left[ \frac{(\eta_L + \eta_E) \Delta y_L + (\eta_N + \eta_{NE}) \Delta y_N}{4\Delta y'_L} - z_B \right]_L \times \left[ \sum_{l=U, UU, \dots} \left( \frac{\partial \rho}{\partial x} \right)_l \Delta \sigma_l + \frac{1}{2} \left( \frac{\partial \rho}{\partial x} \right)_L \Delta \sigma_L \right] \end{aligned} \quad (3.116)$$

where the sum for the index  $l$  is taken from the top to the considered level. For the  $z$  coordinate region,

$$\left( \int_z^{z_B} \frac{\partial \rho}{\partial x} dz' \right)_L = \sum_{l=U, UU, \dots} \left( \frac{\partial \rho}{\partial x} \right)_l \Delta z_l^V + \frac{1}{2} \left( \frac{\partial \rho}{\partial x} \right)_L \Delta z_L^V, \quad (3.117)$$

where the sum for the index  $l$  is taken from the top of the  $z$  coordinate region to the considered level. The corresponding  $y$  derivative terms are represented by simply replacing  $x$  by  $y$ .

In the Laplacian viscosity terms (1.34), (1.35), it is convenient to divide vertical components (i.e., whose subscripts include  $z$ ) of the tensors into two parts for the sake of discretization:

$$\tau_{xz} = \tau'_{xz} + \tau''_{xz}, \quad \tau_{yz} = \tau'_{yz} + \tau''_{yz}, \quad (3.118)$$

where

$$\tau'_{xz} = A_V \frac{\partial u}{\partial z}, \quad \tau''_{xz} = -\frac{\partial A_V}{\partial z} u - A_V \frac{u}{a}, \quad (3.119)$$

$$\tau'_{yz} = A_V \frac{\partial v}{\partial z}, \quad \tau''_{yz} = -\frac{\partial A_V}{\partial z} v - A_V \frac{v}{a}. \quad (3.120)$$

The last two terms of (1.34) and (1.35) are modified accordingly as

$$\mathcal{V}_u = \frac{1}{h_x h_y} \left[ \frac{1}{h_y} \frac{\partial}{\partial x} \left( h_y^2 \frac{\tau_{xx} - \tau_{yy}}{2} \right) + \frac{1}{h_x} \frac{\partial}{\partial y} (h_x^2 \tau_{xy}) \right] + \frac{\partial \tau'_{xz}}{\partial z} + \frac{\tau''_{xz}}{a}, \quad (3.121)$$

$$\mathcal{V}_v = \frac{1}{h_x h_y} \left[ \frac{1}{h_y} \frac{\partial}{\partial x} (h_y^2 \tau_{xy}) + \frac{1}{h_x} \frac{\partial}{\partial y} \left( h_x^2 \frac{\tau_{yy} - \tau_{xx}}{2} \right) \right] + \frac{\partial \tau'_{yz}}{\partial z} + \frac{\tau''_{yz}}{a}. \quad (3.122)$$

These viscosity terms are, of course, defined at V-points.

One of the most convenient ways of discretizing horizontal components of the stress tensor is to define them at T-points. Accordingly, it is natural to define horizontal components of strain rate tensor (see section 1.2.2 for its definition) also at T-points, where velocity at T-points is estimated simply by the average of the four surrounding V-point values, and the horizontal gradient is estimated by the simplest form using the same four-point values. The horizontal divergence term is calculated by the four surrounding T-point values of the horizontal stress tensor components. Although this method is simple and symmetric, it is prone to generate checker-board noise, especially for the case of spatially constant horizontal viscosity. Consider an idealized situation where  $h_x = h_y = \text{const}$  and  $\Delta x = \Delta y = \text{const}$ . For brevity of expression, the metrics are set to unity, and the grid width is set to  $1/4$ , though the choice for these constants does not affect the discussion below. In this case,

$$\varepsilon_{xxL} = u_L + u_S - u_W - u_{SW}, \quad (3.123)$$

$$\varepsilon_{xxE} = u_E + u_{SE} - u_L - u_S, \quad (3.124)$$

$$\varepsilon_{xxN} = u_N + u_L - u_{NW} - u_W, \quad (3.125)$$

$$\varepsilon_{xxNE} = u_{NE} + u_E - u_N - u_L, \quad (3.126)$$

$$\varepsilon_{yyL} = v_L + v_S - v_W - v_{SW}, \quad (3.127)$$

$$\varepsilon_{yyE} = v_E + v_{SE} - v_L - v_S, \quad (3.128)$$

$$\varepsilon_{yyN} = v_N + v_L - v_{NW} - v_W, \quad (3.129)$$

$$\varepsilon_{yyNE} = v_{NE} + v_E - v_N - v_L, \quad (3.130)$$

$$2\varepsilon_{xyL} = u_L + u_W - u_S - u_{SW} + v_L + v_S - v_W - v_{SW}, \quad (3.131)$$

$$2\varepsilon_{xyE} = u_E + u_L - u_{SE} - u_S + v_E + v_{SE} - v_L - v_S, \quad (3.132)$$

$$2\varepsilon_{xyN} = u_N + u_{NW} - u_L - u_W + v_N + v_L - v_{NW} - v_W, \quad (3.133)$$

$$2\varepsilon_{xyNE} = u_{NE} + u_N - u_E - u_L + v_{NE} + v_E - v_N - v_L. \quad (3.134)$$

When the horizontal viscosity coefficient  $A_H$  is also constant, the horizontal divergence term of  $\mathcal{V}_{uL}$  becomes

$$A_H(u_{NE} + u_{SE} + u_{NW} + u_{SW} - 4u_L). \quad (3.135)$$

Thus, there is no direct coupling between  $u_L$  and its four nearest grid point values. For the case of the Laplacian horizontal viscosity with a prescribed (i.e., does not depend on velocity) coefficient, therefore, the horizontal components of the strain rate tensor are defined by

$$\begin{aligned} (\varepsilon_{xx} - \varepsilon_{yy})_{uL} &= \frac{2}{h_{xL}^V + h_{xW}^V} \frac{u_L - u_W}{\Delta x} + \frac{h_{xyL}^V + h_{xyW}^V}{2} \frac{v_L + v_W}{2} \\ &\quad - \frac{2}{h_{yL}^V + h_{yW}^V} \frac{v_N + v_{NW} - v_S - v_{SW}}{2(\Delta y_L + \Delta y_N)} - \frac{h_{yxL}^V + h_{yxW}^V}{2} \frac{u_L + u_W}{2}, \end{aligned} \quad (3.136)$$

$$\begin{aligned} 2(\varepsilon_{xy})_{uL} &= \frac{2}{h_{yL}^V + h_{yS}^V} \frac{u_L - u_S}{\Delta y_L} - \frac{h_{yxL}^V + h_{yxS}^V}{2} \frac{v_L + v_S}{2} \\ &\quad + \frac{2}{h_{xL}^V + h_{xS}^V} \frac{v_E + v_{SE} - v_W - v_{SW}}{4\Delta x} - \frac{h_{xyL}^V + h_{xyS}^V}{2} \frac{u_L + u_S}{2}, \end{aligned} \quad (3.137)$$

$$(\varepsilon_{yy} - \varepsilon_{xx})_{vL} = \frac{2}{h_{yL}^V + h_{yS}^V} \frac{v_L - v_S}{\Delta y_L} + \frac{h_{yxL}^V + h_{yxS}^V}{2} \frac{u_L + u_S}{2}$$

$$-\frac{2}{h_{xL}^V + h_{xS}^V} \frac{u_E + u_{SE} - u_W - u_{SW}}{4\Delta x} - \frac{h_{xyL}^V + h_{xyS}^V}{2} \frac{v_L + v_S}{2}, \quad (3.138)$$

$$2(\varepsilon_{xy})_{vL} = \frac{2}{h_{xL}^V + h_{xW}^V} \frac{v_L - v_W}{\Delta x} - \frac{h_{yxL}^V + h_{yxW}^V}{2} \frac{v_L + v_W}{2} \quad (3.139)$$

$$+\frac{2}{h_{yL}^V + h_{yW}^V} \frac{u_N + u_{NW} - u_S - u_{SW}}{2(\Delta y_L + \Delta y_N)} - \frac{h_{xyL}^V + h_{xyW}^V}{2} \frac{u_L + u_W}{2}, \quad (3.140)$$

where  $(\varepsilon_{xx} - \varepsilon_{yy})_{uL}$  and  $(\varepsilon_{xy})_{uL}$  are defined at the same points as  $F_{xL}^u$  and  $F_{xL}^v$  and used in  $\mathcal{V}_{uL}$ , while  $(\varepsilon_{yy} - \varepsilon_{xx})_{vL}$  and  $(\varepsilon_{xy})_{vL}$  are defined at the same points as  $F_{yL}^u$  and  $F_{yL}^v$  and used in  $\mathcal{V}_{vL}$ . Horizontal components of the stress tensor are defined at the same points as the corresponding components of the strain rate tensor. Then, the horizontal part of the viscosity terms are represented by

$$\left\{ \frac{1}{h_x h_y} \left[ \frac{1}{h_y} \frac{\partial}{\partial x} \left( h_y^2 \frac{\tau_{xx} - \tau_{yy}}{2} \right) + \frac{1}{h_x} \frac{\partial}{\partial y} (h_x^2 \tau_{xy}) \right] \right\}_L$$

$$= \frac{1}{h_{xL}^V h_{yL}^V} \left\{ \frac{1}{h_{yL}^V \Delta x} \left[ \left( \frac{h_{yE}^V + h_{yL}^V}{2} \right)^2 \frac{(\tau_{xx} - \tau_{yy})_{uE}}{2} - \left( \frac{h_{yL}^V + h_{yW}^V}{2} \right)^2 \frac{(\tau_{xx} - \tau_{yy})_{uL}}{2} \right] \right.$$

$$\left. + \frac{1}{h_{xL}^V \Delta y'_L} \left[ \left( \frac{h_{xN}^V + h_{xL}^V}{2} \right)^2 (\tau_{xy})_{uN} - \left( \frac{h_{xL}^V + h_{xS}^V}{2} \right)^2 (\tau_{xy})_{uL} \right] \right\}, \quad (3.141)$$

$$\left\{ \frac{1}{h_x h_y} \left[ \frac{1}{h_y} \frac{\partial}{\partial x} (h_y^2 \tau_{xy}) + \frac{1}{h_x} \frac{\partial}{\partial y} \left( h_x^2 \frac{\tau_{yy} - \tau_{xx}}{2} \right) \right] \right\}_L$$

$$= \frac{1}{h_{xL}^V h_{yL}^V} \left\{ \frac{1}{h_{yL}^V \Delta x} \left[ \left( \frac{h_{yE}^V + h_{yL}^V}{2} \right)^2 (\tau_{xy})_{vE} - \left( \frac{h_{yL}^V + h_{yW}^V}{2} \right)^2 (\tau_{xy})_{vL} \right] \right.$$

$$\left. + \frac{1}{h_{xL}^V \Delta y'_L} \left[ \left( \frac{h_{xN}^V + h_{xL}^V}{2} \right)^2 \frac{(\tau_{yy} - \tau_{xx})_{vN}}{2} - \left( \frac{h_{xL}^V + h_{xS}^V}{2} \right)^2 \frac{(\tau_{yy} - \tau_{xx})_{vL}}{2} \right] \right\}, \quad (3.142)$$

where

$$(\tau_{xx} - \tau_{yy})_u = 2A_H(\varepsilon_{xx} - \varepsilon_{yy})_u, \quad (3.143)$$

$$(\tau_{xy})_u = 2A_H(\varepsilon_{xy})_u \quad (3.144)$$

$$(\tau_{yy} - \tau_{xx})_v = 2A_H(\varepsilon_{yy} - \varepsilon_{xx})_v, \quad (3.145)$$

$$(\tau_{xy})_v = 2A_H(\varepsilon_{xy})_v. \quad (3.146)$$

For the vertical components of the stress tensor, it is convenient to define  $\tau'_{xz}$   $\tau'_{yz}$  at WV-points, and  $\tau''_{xz}$  and  $\tau''_{yz}$  at V-points. Their definition is straightforward:

$$\tau'_{xzL} = (A_V)_L \frac{u_U - u_L}{\Delta z'_L}, \quad (3.147)$$

$$\tau'_{yzL} = (A_V)_L \frac{v_U - v_L}{\Delta z'_L}, \quad (3.148)$$

$$\tau''_{xzL} = -\frac{(A_V)_L - (A_V)_D}{\Delta z_L} u_L - \frac{(A_V)_L + (A_V)_D}{2} \frac{u_L}{a}, \quad (3.149)$$

$$\tau''_{yzL} = -\frac{(A_V)_L - (A_V)_D}{\Delta z_L} v_L - \frac{(A_V)_L + (A_V)_D}{2} \frac{v_L}{a}. \quad (3.150)$$

The vertical part of the viscosity terms are

$$\left( \frac{\partial \tau'_{xz}}{\partial z} + \frac{\tau''_{xz}}{a} \right)_L = \frac{\tau'_{xzL} - \tau'_{xzD}}{\Delta z_L} + \frac{\tau''_{xzL}}{a}, \quad (3.151)$$

$$\left( \frac{\partial \tau'_{yz}}{\partial z} + \frac{\tau''_{yz}}{a} \right)_L = \frac{\tau'_{yzL} - \tau'_{yzD}}{\Delta z_L} + \frac{\tau''_{yzL}}{a} \quad (3.152)$$

The advection terms of the  $\sigma$  coordinate momentum equations (1.18) and (1.19) are represented by the advection form. In their calculation, however, a pseudo-flux form<sup>3</sup> is used:

$$\frac{u}{h_x} \frac{\partial u}{\partial x} + \frac{v}{h_y} \frac{\partial u}{\partial y} + \omega \frac{\partial u}{\partial \sigma} = \frac{1}{h_x h_y} \left[ \frac{\partial}{\partial x} (h_y u u) + \frac{\partial}{\partial y} (h_x v u) \right] + \frac{\partial}{\partial \sigma} (\omega u) - u \operatorname{div} \mathbf{v}, \quad (3.153)$$

$$\frac{u}{h_x} \frac{\partial v}{\partial x} + \frac{v}{h_y} \frac{\partial v}{\partial y} + \omega \frac{\partial v}{\partial \sigma} = \frac{1}{h_x h_y} \left[ \frac{\partial}{\partial x} (h_y u v) + \frac{\partial}{\partial y} (h_x v v) \right] + \frac{\partial}{\partial \sigma} (\omega v) - v \operatorname{div} \mathbf{v}, \quad (3.154)$$

where  $\operatorname{div} \mathbf{v}$  is defined by

$$\operatorname{div} \mathbf{v} = \frac{1}{h_x h_y} \left[ \frac{\partial}{\partial x} (h_y u) + \frac{\partial}{\partial y} (h_x v) \right] + \frac{\partial \omega}{\partial \sigma}. \quad (3.155)$$

Excluding the term of  $\operatorname{div} \mathbf{v}$ , the right hand sides of (3.153) and (3.154) take the same form as the flux convergence terms of (3.93) and (3.106), respectively. So, they are discretized in the same way as the previous, by just replacing  $\Delta z$  by  $\Delta \sigma$  and  $w$  by  $\omega$ . Since  $\Delta \sigma$  does not horizontally vary, expressions for the horizontal components of the momentum advection velocity (3.90) and (3.91) are much simplified. The discretized representation of  $\operatorname{div} \mathbf{v}$  is given by

$$\frac{1}{h_{xL}^V h_{yL}^V} \left[ \frac{(h_{yE}^V + h_{yL}^V) u_E^a + (h_{yL}^V + h_{yW}^V) u_L^a}{2\Delta x} + \frac{(h_{xN}^V + h_{xL}^V) v_N^a + (h_{xL}^V + h_{xS}^V) u_L^a}{2\Delta y'_L} \right] + \frac{\omega_L^a - \omega_D^a}{\Delta \sigma_L}. \quad (3.156)$$

The other terms of the  $\sigma$  coordinate momentum equations are discretized in the same manner as in the  $z$  coordinate case.

Grid point values of horizontal velocity components are defined by

$$u_L^n = \frac{U_L^n}{H_L^V} + u_L'^n, \quad (3.157)$$

$$v_L^n = \frac{V_L^n}{H_L^V} + v_L'^n, \quad (3.158)$$

where (1.92) and (1.93) are used with setting  $\eta$  to zero.

### 3.3.5 External Mode Equations

Spatial discretization of the sea level equation (1.27) is achieved based on the same consideration as for the continuity equation. Its horizontal area integral over the grid box containing  $\eta_L$  is represented as

$$\frac{\partial \eta_L}{\partial t} \Delta x \Delta y_L h_{xL}^T h_{yL}^T = -(F_{xE}^\eta - F_{xL}^\eta) - (F_{yN}^\eta - F_{yL}^\eta), \quad (3.159)$$

where

$$F_{xL}^\eta = \frac{h_{yW}^V U_W + h_{ySW}^V U_{SW}}{2} \Delta y_L, \quad (3.160)$$

$$F_{yL}^\eta = \frac{h_{xS}^V V_W + h_{xSW}^V V_{SW}}{2} \Delta x \quad (3.161)$$

are equivalent to vertical integral of the fluid volume flux (3.64) and (3.65).

<sup>3</sup>The true flux form includes contribution of  $(\eta - z_B)$

The discretized representation for (1.80) and (1.81) is

$$\frac{\partial U_L}{\partial t} - f_L V_L = -\frac{H_L^V}{\rho_0 h_{xL}^V} \left[ g \left( \frac{\partial \eta}{\partial x} \right)_L + \left( \frac{\partial P_\eta}{\partial x} \right)_L \right] + X'_L + (\mathcal{V}_U)_L, \quad (3.162)$$

$$\frac{\partial V_L}{\partial t} + f_L U_L = -\frac{H_L^V}{\rho_0 h_{yL}^V} \left[ g \left( \frac{\partial \eta}{\partial y} \right)_L + \left( \frac{\partial P_\eta}{\partial y} \right)_L \right] + Y'_L + (\mathcal{V}_V)_L, \quad (3.163)$$

where  $f_L$  is the value of the Coriolis parameter at the V-point labeled by  $L$ . Explicit representation for the horizontal gradient terms is given by (3.114) and (3.115). The terms  $X'_L$  and  $Y'_L$  are obtained by vertically summing up the terms appearing in the internal mode equations. The viscosity term is represented by the same manner as for the internal mode equations.

The system of the discretized equations (3.159), (3.162) and (3.163) does not contain a mechanism eliminating checker-board noise in sea level. For the sake of numerical stability, therefore, the Laplacian horizontal diffusion term is added to the sea level equation. So, the equation actually solved is

$$\frac{\partial \eta}{\partial t} = -\frac{1}{h_x h_y} \left[ \frac{\partial}{\partial x} (h_y U) + \frac{\partial}{\partial y} (h_x V) \right] + \frac{1}{h_x h_y} \left[ \frac{\partial}{\partial x} \left( K_\eta \frac{h_y}{h_x} \frac{\partial \eta}{\partial x} \right) + \frac{\partial}{\partial y} \left( K_\eta \frac{h_x}{h_y} \frac{\partial \eta}{\partial y} \right) \right], \quad (3.164)$$

where  $K_\eta$  is the coefficient for sea level diffusion. The diffusion term is temporally discretized by the forward-in-time method, and the method of its spatial discretization is the same as that of the tracer diffusion term. Let  $F^{\eta d}$  denote diffusive flux of sea level. The equation (3.159) now becomes

$$\frac{\partial \eta_L}{\partial t} \Delta x \Delta y_L h_{xL}^T h_{yL}^T = -(F_{xE}^\eta - F_{xL}^\eta) - (F_{yN}^\eta - F_{yL}^\eta) + (F_{xE}^{\eta d} - F_{xL}^{\eta d}) + (F_{yN}^{\eta d} - F_{yL}^{\eta d}), \quad (3.165)$$

where

$$F_{xL}^{\eta d} = K_\eta \frac{h_{yW}^V + h_{ySW}^V}{h_{xL}^T + h_{xW}^T} \frac{\eta_L - \eta_W}{\Delta x} \Delta y_L, \quad (3.166)$$

$$F_{yL}^{\eta d} = K_\eta \frac{h_{xS}^V + h_{xSW}^V}{h_{yL}^T + h_{yS}^T} \frac{\eta_L - \eta_S}{\Delta y'_S} \Delta x. \quad (3.167)$$

Changes of sea level must accompany redistribution of the tracer quantities in the  $\sigma$  coordinate region. Correction for the tracer  $S$  is represented by

$$\frac{\partial}{\partial t} [(\eta_L - z_B) S_L] h_{xL}^T h_{yL}^T \Delta x \Delta y_L = (F_{xE}^{Sc} - F_{xL}^{Sc}) + (F_{yN}^{Sc} - F_{yL}^{Sc}), \quad (3.168)$$

where the correction flux  $F^{Sc}$  is assumed to transport the tracer in the down-gradient direction of sea level:

$$F_{xL}^{Sc} = \frac{F_{xL}^{\eta d} + |F_{xL}^{\eta d}|}{2} S_L + \frac{F_{xL}^{\eta d} - |F_{xL}^{\eta d}|}{2} S_W, \quad (3.169)$$

$$F_{yL}^{Sc} = \frac{F_{yL}^{\eta d} + |F_{yL}^{\eta d}|}{2} S_L + \frac{F_{yL}^{\eta d} - |F_{yL}^{\eta d}|}{2} S_S. \quad (3.170)$$

## 3.4 Treatment of Boundary

### 3.4.1 Cyclic Boundary Condition

The model domain is assumed to cyclically connected in the  $x$  direction. It is realized in the model by putting extra grids to the east (west) of the eastern (western) end of the domain. In the standard configuration of COCO, there are two extra columns of grids both to the west and east. The number of extra grids can easily be changed in the model. The values of variables at these extra grid points are copied from the corresponding

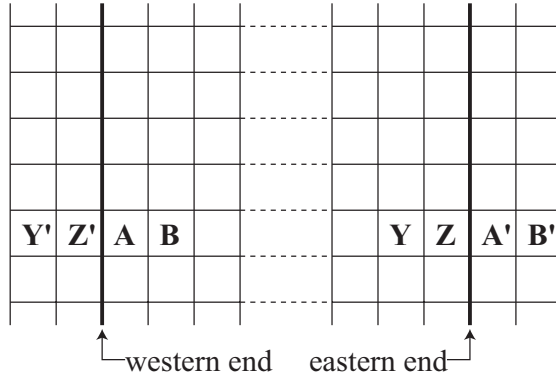


Figure 3.6: Grid configuration for the cyclic boundary in the  $x$  direction. The values at the grids labeled by the primed symbols are copied from the grids of the respective non-primed symbols.

grids so that the cyclic condition is realized (see Figure 3.6). When it is intended not to apply the cyclic boundary condition, there should at least one coastline connecting the northern and southern ends of the domain.

Although there is no need to cyclically connect the domain in the  $y$  direction, there also are extra grids to the north (south) of the northern (southern) end of the model domain. When the model is parallelized, information from other processors is passed on to these extra grids.

### 3.4.2 Masking Array and Boundary Condition

In order to exclude land grid points from calculation, masking arrays are defined in the model. Let  $M^T$  and  $M^V$  denote masking arrays for T-points and V-points, respectively. The grid point value of  $M^T$  takes zero when the T-point-centered grid box labeled by  $L$  is land, and is unity otherwise:

$$M_L^T = \begin{cases} 0 & \text{for land grids} \\ 1 & \text{for ocean grids} \end{cases} \quad (3.171)$$

For the grids partially occupied by land, its value is also unity.  $M_L^V$  is zero where the corresponding V-point is land or on coast, and is unity elsewhere. Its values are defined by

$$M_L^V = M_L^T \cdot M_E^T \cdot M_N^T \cdot M_{NE}^T \quad (3.172)$$

Masking arrays for fluxes are also defined to adequately realize zero-flux boundary conditions. Let  $M_x^{FT}$ ,  $M_y^{FT}$  and  $M_z^{FT}$  denote masking arrays for the fluxes of T-point variables in the  $x$ ,  $y$  and  $z$  directions, respectively. Their grid point values are defined by

$$M_{xL}^{FT} = M_L^T \cdot M_W^T, \quad (3.173)$$

$$M_{yL}^{FT} = M_L^T \cdot M_S^T, \quad (3.174)$$

$$M_{zL}^{FT} = M_L^T \cdot M_U^T. \quad (3.175)$$

For the fluxes of V-point variables, masking arrays are defined by

$$M_{xL}^{FV} = M_L^T \cdot M_N^T, \quad (3.176)$$

$$M_{yL}^{FV} = M_L^T \cdot M_E^T, \quad (3.177)$$

$$M_{zL}^{FV} = [1 - (1 - M_L^T)(1 - M_E^T)(1 - M_N^T)(1 - M_{NE}^T)] \cdot M_U^T \cdot M_{UE}^T \cdot M_{UN}^T \cdot M_{UNE}^T. \quad (3.178)$$

The boundary conditions for temperature and salinity on solid boundaries (1.56) and (1.57) are satisfied by setting their flux in the direction normal to the boundaries to zero. Tracer fluxes are calculated for all the grids regardless of land or sea, including the extra grids for the cyclic boundary. Then, they are multiplied by the above-defined flux masking arrays for T-point variables. Note that the actual definition of  $M_x^{FT}$  and  $M_y^{FT}$  in the model is slightly different from the above. They are further multiplied by the grid thickness for the convenience of actual use:

$$M_{xL}^{FT} = M_L^T \cdot M_W^T \times \min(\Delta z_L, \Delta z_W), \quad (3.179)$$

$$M_{yL}^{FT} = M_L^T \cdot M_S^T \times \min(\Delta z_L, \Delta z_S). \quad (3.180)$$

Note that the grid thickness for the  $\sigma$  coordinate region is defined by  $\Delta z_L = -z_B \Delta \sigma_L$ . These masking arrays are used only for the calculation of diffusive tracer fluxes. Advective tracer fluxes need not to be multiplied by the masking arrays, as velocity is always set to zero on land points.

The no-slip boundary conditions (1.44) and (1.45) are realized by simply multiplying  $u$  and  $v$  by  $M^V$ . Then, advective momentum fluxes on boundaries become zero without taking a special care, as in the case of advective tracer fluxes. The masking arrays for V-point variable fluxes are used only in viscosity calculation. As in the case of the masking arrays for T-point variable fluxes, the actual definition of  $M_x^{FV}$  and  $M_y^{FV}$  in the model is multiplied by the grid thickness:

$$M_{xL}^{FV} = M_L^T \cdot M_N^T \times \min(\Delta z_L^V, \Delta z_W^V), \quad (3.181)$$

$$M_{yL}^{FV} = M_L^T \cdot M_E^T \times \min(\Delta z_L^V, \Delta z_S^V). \quad (3.182)$$

Vertical velocity at WT-points on the ocean floor is always regarded as zero. See the comment on (3.58). At the sea surface,  $\omega$  is identically zero by definition. Note that it is not explicitly used anywhere. Vertical velocity at WV-points is naturally derived by (3.92). It takes nonzero values at the corner of topographical steps (see Figure 3.2: the symbol  $W$  is placed only where vertical velocity could take nonzero values), and the vertical momentum flux is explicitly calculated for those grids.

## Chapter 4

# Numerical Algorithm and Physical Parameterization in Standard Use

### 4.1 Tracer Advection

A third-order, upstream weighted algorithm is the standard choice for tracer advection in COCO. Two-dimensional horizontal advection and one-dimensional vertical advection are separately treated. The algorithm for vertical advection is the Quadratic Upstream Interpolation for Convective Kinematics with Estimated Streaming Terms (QUICKEST) of *Leonard [1979]*. Its multidimensional extension, which is called the Uniformly Third-Order Polynomial Interpolation Algorithm (UTOPIA) [*Leonard et al., 1993, 1994*], is used for horizontal advection.

UTOPIA can be formulated in three-dimension, but fully three-dimensional UTOPIA is far more costly than the combination of vertical QUICKEST and horizontal UTOPIA. In addition, coding of three-dimensional UTOPIA becomes far more complicated than that of two-dimensional UTOPIA. There is a way, called COSMIC [*Leonard et al., 1996*], to realize an algorithm equivalent to three-dimensional UTOPIA by repeatedly applying QUICKEST. Although its coding is very simple, its computational cost is no less than three-dimensional UTOPIA. The separation of vertical and horizontal advection means that the effect of slantwise tracer transport is neglected. As long as horizontal-vertical grid aspect ratio (and also the ratio of horizontal advection speed to vertical advection speed) is much larger than unity, that effect is actually negligible.

#### 4.1.1 QUICKEST

Let us consider finite difference discretization of a flux-form, one-dimensional advection equation for tracer  $\psi$ :

$$\frac{\partial \psi}{\partial t} + \frac{\partial}{\partial z}(w\psi) = 0, \quad (4.1)$$

When the equation is temporally differenced by use of the forward-in-time scheme, flux-form spatial differencing yields

$$\frac{\psi_L^{n+1} - \psi_L^n}{\Delta t} = \frac{F_L^{\psi^n} - F_D^{\psi^n}}{\Delta z_L}. \quad (4.2)$$

See Figures 3.2, 3.3 and 3.5 for the arrangement of grid point values.

Integration of  $\psi^n$  over one spatial grid yields

$$\begin{aligned}
& \int_{z_L - \Delta z_L/2}^{z_L + \Delta z_L/2} \psi^n dz \\
&= \int_{z_L - \Delta z_L/2}^{z_L + \Delta z_L/2} \left[ \psi_L^n + (z - z_L) \psi_{zL}^n + \frac{(z - z_L)^2}{2} \psi_{zzL}^n + \frac{(z - z_L)^3}{6} \psi_{zzzL}^n + \dots \right] dz \\
&= \Delta z_L \psi_L^n + \frac{\Delta z_L^3}{24} \psi_{zzL}^n + O(\Delta z^5),
\end{aligned} \tag{4.3}$$

where the subscript  $z$  indicates spatial differentiation. Thus, integration of  $\partial\psi/\partial t$  over one time level and one spatial grid becomes

$$\begin{aligned}
\int_{t^n}^{t^{n+1}} dt \int_{z_L - \Delta z_L/2}^{z_L + \Delta z_L/2} dz \frac{\partial\psi}{\partial t} &= \int_{z_L - \Delta z_L/2}^{z_L + \Delta z_L/2} dz (\psi^{n+1} - \psi^n) \\
&= \Delta z_L \left[ (\psi_L^{n+1} - \psi_L^n) + \frac{\Delta z_L^2}{24} (\psi_{zzL}^{n+1} - \psi_{zzL}^n) + O(\Delta z^4) \right].
\end{aligned} \tag{4.4}$$

It holds that

$$\begin{aligned}
\psi_{zzL}^{n+1} - \psi_{zzL}^n &= \Delta t \left( \frac{\partial\psi_{zz}}{\partial t} \right)_L^n + O(\Delta t^2) \\
&= -\Delta t \left\{ \frac{\partial^2}{\partial z^2} \left[ \frac{\partial}{\partial z} (w\psi) \right] \right\}_L^n + O(\Delta t^2) \\
&= -\frac{\Delta t}{\Delta z_L} (w_L^n \psi_{zzu}^n - w_D^n \psi_{zzd}^n) + O(\Delta t^2) + O(w\Delta t),
\end{aligned} \tag{4.5}$$

where the subscripts  $u$  and  $d$  denote the positions of upper and lower grid boundaries, respectively, i.e.,  $\psi_{zzu}$  ( $\psi_{zzd}$ ) is defined at the same point as  $w_L$  ( $w_D$ ). It is assumed that the order of accuracy for the estimation of  $\psi_{zz}$  is  $O(\Delta z)$ , which yields error of the order of  $O(w\Delta t)$  in the calculation above. Therefore, the integration of  $\partial\psi/\partial t$  is represented by

$$\begin{aligned}
& \int_{t^n}^{t^{n+1}} dt \int_{z_L - \Delta z_L/2}^{z_L + \Delta z_L/2} dz \frac{\partial\psi}{\partial t} \\
&= \Delta z_L \left[ (\psi_L^{n+1} - \psi_L^n) + \frac{\Delta t \Delta z_L}{24} (w_L^n \psi_{zzu}^n - w_D^n \psi_{zzd}^n) \right] \\
&\quad + O(w\Delta t \Delta z^2) + O(\Delta t^2 \Delta z^3) + O(\Delta z^5).
\end{aligned} \tag{4.6}$$

Here,  $O(w\Delta t \Delta z^2) \sim O(\Delta z^3)$  as the Courant number  $w\Delta t/\Delta z$  is chosen to be less than unity. On the other hand, integration of  $\partial(w\psi)/\partial z$  over one time level and one spatial grid is represented by

$$\begin{aligned}
\int_{t^n}^{t^{n+1}} dt \int_{z_L - \Delta z_L/2}^{z_L + \Delta z_L/2} dz \frac{\partial}{\partial z} (w\psi) &= \int_{t^n}^{t^{n+1}} dt (w_L \psi_u - w_D \psi_d) \\
&= \Delta t \left( \overline{w_L \psi_u}^n - \overline{w_D \psi_d}^n \right) + O(\Delta z^3),
\end{aligned} \tag{4.7}$$

where the time average  $\overline{w_L \psi_u}^n$  is estimated such that this representation guarantees the third-order accuracy, whose method is described later. Therefore, integration of (4.1) over one time level and one spatial grid results in

$$\begin{aligned}
\psi_L^{n+1} &= \psi_L^n - \frac{\Delta t}{\Delta z_L} \left[ \left( \overline{w_L \psi_u}^n - \overline{w_D \psi_d}^n \right) \right. \\
&\quad \left. - \frac{\Delta z_L^2}{24} (w_L^n \psi_{zzu}^n - w_D^n \psi_{zzd}^n) \right] + O(\Delta z^3),
\end{aligned} \tag{4.8}$$

on condition that  $\psi_{zz}$  is estimated with an appropriate accuracy. It means that the finite differenced advection equation (4.2) has the third-order accuracy when the flux is estimated by

$$F_L^{\psi^n} = -\overline{w_L \psi_u}^n + \frac{\Delta z_L^2}{24} w_L^n \psi_{zzu}^n. \quad (4.9)$$

When  $w$  is constant or its variation is negligible within the accuracy now under consideration, it is represented by

$$F_L^n = -w_L^n \left( \bar{\psi}_u^n - \frac{\Delta z_L^2}{24} \psi_{zzu}^n \right) \equiv -w_L^n \tilde{\psi}_u^n. \quad (4.10)$$

This case is considered below.

The value of  $\psi^n$  around  $z = z_u$  (the position where  $\psi_u$  is defined) is here approximated by a quadratic expression:

$$\psi^n = c_0 + c_1(z - z_u) + c_2(z - z_u)^2. \quad (4.11)$$

The coefficients  $c_0$ ,  $c_1$ , and  $c_2$  are determined from the relationships

$$\psi_D^n = c_0 - c_1 \left( \Delta z_L + \frac{\Delta z_D}{2} \right) + c_2 \left( \Delta z_L + \frac{\Delta z_D}{2} \right)^2, \quad (4.12)$$

$$\psi_L^n = c_0 - c_1 \frac{\Delta z_L}{2} + c_2 \frac{\Delta z_L^2}{4}, \quad (4.13)$$

$$\psi_U^n = c_0 + c_1 \frac{\Delta z_U}{2} + c_2 \frac{\Delta z_U^2}{4}, \quad (4.14)$$

$$\psi_{UU}^n = c_0 + c_1 \left( \Delta z_U + \frac{\Delta z_{UU}}{2} \right) + c_2 \left( \Delta z_U + \frac{\Delta z_{UU}}{2} \right)^2. \quad (4.15)$$

The order of accuracy for these estimates is  $O(\Delta z^3)$ . Only three of them are used to determine the coefficients, and the choice depends on the sign of  $w_L^n$ . That is, the expressions for the adjacent points,  $\psi_L^n$  and  $\psi_U^n$ , and either of  $\psi_D^n$  or  $\psi_{UU}^n$  in the upstream is used. Therefore, when  $w_L^n$  is positive,

$$\begin{aligned} c_0 &= \frac{\Delta z_U \psi_L^n + \Delta z_L \psi_U^n}{2\Delta z'_L} - \frac{\Delta z_L \Delta z_U}{4} c_2, \\ c_1 &= \frac{\psi_U^n - \psi_L^n}{\Delta z'_L} + \frac{\Delta z_L - \Delta z_U}{2} c_2, \\ c_2 &= \frac{1}{\Delta z'_L + \Delta z'_D} \left( \frac{\psi_D^n - \psi_L^n}{\Delta z'_L} - \frac{\psi_L^n - \psi_U^n}{\Delta z'_D} \right). \end{aligned} \quad (4.16)$$

When  $w_L^n$  is negative,

$$\begin{aligned} c_0 &= \frac{\Delta z_U \psi_L^n + \Delta z_L \psi_U^n}{2\Delta z'_L} - \frac{\Delta z_L \Delta z_U}{4} c_2, \\ c_1 &= \frac{\psi_U^n - \psi_L^n}{\Delta z'_L} + \frac{\Delta z_L - \Delta z_U}{2} c_2, \\ c_2 &= \frac{1}{\Delta z'_L + \Delta z'_U} \left( \frac{\psi_L^n - \psi_U^n}{\Delta z'_L} - \frac{\psi_U^n - \psi_{UU}^n}{\Delta z'_U} \right). \end{aligned} \quad (4.17)$$

The instantaneous value of  $\psi_u^n$  coincides with  $c_0$  derived above. Since the quantity  $\psi$  is advected, time average of  $\psi_u^n$  over the time interval  $\Delta t$  is estimated by the spatial average of  $\psi^n$  over the region  $[z_u - w_L^n \Delta t, z_u]$  for positive  $w_L^n$  and the region  $[z_u, z_u - w_L^n \Delta t]$  for negative  $w_L^n$ . Regardless of the sign of  $w_L^n$ , it becomes

$$\begin{aligned} \bar{\psi}_u^n &= \frac{1}{w_L^n \Delta t} \int_{z_u - w_L^n \Delta t}^{z_u} \psi^n dz \\ &= c_0 - c_1 \frac{w_L^n \Delta t}{2} + c_2 \frac{(w_L^n \Delta t)^2}{3}. \end{aligned} \quad (4.18)$$

This estimate retains the accuracy of  $O(\Delta z^3)$ , as the estimate of  $\psi^n$  has that accuracy over the region of integration. Since  $\psi_{zzu}^n$  equals to  $2c_2$  and its accuracy is  $O(\Delta z)$ , the expression

$$\tilde{\psi}_u^n = c_0 - c_1 \frac{w_L^n \Delta t}{2} + c_2 \left( \frac{(w_L^n \Delta t)^2}{3} - \frac{\Delta z_L^2}{12} \right) \quad (4.19)$$

has the accuracy of  $O(\Delta z^3)$ . Note that when the temporal variation of  $\psi$  within the integration time interval is neglected, i.e., when  $\tilde{\psi}_u^n$  is estimated by  $c_0$ , the scheme is called QUICK. QUICK does not guarantee the third-order accuracy for the finite differenced expression of (4.1). See *Leonard [1979]* for its detail.

#### 4.1.2 Flux Limiter for One-Dimensional Advection

The quadratic interpolation (4.11) could estimate a false minimum or maximum, i.e., the estimated  $\psi_u$  could become smaller (larger) than both of  $\psi_L$  and  $\psi_U$ . Such an overshooting estimate violates the monotonicity preserving nature<sup>1</sup> of advection. The simplest way of avoiding such a false minimum or maximum is bounding  $\psi_u$  by

$$\min(\psi_L, \psi_U) \leq \psi_u \leq \max(\psi_L, \psi_U). \quad (4.20)$$

However, this simplest way could also fail from another respect, as the estimated  $\psi_u$  could become the downstream value. The downstream advection scheme with the forward-in-time method inevitably leads to numerical instability.

The method of limiting the estimate of  $\psi_u$  adopted here is one devised by *Leonard [1991]*. Here we first describe the case of  $w_L > 0$ . Let  $\delta$  and  $\gamma$  be defined by

$$\delta = \left( \frac{\psi_U - \psi_L}{\Delta z'_L} + \frac{\psi_L - \psi_D}{\Delta z'_D} \right) \Delta z_L, \quad (4.21)$$

$$\gamma = \frac{\psi_U - \psi_L}{\Delta z'_L} - \frac{\psi_L - \psi_D}{\Delta z'_D}. \quad (4.22)$$

The limiting criterion is described as follows:

$$\tilde{\psi}_u = \psi_L \quad \text{when} \quad |\gamma \Delta z_L| > |\delta|. \quad (4.23)$$

Otherwise,

$$\psi_L \leq \tilde{\psi}_u \leq \min \left( \psi_D + \frac{\psi_L - \psi_D}{w_L \Delta t} \Delta z'_L, \psi_U \right) \quad \text{when} \quad \delta > 0, \quad (4.24)$$

$$\max \left( \psi_D + \frac{\psi_L - \psi_D}{w_L \Delta t} \Delta z'_L, \psi_U \right) \leq \tilde{\psi}_u \leq \psi_L \quad \text{when} \quad \delta < 0. \quad (4.25)$$

For the case of  $w_L < 0$ ,  $\delta$  and  $\gamma$  are defined by

$$\delta = \psi_L - \psi_{UU}, \quad (4.26)$$

$$\gamma = \frac{\psi_L - \psi_U}{\Delta z'_L} - \frac{\psi_U - \psi_{UU}}{\Delta z'_U}, \quad (4.27)$$

and the limiting criterion is described as follows:

$$\tilde{\psi}_u = \psi_U \quad \text{when} \quad |\gamma \Delta z_U| > |\delta|. \quad (4.28)$$

Otherwise,

$$\psi_U \leq \tilde{\psi}_u \leq \min \left( \psi_{UU} + \frac{\psi_U - \psi_{UU}}{|w_L| \Delta t} \Delta z'_L, \psi_L \right) \quad \text{when} \quad \delta > 0, \quad (4.29)$$

$$\max \left( \psi_{UU} + \frac{\psi_U - \psi_{UU}}{|w_L| \Delta t} \Delta z'_L, \psi_U \right) \leq \tilde{\psi}_u \leq \psi_U \quad \text{when} \quad \delta < 0. \quad (4.30)$$

---

<sup>1</sup>Advection of monotonically varying quantity by uniform velocity would not generate any minima or maxima.

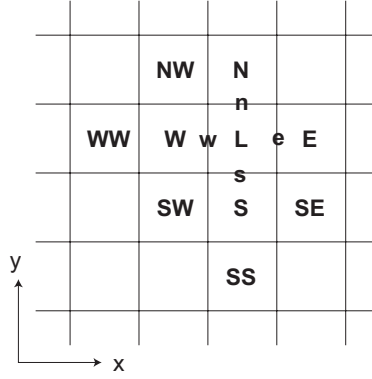


Figure 4.1: The arrangement of the labels denoting grid points.

### 4.1.3 Two-Dimensional UTOPIA

Now, a flux-form two-dimensional advection equation

$$\frac{\partial \psi}{\partial t} + \frac{1}{h_x h_y} \left[ \frac{\partial}{\partial x} (h_y u \psi) + \frac{\partial}{\partial y} (h_x v \psi) \right] = 0 \quad (4.31)$$

is considered. It is assumed that the two-dimensional continuity equation

$$\frac{1}{h_x h_y} \left[ \frac{\partial}{\partial x} (h_y u) + \frac{\partial}{\partial y} (h_x v) \right] = 0 \quad (4.32)$$

is satisfied. The required grid stencil is wider than previously defined, so its labeling is illustrated in Figure 4.1. Let us define  $\chi$ ,  $\phi$  and  $\theta$  by

$$\chi = h_y u, \quad \phi = h_x v, \quad \theta = h_x h_y \psi. \quad (4.33)$$

The equations (4.31) and (4.32) are expressed as

$$\frac{\partial \psi}{\partial t} = -\frac{1}{h_x h_y} \left[ \frac{\partial}{\partial x} (\chi \psi) + \frac{\partial}{\partial y} (\phi \psi) \right], \quad (4.34)$$

$$\frac{\partial \chi}{\partial x} + \frac{\partial \phi}{\partial y} = 0. \quad (4.35)$$

It is then assumed that  $\chi$  and  $\phi$  is spatially uniform.

With a procedure similar to the one-dimensional case, integration of the right hand side of (4.34) over one time level and one spatial grid yields

$$\begin{aligned} & \int_{t^n}^{t^{n+1}} dt \int_{x_L - \Delta x/2}^{x_L + \Delta x/2} dx \int_{y_L - \Delta y_L/2}^{y_L + \Delta y_L/2} dy h_x h_y \times \frac{1}{h_x h_y} \left[ \frac{\partial}{\partial x} (\chi \psi) + \frac{\partial}{\partial y} (\phi \psi) \right] \\ &= \Delta t \left[ (\chi_e^n \bar{\psi}_e^n - \chi_w^n \bar{\psi}_w^n) \Delta y_L + (\phi_n^n \bar{\psi}_n^n - \phi_s^n \bar{\psi}_s^n) \Delta x \right]. \end{aligned} \quad (4.36)$$

Integration of the left hand side is

$$\begin{aligned} & \int_{t^n}^{t^{n+1}} dt \int_{x_L - \Delta x/2}^{x_L + \Delta x/2} dx \int_{y_L - \Delta y_L/2}^{y_L + \Delta y_L/2} dy h_x h_y \frac{\partial \psi}{\partial t} \\ &= \int_{x_L - \Delta x/2}^{x_L + \Delta x/2} dx \int_{y_L - \Delta y_L/2}^{y_L + \Delta y_L/2} dy (\theta^{n+1} - \theta^n) \\ &= \Delta x \Delta y_L \left[ (\theta_L^{n+1} - \theta_L^n) + \frac{\Delta x^2}{24} (\theta_{xxL}^{n+1} - \theta_{xxL}^n) + \frac{\Delta y_L^2}{24} (\theta_{yyL}^{n+1} - \theta_{yyL}^n) \right]. \end{aligned} \quad (4.37)$$

Note that the symbols denoting the accuracy, such as  $O(\Delta x)$ , are omitted, as the discussion for the accuracy goes parallel with the one-dimensional case. As in the one-dimensional case,

$$\theta_{xxL}^{n+1} - \theta_{xxL}^n = -\Delta t \left[ \frac{\chi_e^n \psi_{xxe}^n - \chi_w^n \psi_{xxw}^n}{\Delta x} + \frac{\phi_n^n \psi_{xxn}^n - \phi_s^n \psi_{xxs}^n}{\Delta y_L} \right], \quad (4.38)$$

$$\theta_{yyL}^{n+1} - \theta_{yyL}^n = -\Delta t \left[ \frac{\chi_e^n \psi_{yye}^n - \chi_w^n \psi_{yyw}^n}{\Delta x} + \frac{\phi_n^n \psi_{yy n}^n - \phi_s^n \psi_{yy s}^n}{\Delta y_L} \right]. \quad (4.39)$$

Finite differenced representation of (4.31) now becomes

$$\psi_L^{n+1} = \psi_L^n - \frac{\Delta t}{h_x h_y} \left( \frac{\chi_e^n \tilde{\psi}_e^n - \chi_w^n \tilde{\psi}_w^n}{\Delta x} + \frac{\phi_n^n \tilde{\psi}_n^n - \phi_s^n \tilde{\psi}_s^n}{\Delta y_L} \right), \quad (4.40)$$

where

$$\tilde{\psi}_w^n = \bar{\psi}_w^n - \frac{\Delta x^2}{24} \psi_{xxw}^n - \frac{\Delta y_L^2}{24} \psi_{yyw}^n, \quad (4.41)$$

$$\tilde{\psi}_s^n = \bar{\psi}_s^n - \frac{\Delta x^2}{24} \psi_{xxs}^n - \frac{\Delta y_L^2}{24} \psi_{yy s}^n. \quad (4.42)$$

Let us represent the quadratic approximation for  $\psi^n$  around  $(x_w, y_w)$  and  $(x_s, y_s)$  by

$$\begin{aligned} \psi^n &= c_{00} + c_{10}(x - x_w) + c_{20}(x - x_w)^2 \\ &\quad + c_{01}(y - y_w) + c_{02}(y - y_w)^2 + c_{11}(x - x_w)(y - y_w), \end{aligned} \quad (4.43)$$

$$\begin{aligned} \psi^n &= d_{00} + d_{01}(y - y_s) + d_{02}(y - y_s)^2 \\ &\quad + d_{10}(x - x_s) + d_{20}(x - x_s)^2 + d_{11}(x - x_s)(y - y_s), \end{aligned} \quad (4.44)$$

respectively. The first expression yields

$$\psi_L^n = c_{00} + c_{10} \frac{\Delta x}{2} + c_{20} \frac{\Delta x^2}{4}, \quad (4.45)$$

$$\psi_W^n = c_{00} - c_{10} \frac{\Delta x}{2} + c_{20} \frac{\Delta x^2}{4}, \quad (4.46)$$

$$\psi_E^n = c_{00} + c_{10} \frac{3\Delta x}{2} + c_{20} \frac{9\Delta x^2}{4}, \quad (4.47)$$

$$\psi_{WW}^n = c_{00} - c_{10} \frac{3\Delta x}{2} + c_{20} \frac{9\Delta x^2}{4}, \quad (4.48)$$

$$\psi_N^n = \psi_L^n + c_{01} \Delta y'_L + c_{02} \Delta y_L'^2 + c_{11} \frac{\Delta x \Delta y'_L}{2}, \quad (4.49)$$

$$\psi_S^n = \psi_L^n - c_{01} \Delta y'_S + c_{02} \Delta y_S'^2 - c_{11} \frac{\Delta x \Delta y'_S}{2}, \quad (4.50)$$

$$\psi_{NW}^n = \psi_W^n + c_{01} \Delta y'_L + c_{02} \Delta y_L'^2 - c_{11} \frac{\Delta x \Delta y'_L}{2}, \quad (4.51)$$

$$\psi_{SW}^n = \psi_W^n - c_{01} \Delta y'_S + c_{02} \Delta y_S'^2 + c_{11} \frac{\Delta x \Delta y'_S}{2} \quad (4.52)$$

around  $(x_w, y_w)$ . There are six coefficients to be determined, so six of the above expressions are necessary. The choice depends on the sign of  $u_w^n$  and  $v_w^n$ :  $\psi_L^n, \psi_W^n$ , either of  $\psi_E^n$  or  $\psi_{WW}^n$  in the upstream, and three of  $\psi_N^n, \psi_S^n, \psi_{NW}^n$ , and  $\psi_{SW}^n$  excluding one in the downstream. The choice is summarized as

$$\begin{aligned} u_w^n > 0, v_w^n > 0 &\Rightarrow \psi_L^n, \psi_W^n, \psi_{WW}^n, \psi_S^n, \psi_{NW}^n, \psi_{SW}^n; \\ u_w^n < 0, v_w^n > 0 &\Rightarrow \psi_L^n, \psi_W^n, \psi_E^n, \psi_N^n, \psi_S^n, \psi_{SW}^n; \\ u_w^n > 0, v_w^n < 0 &\Rightarrow \psi_L^n, \psi_W^n, \psi_{WW}^n, \psi_N^n, \psi_{NW}^n, \psi_{SW}^n; \\ u_w^n < 0, v_w^n < 0 &\Rightarrow \psi_L^n, \psi_W^n, \psi_E^n, \psi_N^n, \psi_S^n, \psi_{NW}^n. \end{aligned} \quad (4.53)$$

The resulting representation for the coefficients are:

	$u_w > 0, v_w > 0$	$u_w < 0, v_w > 0$	$u_w > 0, v_w < 0$	$u_w < 0, v_w < 0$
$c_{20}$	$\frac{\psi_L - 2\psi_W + \psi_{WW}}{2\Delta x^2}$	$\frac{\psi_E - 2\psi_L + \psi_W}{2\Delta x^2}$	$\frac{\psi_L - 2\psi_W + \psi_{WW}}{2\Delta x^2}$	$\frac{\psi_E - 2\psi_L + \psi_W}{2\Delta x^2}$
$c_{01}$	$c_{01-A}$	$c_{01-B}$	$c_{01-B}$	$c_{01-A}$
$c_{02}$	$c_{01-A}$	$c_{01-B}$	$c_{01-A}$	$c_{01-B}$
$c_{11}$	$\frac{\psi_{SW} - \psi_W - \psi_S + \psi_L}{\Delta x \Delta y'_S}$	$\frac{\psi_{SW} - \psi_W - \psi_S + \psi_L}{\Delta x \Delta y'_S}$	$\frac{\psi_N - \psi_L - \psi_{NW} + \psi_W}{\Delta x \Delta y'_L}$	$\frac{\psi_N - \psi_L - \psi_{NW} + \psi_W}{\Delta x \Delta y'_L}$

$$\begin{aligned}
c_{00} &= \frac{\psi_L + \psi_W}{2} - c_{20} \frac{\Delta x^2}{4} \\
c_{10} &= \frac{\psi_L - \psi_W}{\Delta x} \\
c_{01-A} &= \frac{(\psi_{NW} - \psi_W) \Delta y'_S - (\psi_S - \psi_L) \Delta y'_L}{2 \Delta y'_L \Delta y'_S} - c_{02} \frac{\Delta y'_L - \Delta y'_S}{2} \\
c_{01-B} &= \frac{(\psi_N - \psi_L) \Delta y'_S - (\psi_{SW} - \psi_W) \Delta y'_L}{2 \Delta y'_L \Delta y'_S} - c_{02} \frac{\Delta y'_L - \Delta y'_S}{2} \\
c_{02-A} &= \frac{(\psi_{NW} - \psi_W) \Delta y'_S + (\psi_{SW} - \psi_W) \Delta y'_L}{\Delta y'_L \Delta y'_S (\Delta y'_L + \Delta y'_S)} \\
c_{02-B} &= \frac{(\psi_N - \psi_L) \Delta y'_S + (\psi_S - \psi_L) \Delta y'_L}{\Delta y'_L \Delta y'_S (\Delta y'_L + \Delta y'_S)} \tag{4.54}
\end{aligned}$$

where the superscript  $n$  is omitted. Similar consideration results in

	$u_s > 0, v_s > 0$	$u_s > 0, v_s < 0$	$u_s < 0, v_s > 0$	$u_s < 0, v_s < 0$
$d_{02}$	$d_{02-A}$	$d_{02-B}$	$d_{02-A}$	$d_{02-B}$
$d_{20}$	$\frac{\psi_{SE} - 2\psi_S + \psi_{SW}}{2\Delta x^2}$	$\frac{\psi_E - 2\psi_L + \psi_W}{2\Delta x^2}$	$\frac{\psi_{SE} - 2\psi_S + \psi_{SW}}{2\Delta x^2}$	$\frac{\psi_E - 2\psi_L + \psi_W}{2\Delta x^2}$
$d_{11}$	$\frac{\psi_{SW} - \psi_S - \psi_W + \psi_L}{\Delta x (\Delta y_L + \Delta y_S)/2}$	$\frac{\psi_{SW} - \psi_S - \psi_W + \psi_L}{\Delta x (\Delta y_L + \Delta y_S)/2}$	$\frac{\psi_E - \psi_L - \psi_{SE} + \psi_S}{\Delta x (\Delta y_L + \Delta y_S)/2}$	$\frac{\psi_E - \psi_L - \psi_{SE} + \psi_S}{\Delta x (\Delta y_L + \Delta y_S)/2}$

$$\begin{aligned}
d_{00} &= \frac{\psi_L \Delta \varphi_S + \psi_S \Delta \varphi_L}{\Delta y_L + \Delta y_S} - d_{02} \frac{\Delta y_L \Delta y_S}{4} \\
d_{01} &= \frac{2(\psi_L - \psi_S)}{\Delta y_L + \Delta y_S} - d_{02} \frac{\Delta y_L - \Delta y_S}{2} \\
d_{02-A} &= 4 \frac{(\psi_L - \psi_S)(\Delta y_S + \Delta y_{SS}) - (\psi_S - \psi_{SS})(\Delta y_L + \Delta y_S)}{(\Delta y_L + \Delta y_S)(\Delta y_S + \Delta y_{SS})(\Delta y_L + 2\Delta y_S + \Delta y_{SS})} \\
d_{02-B} &= 4 \frac{(\psi_N - \psi_L)(\Delta y_L + \Delta y_S) - (\psi_L - \psi_S)(\Delta y_N + \Delta y_L)}{(\Delta y_N + \Delta y_L)(\Delta y_L + \Delta y_S)(\Delta y_N + 2\Delta y_L + \Delta y_S)} \\
d_{10} &= \frac{\psi_L - \psi_W}{\Delta x} + d_{20} \Delta x - d_{11} \frac{\Delta y_L}{2} \quad \text{or} \quad \frac{\psi_E - \psi_L}{\Delta x} + d_{20} \Delta x - d_{11} \frac{\Delta y_L}{2} \tag{4.55}
\end{aligned}$$

Two expressions are given for  $d_{10}$ , and the choice should be made in accordance with the sign of the advection velocity. For instance,  $\psi_W$  is not to be used when  $u_s > 0$  and  $v_s < 0$ , so the second expression is valid in that case. When it is the case that the both expressions are available, they result in the same expression.

The estimation of  $\bar{\psi}_w^n$  and  $\bar{\psi}_s^n$  is realized by spatially averaging  $\psi_w^n$  and  $\psi_s^n$ , respectively, as in the one-dimensional case. For  $\bar{\psi}_w^n$ , the region for the average is determined by the area expanded by the vector  $(u_w \Delta t, v_w \Delta t)$  and the western boundary of the grid box  $L$ . It is illustrated in Figure 4.2. By introducing the variables,

$$\xi_w = \frac{2u_w}{h_{xL}^T + h_{xW}^T}, \quad \eta_w = \frac{2v_w}{h_{yL}^T + h_{yW}^T}, \tag{4.56}$$

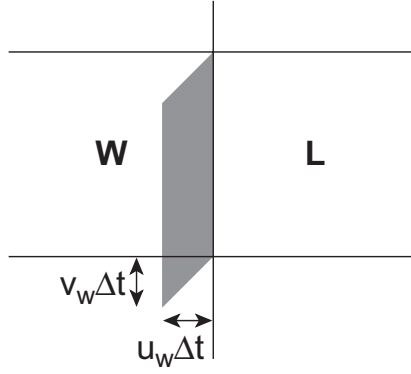


Figure 4.2: The area for average in estimating  $\bar{\psi}_w^n$  when  $u_w > 0$  and  $v_w > 0$ .

$$\xi_s = \frac{2u_s}{h_{xL}^T + h_{xS}^T}, \quad \eta_s = \frac{2v_s}{h_{yL}^T + h_{yS}^T}, \quad (4.57)$$

the average is calculated as

$$\begin{aligned} \bar{\psi}_w^n &= \frac{1}{\xi_w^n \Delta t \Delta y_L} \left[ \int_{x_w - \xi_w^n \Delta t}^{x_w} dx \int_{y_w - \Delta y_L/2 - \eta_w^n \Delta t}^{y_w + \Delta y_L/2 - \eta_w^n \Delta t} dy \psi^n + \int_{x_w - \xi_w^n \Delta t}^{x_w} dx \int_{y_w - \Delta y_L/2}^{y_w + \Delta y_L/2} dy \psi^n \right] \times \frac{1}{2} \\ &= c_{00} - \frac{1}{2} \xi_w^n \Delta t c_{10} + \frac{1}{3} (\xi_w^n \Delta t)^2 c_{20} \\ &\quad - \frac{1}{2} \eta_w^n \Delta t c_{01} + \left( \frac{\Delta y_L^2}{12} + \frac{1}{2} (\eta_w^n \Delta t)^2 \right) c_{02} + \frac{1}{4} \xi_w^n \Delta t \eta_w^n \Delta t c_{11}, \end{aligned} \quad (4.58)$$

$$\begin{aligned} \bar{\psi}_s^n &= \frac{1}{\Delta x \eta_s^n \Delta t} \left[ \int_{y_s - \eta_s^n \Delta t}^{y_s} dy \int_{x_s - \Delta x/2 - \xi_s^n \Delta t}^{x_s + \Delta x/2 - \xi_s^n \Delta t} dx \psi^n + \int_{y_s - \eta_s^n \Delta t}^{y_s} dy \int_{x_s - \Delta x/2}^{x_s + \Delta x/2} dx \psi^n \right] \times \frac{1}{2} \\ &= d_{00} - \frac{1}{2} \eta_s^n \Delta t d_{01} + \frac{1}{3} (\eta_s^n \Delta t)^2 d_{02} \\ &\quad - \frac{1}{2} \xi_s^n \Delta t d_{10} + \left( \frac{\Delta x^2}{12} + \frac{1}{2} (\xi_s^n \Delta t)^2 \right) d_{20} + \frac{1}{4} \xi_s^n \Delta t \eta_s^n \Delta t d_{11}. \end{aligned} \quad (4.59)$$

Since  $\psi_{xxl}^n = 2c_{20}$ ,  $\psi_{yyt}^n = 2c_{02}$ ,  $\psi_{xxd}^n = 2d_{20}$ , and  $\psi_{yyd}^n = 2d_{02}$ , the final expressions are

$$\begin{aligned} \tilde{\psi}_w^n &= c_{00} - \frac{1}{2} \xi_w^n \Delta t c_{10} + \left( \frac{1}{3} (\xi_w^n \Delta t)^2 - \frac{\Delta x^2}{12} \right) c_{20} \\ &\quad - \frac{1}{2} \eta_w^n \Delta t c_{01} + \frac{1}{2} (\eta_w^n \Delta t)^2 c_{02} + \frac{1}{4} \xi_w^n \Delta t \eta_w^n \Delta t c_{11}, \end{aligned} \quad (4.60)$$

$$\begin{aligned} \tilde{\psi}_s^n &= d_{00} - \frac{1}{2} \eta_s^n \Delta t d_{01} + \left( \frac{1}{3} (\eta_s^n \Delta t)^2 - \frac{\Delta y_L^2}{12} \right) d_{02} \\ &\quad - \frac{1}{2} \xi_s^n \Delta t d_{10} + \frac{1}{2} (\xi_s^n \Delta t)^2 d_{20} + \frac{1}{4} \xi_s^n \Delta t \eta_s^n \Delta t d_{11}. \end{aligned} \quad (4.61)$$

Advection velocity  $u_w$  and  $v_s$  are estimated from the fluid volume flux (3.64) and (3.65) as

$$u_w \frac{h_{yL}^T + h_{yW}^T}{2} \Delta y_L M_{xL}^{FT} = F_{xL}^V, \quad (4.62)$$

$$v_s \frac{h_{xL}^T + h_{xS}^T}{2} \Delta x M_{yL}^{FT} = F_{yL}^V, \quad (4.63)$$

where  $M$  represents the masking arrays defined in section 3.4.2, and  $u_s$  and  $v_w$  are estimated in a consistent

way as

$$u_s \frac{h_{yL}^T + h_{yS}^T}{2} M_{yL}^{FT} = \frac{1}{2} (h_{yS}^V u_S^t \Delta z_S^V + h_{ySW}^V u_{SW}^t \Delta z_{SW}^V), \quad (4.64)$$

$$v_w \frac{h_{xL}^T + h_{xW}^T}{2} M_{xL}^{FT} = \frac{1}{2} (h_{xW}^V v_W^t \Delta z_W^V + h_{xSW}^V v_{SW}^t \Delta z_{SW}^V). \quad (4.65)$$

#### 4.1.4 Flux Limiter for Two-Dimensional Advection

As in the case of the one-dimensional advection, flux limiter is required to guarantee monotonicity preservation. One possible solution is to apply a one-dimensional limiter, such as introduced previously, to each direction. This approach certainly preserve monotonicity, but shape of tracer distribution is sometimes severely distorted<sup>2</sup>. The one introduced here is a two-dimensional limiter of *Leonard et al. [1993]*.

Let us first consider the limiter for the  $x$  direction flux. For the sake of brevity of expressions, the following notations are introduced. The Courant numbers  $c_x$  and  $c_y$  are defined by

$$c_{xw} = \frac{\xi_w \Delta t}{\Delta x}, \quad c_{yw} = \frac{\eta_w \Delta t}{\Delta y_L}, \quad (4.66)$$

where the subscript  $w$  indicates that these quantities are defined at the western face of the T-point-centered grid box labeled by  $L$ . With regard to this western face, three of the four grid point values  $\psi_{WW}$ ,  $\psi_W$ ,  $\psi_L$  and  $\psi_E$  are used to represent the  $x$  direction flux. Let us represent the upstream, center and downstream values of the three used grid point values by  $\psi_{up}$ ,  $\psi_{cn}$  and  $\psi_{dn}$ , respectively:

$$\psi_{up} = \psi_{WW}, \quad \psi_{cn} = \psi_W, \quad \psi_{dn} = \psi_L \quad \text{when } c_{xw} > 0, \quad (4.67)$$

$$\psi_{up} = \psi_E, \quad \psi_{cn} = \psi_L, \quad \psi_{dn} = \psi_W \quad \text{when } c_{xw} < 0. \quad (4.68)$$

Likewise, the grid point values of the northern and southern sides of  $\psi_{cn}$  are described by  $\psi_{nn}$  and  $\psi_{ss}$ , respectively:

$$\psi_{nn} = \psi_{NW}, \quad \psi_{ss} = \psi_{SW} \quad \text{when } c_{xw} > 0, \quad (4.69)$$

$$\psi_{nn} = \psi_N, \quad \psi_{ss} = \psi_S \quad \text{when } c_{xw} < 0. \quad (4.70)$$

Finally,  $\psi_{\text{diff}}$  and  $\psi_{\text{curv}}$  are defined by

$$\psi_{\text{diff}} = \psi_{dn} - \psi_{up}, \quad (4.71)$$

$$\psi_{\text{curv}} = \psi_{dn} - 2\psi_{cn} + \psi_{up}. \quad (4.72)$$

By defining

$$\tilde{\psi}'_w = \tilde{\psi}_w + \frac{1}{2} \left[ \frac{c_{yw} + |c_{yw}|}{2} (\psi_{cn} - \psi_{ss}) + \frac{c_{yw} - |c_{yw}|}{2} (\psi_{nn} - \psi_{cn}) \right], \quad (4.73)$$

the limiting criterion is given as follows:

$$\tilde{\psi}'_w = \psi_{cn} \quad \text{when } |\psi_{\text{curv}}| > |\psi_{\text{diff}}|. \quad (4.74)$$

Otherwise,  $\tilde{\psi}'_w$  is bounded by  $\psi_{\text{max}}$  and  $\psi_{\text{min}}$  which are defined by

$$\psi_{\text{max}} = \min \left( \psi_{dn}, \psi_{up} + (\psi_{cn} - \psi_{up}) \frac{(1 + |c_{xw} c_{yw}|)}{|c_{xw}| + |c_{yw}|} \right), \quad \psi_{\text{min}} = \psi_{cn} \quad \text{when } \psi_{\text{diff}} > 0, \quad (4.75)$$

$$\psi_{\text{max}} = \psi_{cn}, \quad \psi_{\text{min}} = \max(\psi_{dn}, \psi_{dn} + (\psi_{cn} - \psi_{dn}) |c_{yw}|) \quad \text{when } \psi_{\text{diff}} < 0. \quad (4.76)$$

---

<sup>2</sup>Advection by spatially uniform velocity fields does not change the shape of distribution of the advected tracer. This property is called shape preservation.

Then,  $\tilde{\psi}_w$  is finally determined as

$$\tilde{\psi}_w = \tilde{\psi}'_w - \frac{1}{2} \left[ \frac{c_{yw} + |c_{yw}|}{2} (\psi_{cn} - \psi_{ss}) + \frac{c_{yw} - |c_{yw}|}{2} (\psi_{nn} - \psi_{cn}) \right]. \quad (4.77)$$

Consideration for the  $y$  direction limiter is basically the same as the above. The Courant numbers are defined by

$$c_{xs} = \frac{\xi_s \Delta t}{\Delta x}, \quad c_{ys} = \frac{\eta_s \Delta t}{\Delta y_L}, \quad (4.78)$$

and  $\psi_{up}$ ,  $\psi_{cn}$  and  $\psi_{dn}$  are represented by

$$\psi_{up} = \psi_{SS}, \quad \psi_{cn} = \psi_S, \quad \psi_{dn} = \psi_L \quad \text{when } c_{ys} > 0, \quad (4.79)$$

$$\psi_{up} = \psi_N, \quad \psi_{cn} = \psi_L, \quad \psi_{dn} = \psi_S \quad \text{when } c_{ys} < 0. \quad (4.80)$$

The grid point values of the eastern and western sides of  $\psi_{cn}$ ,  $\psi_{ee}$  and  $\psi_{ww}$ , are represented by

$$\psi_{ee} = \psi_{SE}, \quad \psi_{ww} = \psi_{SW} \quad \text{when } c_{ys} > 0, \quad (4.81)$$

$$\psi_{ee} = \psi_E, \quad \psi_{ww} = \psi_W \quad \text{when } c_{ys} < 0. \quad (4.82)$$

The definition for  $\psi_{\text{diff}}$  is the same as the previous, but that for  $\psi_{\text{curv}}$  is slightly modified due to the variable grid spacing in the  $y$  direction:

$$\psi_{\text{diff}} = \psi_{dn} - \psi_{up}, \quad (4.83)$$

$$\psi_{\text{curv}} = \left( \frac{\psi_{dn} - \psi_{cn}}{\Delta y'_S} - \frac{\psi_{cn} - \psi_{up}}{\Delta y'_{up}} \right) \Delta y_{cn}, \quad (4.84)$$

where

$$\Delta y'_{up} = \Delta y'_{SS}, \quad \Delta y_{cn} = \Delta y_S \quad \text{when } c_{ys} > 0, \quad (4.85)$$

$$\Delta y'_{up} = \Delta y'_L, \quad \Delta y_{cn} = \Delta y_L \quad \text{when } c_{ys} < 0. \quad (4.86)$$

By defining

$$\tilde{\psi}'_s = \tilde{\psi}_s + \frac{1}{2} \left[ \frac{c_{xs} + |c_{xs}|}{2} (\psi_{cn} - \psi_{ww}) + \frac{c_{xs} - |c_{xs}|}{2} (\psi_{ee} - \psi_{cn}) \right], \quad (4.87)$$

the limiting criterion is given as follows:

$$\tilde{\psi}'_s = \psi_{cn} \quad \text{when } |\psi_{\text{curv}}| > |\psi_{\text{diff}}|. \quad (4.88)$$

Otherwise,  $\tilde{\psi}'_s$  is bounded by  $\psi_{\text{max}}$  and  $\psi_{\text{min}}$  which are defined by

$$\psi_{\text{max}} = \min \left( \psi_{dn}, \psi_{up} + (\psi_{cn} - \psi_{up}) \frac{(1 + |c_{xs} c_{ys}|)}{|c_{xs}| + |c_{ys}|} \right), \quad \psi_{\text{min}} = \psi_{cn} \quad \text{when } \psi_{\text{diff}} > 0, \quad (4.89)$$

$$\psi_{\text{max}} = \psi_{cn}, \quad \psi_{\text{min}} = \max(\psi_{dn}, \psi_{dn} + (\psi_{cn} - \psi_{dn}) |c_{xs}|) \quad \text{when } \psi_{\text{diff}} < 0. \quad (4.90)$$

Then,  $\tilde{\psi}_s$  is finally determined as

$$\tilde{\psi}_s = \tilde{\psi}'_s - \frac{1}{2} \left[ \frac{c_{xs} + |c_{xs}|}{2} (\psi_{cn} - \psi_{ww}) + \frac{c_{xs} - |c_{xs}|}{2} (\psi_{ee} - \psi_{cn}) \right]. \quad (4.91)$$

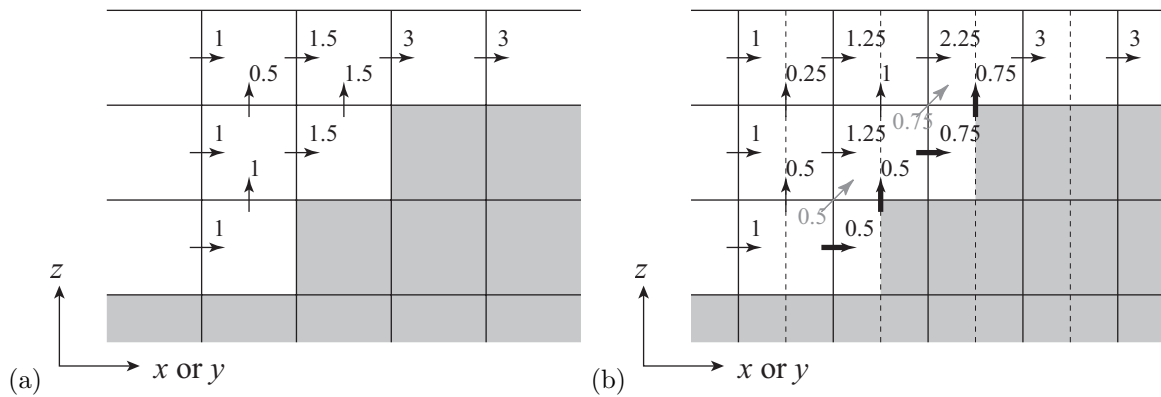


Figure 4.3: (a) Fluid volume budget of T-point centered boxes for horizontal inflow over a sloping bottom. The shaded boxes indicate land grids. (b) Corresponding fluid volume budget for V-point centered boxes. The dotted vertical lines indicate boundaries for the T-point-centered boxes.

## 4.2 Momentum Advection

The centered-in-space differencing scheme for the momentum advection described in chapter 3 is the standard choice in the case of non-eddy-resolving resolution. In eddy-resolving (or eddy-permitting) cases, a pseudo-entropy preserving scheme of *Ishizaki and Motoi [1999]* is used. The scheme also takes up/down-slope momentum advection into consideration. Its strategy for discretization is described in detail by themselves, in such a way that it is directly applicable to COCO. Therefore, its discretized representation is not repeated here, and only the basic concept behind is described below. The examples below are also taken from *Ishizaki and Motoi [1999]*.

### 4.2.1 Up/Down-Slope Momentum Advection

Let us consider the case illustrated in Figure 4.3a. The bottom is sloping up toward the right, and there is vertically uniform inflow from the left end. Vertically integrated rightward volume flux is conserved, so rightward velocity becomes gradually larger as the fluid moves to the right. It is assumed rightward velocity is uniformly intensified in vertical (it is actually expected when the fluid is not stratified). The corresponding fluid volume budget for T-point-centered grid boxes is indicated by arrows in Figure 4.3a. Tracer advection is calculated in a way consistent with this fluid volume budget.

By following the method described in section 3.3.4, fluid volume budget for V-point-centered grid boxes is estimated as the black arrows (both thin and thick) in Figure 4.3b. Momentum advection is calculated in a way consistent with this fluid volume budget. There is no volume flux convergence/divergence at any V-point-centered grid box, of course. According to this treatment, the momentum transported with the volume fluxes indicated by thick horizontal arrows (just to the left of lateral boundaries) is interpreted as dissipating out at lateral boundaries; and the vertical volume fluxes indicated by the thick vertical arrows accompany vertical momentum fluxes which slow down the horizontal flows just above. It is a natural consequence of the no-slip lateral boundary condition for the horizontal velocity components (see section 1.3). In a step-like representation of the ocean floor, this no-slip lateral boundary is eventually applied to sloping “bottom,” too. If this kind of momentum dissipation on sloping bottom is not favorable, slantwise momentum advection by the volume fluxes indicated by the gray arrows in Figure 4.3b has to be taken into account.

The case exemplified in Figure 4.3 is very simplified as it is two-dimensional. In an actual application of

this scheme to an OGCM, it is necessary to define eight-direction slantwise momentum advection velocity at each WV-point, in addition to the regular vertical advection.

### 4.2.2 Preservation of Enstrophy

Let us consider discretized representations of the horizontal advection term of the momentum equation (1.1):

$$\frac{\partial}{\partial x}(h_y uu) + \frac{\partial}{\partial y}(h_x vu). \quad (4.92)$$

Only the  $x$ -direction momentum equation is discussed here. Once it is established, the treatment for the  $y$ -direction momentum equation is obvious.

The simplest five-point representation (i.e., momentum at  $N$ ,  $S$ ,  $E$ ,  $W$  and  $L$  appears) is

$$\begin{aligned} & \left[ \frac{\partial}{\partial x}(h_y uu) + \frac{\partial}{\partial y}(h_x vu) \right]_L^{\text{rect}} \\ &= \frac{1}{\Delta x} \left[ (h_y u)_e \frac{u_E + u_L}{2} - (h_y u)_w \frac{u_L + u_W}{2} \right] + \frac{1}{\Delta y'_L} \left[ (h_x v)_n \frac{u_N + u_L}{2} - (h_x v)_s \frac{u_L + u_S}{2} \right], \end{aligned} \quad (4.93)$$

where the upper case labels (subscripts) indicate V-points, and the lower case labels indicate faces (for  $n$ ,  $s$ ,  $e$  and  $w$ ) or vertices (for  $ne$ ,  $se$ ,  $nw$  and  $sw$ ) of the grid box which contains the V-point labeled by  $L$ . This five-point representation corresponds to what is described in section 3.3.4. This is good for conservation of momentum and kinetic energy, but not for enstrophy.

Other discretized representations are possible if a wider grid stencil is allowed to be used. One possible representation is

$$\begin{aligned} \left[ \frac{\partial}{\partial x}(h_y uu) + \frac{\partial}{\partial y}(h_x vu) \right]_L^{\text{diag}} &= \frac{1}{2\Delta x} \left[ (h_y u)_{ne} \frac{u_{NE} + u_L}{2} + (h_y u)_{se} \frac{u_{SE} + u_L}{2} \right. \\ &\quad \left. - (h_y u)_{nw} \frac{u_L + u_{NW}}{2} - (h_y u)_{sw} \frac{u_L + u_{SW}}{2} \right] \\ &\quad + \frac{1}{2\Delta y'_L} \left[ (h_x v)_{ne} \frac{u_{NE} + u_L}{2} + (h_x v)_{nw} \frac{u_L + u_{NW}}{2} \right. \\ &\quad \left. - (h_x v)_{se} \frac{u_{SE} + u_L}{2} + (h_x v)_{sw} \frac{u_L + u_{SW}}{2} \right]. \end{aligned} \quad (4.94)$$

It is rewritten as

$$\begin{aligned} \left[ \frac{\partial}{\partial x}(h_y uu) + \frac{\partial}{\partial y}(h_x vu) \right]_L^{\text{diag}} &= \frac{1}{2\Delta x \Delta y'_L} \left\{ [(h_y u)_{ne} \Delta y'_L + (h_x v)_{ne} \Delta x] \frac{u_{NE} + u_L}{2} \right. \\ &\quad + [(h_y u)_{se} \Delta y'_L - (h_x v)_{se} \Delta x] \frac{u_{SE} + u_L}{2} \\ &\quad - [(h_y u)_{sw} \Delta y'_L + (h_x v)_{sw} \Delta x] \frac{u_L + u_{SW}}{2} \\ &\quad \left. - [(h_y u)_{nw} \Delta y'_L - (h_x v)_{nw} \Delta x] \frac{u_L + u_{NW}}{2} \right\}, \end{aligned} \quad (4.95)$$

so this representation can be interpreted as momentum advection by diagonal direction velocity.

A combination of the above two representations

$$\alpha \left[ \frac{\partial}{\partial x}(h_y uu) + \frac{\partial}{\partial y}(h_x vu) \right]_L^{\text{rect}} + \beta \left[ \frac{\partial}{\partial x}(h_y uu) + \frac{\partial}{\partial y}(h_x vu) \right]_L^{\text{diag}} \quad (4.96)$$

under the condition

$$\alpha + \beta = 1 \quad (4.97)$$

is also valid. By choosing  $\alpha = 2/3$  and  $\beta = 1/3$ , the discretized representation for momentum advection conserves pseudo-*enstrophy*, similar to the *enstrophy-preserving* scheme of *Arakawa [1966]*. Here, pseudo-*enstrophy* preservation means that quantities defined by

$$\left[ \frac{1}{h_x h_y} \frac{\partial}{\partial x} (h_y v) \right]^2, \quad \left[ \frac{1}{h_x h_y} \frac{\partial}{\partial y} (h_x u) \right]^2 \quad (4.98)$$

are conserved, while *enstrophy* is the square of vorticity  $\zeta$ , which is defined by

$$\zeta = \frac{1}{h_x h_y} \left[ \frac{\partial}{\partial x} (h_y v) - \frac{\partial}{\partial y} (h_x u) \right]. \quad (4.99)$$

### 4.3 Horizontal Friction

In non-eddy-resolving cases, the standard choice for horizontal friction is the classical Laplacian (harmonic) viscosity described in section 1.2.2. Value of the horizontal viscosity coefficient is determined by a requirement from numerical stability. Horizontal friction induces a viscous boundary layer along oceanic western boundary, and its width is dependent on the viscosity coefficient. Numerical instability occurs when this viscous boundary layer is not resolved [*Bryan, 1975*]. Let  $\Delta\lambda$  be the grid width in the longitudinal direction of the geographical coordinate system. In order to avoid the numerical instability, the horizontal viscosity coefficient must satisfy

$$A_H > \beta \left( \frac{\sqrt{3}\Delta\lambda}{\pi} \right)^3, \quad (4.100)$$

where  $\beta$  is the meridional (in the geographical coordinate) derivative of the Coriolis parameter.

#### 4.3.1 Two-coefficient horizontal viscosity

The general constitutive equation for the case of horizontal-vertical transverse anisotropy is described in appendix D.4.4. *Large et al. [2001]* propose the form of

$$c_1 = A_H + B_H, \quad c_2 = 0, \quad c_3 = B_H - A_V, \quad c_5 = A_V, \quad (4.101)$$

where  $A_H$  and  $B_H$  represent two different horizontal viscosity, and  $A_V$  is vertical viscosity. It is mostly for the sake of improving representation of the Equatorial Under Current in coarse-resolution setups. The constitutive equation becomes

$$\tau_{xx} - \tau_{yy} = 2A_H(\varepsilon_{xx} - \varepsilon_{yy}), \quad (4.102)$$

$$\tau_{xy} = 2B_H\varepsilon_{xy}, \quad (4.103)$$

$$\tau_{xz} = 2A_V\varepsilon_{xz}, \quad (4.104)$$

$$\tau_{yz} = 2A_V\varepsilon_{yz} \quad (4.105)$$

instead of (1.36)–(1.39). The coefficient  $B_H$  is related to viscous western boundary layer, to which the above-mentioned criterion by *Bryan [1975]* should be applied. However, application of this criterion over the whole domain makes no sense in adopting this viscosity formulation. Its application should be limited to regions spanning by a few grids from the western boundary. The coefficient  $A_H$  cannot freely be chosen,

either, as its effect has to eliminate dispersive noise of the centered spatial differencing. It requires the grid Reynolds number, defined by  $V\Delta/A_H$  ( $V$  and  $\Delta$  are horizontal velocity and grid spacing, respectively), be less than two.

### 4.3.2 Shear-dependent viscosity coefficient

In eddy-resolving cases, a biharmonic version of Smagorinsky viscosity [Smagorinsky, 1963] is the first choice. This scheme selectively eliminates smaller scale velocity variations than harmonic and/or constant-coefficient viscosity does. The biharmonic scheme is realized by applying the harmonic scheme described in section 1.2.2 twice. Let  $B_H$  denote the coefficient for horizontal biharmonic diffusion. First, the harmonic viscosity terms  $\mathcal{V}_u$  and  $\mathcal{V}_v$  are calculated as described in section 3.3.4 (the first one of the two described methods), except that the horizontal viscosity coefficient is replaced by  $\sqrt{B_H}$ . Then, by regarding the harmonic viscosity terms as horizontal velocity components, the same procedure is repeated with the same viscosity coefficient  $\sqrt{B_H}$ . Finally, the sign is reversed. Following Griffies and Hallberg [2000], the biharmonic viscosity coefficient is determined as

$$B_H = \frac{1}{8} \left( \frac{C\Delta^2}{\pi} \right)^2 D, \quad (4.106)$$

where  $\Delta$  (spatially variable) is chosen as the smaller one of  $\Delta x$  and  $\Delta y$ , and  $D$  is defined by

$$D = \sqrt{(\varepsilon_{xx} - \varepsilon_{yy})^2 + (2\varepsilon_{xy})^2}. \quad (4.107)$$

$C$  is a nondimensional parameter, whose typical value is  $2 \sim 4$ .

## 4.4 Convection

Vertical convection, which is induced by unstable stratification, is not properly represented in OGCMs because of two reasons. One of the reasons is in the employment of the hydrostatic approximation, which separates the direct link between buoyancy and acceleration of vertical fluid motion. The second reason is related to resolution of OGCMs in actual uses. A typical horizontal scale of vertical convection, or convective plumes, is less than 1 km, which cannot be resolved by regular OGCMs for global or basin-scale modeling. So, there is a need to apply a physical parameterization to remove unstable stratification.

A classical, still widely used, method is the convective adjustment, where unstable water column is artificially homogenized with conserving heat and salt (and other tracers). There are several possible algorithms realizing the convective adjustment. One of the choices is pairwise adjustment. In the pairwise adjustment, potential density of two vertically adjacent grids is compared, and they are mixed when instability is found. For each water column, this pairwise adjustment is applied sequentially from top to bottom. Unstable stratification might not be completely removed by applying this procedure once. If complete removal is intended, the procedure should be repeated several times.

COCO employs the convective adjustment for the standard choice, but its algorithm is not the pairwise adjustment. It is summarized as follows:

1. Set the index  $K$ , indicating the starting level of the convective adjustment, to one (the top level). Set the index  $k$ , indicating the level where instability is currently judged, to two (the second level).
2. Compare potential density of the  $(k - 1)$ -th and  $k$ -th levels. The reference depth of potential density is selected at the  $k$ -th level. If instability is found, go to the step 3. If instability is not found, go to the step 4.

3. Mix the water column between the  $K$ -th level and the  $k$ -th level. Increase  $k$  by one. If the (new)  $k$ -th level is below the ocean floor, the whole procedure ends here. If not, go back to the step 2 with the new  $k$ .
4. Set  $K$  to  $k$ . Then, increase  $k$  by one. If the (new)  $k$ -th level is below the ocean floor, the whole procedure ends here. If not, go back to the step 2 with the new  $k$  and  $K$ .

When there is no heat/salt sink or source in the ocean interior nor at the ocean floor, this algorithm completely removes unstable stratification. Note that complete removal of instability in a single step is not necessarily physically plausible.

Another simple way is to enhance vertical diffusivity where stratification is unstable. This method is also prepared in the COCO model package. The enhanced value of vertical diffusivity is a model parameter, taking  $1 \text{ m}^2 \text{ s}^{-1}$  for example.

Both of the above methods are unable to represent the effect of penetrative convection. Because the actual horizontal scale of convective plumes is much less than the usual horizontal grid size of OGCMs, actual convective plumes do not lose (negative) buoyancy at the level where the convective adjustment reaches. As a result, the convective adjustment could underestimate dense water input into deep layers by overly homogenizing upper part of water columns.

## 4.5 Surface Mixed Layer

The standard surface mixed layer parameterization of COCO is based on the turbulence closure of *Noh and Kim [1999]*, which is a derivative of the level 2.5 turbulence closure of *Mellor and Yamada [1982]*. A slight modification is applied to the original parameterization. Its formulation is repeated here with the applied modification. The method of time differencing is also described.

In the level 2.5 turbulence closure, turbulent kinetic energy (TKE)  $E$  is the only prognostic variable for subgrid-scale motions, and vertical diffusivity  $K_V$  and vertical viscosity  $A_V$  are estimated as a function of TKE and other turbulence-related parameters. Time evolution of TKE is controlled by vertical diffusion, production due to vertical shear, reduction associated with vertical diffusion of buoyancy<sup>3</sup>, and dissipation:

$$\frac{\partial E}{\partial t} = \frac{\partial}{\partial z} \left( K_E \frac{\partial E}{\partial z} \right) + A_V \left[ \left( \frac{\partial u}{\partial z} \right)^2 + \left( \frac{\partial v}{\partial z} \right)^2 \right] + \frac{g}{\rho_0} K_V \frac{\partial \rho}{\partial z} - \varepsilon. \quad (4.108)$$

$K_E$  is the vertical diffusivity of TKE, and the dissipation term  $\varepsilon$  is represented by

$$\varepsilon = \frac{Cq^3}{l}, \quad (4.109)$$

where  $C$  is a constant of proportionality,  $q = \sqrt{2E}$  is the root-mean-square velocity of turbulence, and  $l$  is the turbulence length scale. Vertical diffusivity and viscosity are given by

$$A_V = Sql, \quad K_V = \frac{A_V}{P_r}, \quad K_E = \frac{A_V}{\sigma}. \quad (4.110)$$

The coefficient  $\sigma$  is a constant, taken to be 1.95. The coefficients  $S$  and  $C$  are represented by

$$S = \frac{S_0}{\sqrt{1 + \alpha R_{it}}}, \quad C = C_0 \sqrt{1 + \alpha R_{it}}, \quad (4.111)$$

---

<sup>3</sup>Vertical diffusion of buoyancy (temperature and salinity) under stable stratification increases potential energy of a water column. In the case of eddy-induced turbulent mixing, it means conversion of TKE to potential energy, so vertical diffusion of buoyancy is a sink of TKE.

where  $R_{it}$  is a turbulence Richardson number defined by

$$R_{it} = \left( \frac{Nl}{q} \right)^2 \quad (4.112)$$

and  $\alpha$  is a constant of proportionality, which is set to 3. The buoyancy frequency  $N$  is defined by

$$N^2 = -\frac{g}{\rho_0} \frac{\partial \rho}{\partial z}. \quad (4.113)$$

The values of  $S$  and  $C$  at neutral stability (the case of  $R_{it} = 0$ ) are given as  $S_0 = 0.39$  and  $C_0 = 0.06$ .

The coefficient  $P_r$  is constant in the original formulation. However, experimental and theoretical studies have indicated that  $P_r$  changes in proportion with the turbulence Richardson number in the limit of strong stratification, while it becomes almost constant for high turbulence [Baum and Caponi, 1992]<sup>4</sup>. On the other hand, observations and laboratory experiments also indicate that  $P_r$  is proportional to the (regular) Richardson number defined by

$$R_i = \frac{N^2}{(\partial u / \partial z)^2 + (\partial v / \partial z)^2} \quad (4.114)$$

when fluid is strongly stratified [Kondo et al., 1978]. Here we follow the latter formulation:

$$P_r = P_{r0} + \beta R_i, \quad (4.115)$$

where  $P_{r0} = 0.8$  and  $\beta = 7$ .

The sea surface boundary condition for TKE is given by

$$K_E \frac{\partial E}{\partial z} \Big|_{\text{surface}} = m u_*^3, \quad (4.116)$$

where the frictional velocity  $u_*$  is defined by

$$u_*^2 = \frac{\sqrt{\tau_x^2 + \tau_y^2}}{\rho_0} \quad (4.117)$$

and the constant of proportionality  $m$  is taken to be 100.

The turbulence length scale is calculated by

$$l = \frac{\kappa(d + z_0)}{1 + \kappa(d + z_0)/h}, \quad (4.118)$$

where  $\kappa = 0.4$  is the von Karman constant,  $d$  is depth from the sea surface (positive value),  $z_0$  is a roughness length scale at the sea surface, and  $h$  is depth of the sea surface mixed layer. The roughness length scale is selected to be 1 m, and the depth of the mixed layer is defined by the level above which vertical diffusivity is larger than a background value (typically of the order of  $1 \times 10^{-5} \text{ m}^2 \text{ s}^{-1}$ ).

In numerically solving (4.108), the vertical diffusion term is discretized by the backward-in-time method, as in the case of tracer diffusion and viscosity. Furthermore, the other terms in the right hand side of (4.108) also include contribution from TKE, and the simple forward-in-time discretization could induce numerical instability when the ‘‘coefficient’’ of TKE becomes very large. Since these terms are nonlinear in terms of their dependence on TKE, they are semi-implicitly discretized in time. The TKE equation (4.108) can be rewritten as

$$\frac{\partial E}{\partial t} = \frac{\partial}{\partial z} \left( K_E \frac{\partial E}{\partial z} \right) - \gamma E - \delta E, \quad (4.119)$$

<sup>4</sup>They suggest to parameterize  $P_r$  by  $\sim 1$  for  $R_{it} < 0.14$  and  $R_{it}/0.14$  for  $R_{it} > 0.14$ .

where

$$\gamma = \frac{2S_0 l}{q\sqrt{1 + \alpha R_{it}}} \left[ \frac{N^2}{P_r} - \left( \frac{\partial u}{\partial z} \right)^2 - \left( \frac{\partial v}{\partial z} \right)^2 \right] \quad (4.120)$$

$$\delta = \frac{2C_0 q \sqrt{1 + \alpha R_{it}}}{l} \quad (4.121)$$

Although the coefficients  $\gamma$  and  $\delta$  include  $q = \sqrt{2E}$ , their dependence is ignored in considering time discretization. The coefficient of the dissipation term,  $\delta$ , is always positive, and the dissipation term is always discretized by the backward-in-time method. The coefficient  $\gamma$ , on the other hand, could become negative. When it is negative, the backward-in-time method should not be used, because it underestimates growth of turbulence and results in too shallow mixed layer. Let us now consider time integration of an equation

$$\frac{\partial E}{\partial t} = -\gamma E \quad (4.122)$$

from the  $n$ -th time level to the  $(n + 1)$ -th time level. Its exact solution is

$$E^{n+1} = e^{-\gamma \Delta t} E^n. \quad (4.123)$$

In time-differencing (4.122), let us express the right hand side by a weighted average of the  $n$ -th and  $(n+1)$ -th time level values as:

$$\frac{E^{n+1} - E^n}{\Delta t} = -\gamma [(1 - \mu)E^{n+1} + \mu E^n]. \quad (4.124)$$

When the weight  $\mu$  is chosen as

$$\mu = \frac{1}{\gamma \Delta t} + \frac{e^{-\gamma \Delta t}}{e^{-\gamma \Delta t} - 1}, \quad (4.125)$$

the finite-differenced equation returns the exact solution. Therefore, the second term of the right hand side of (4.119) is time-differenced in this way. Although this expression is valid for any  $\gamma$  other than zero, there is a problem in actual computation when  $\gamma$  is a large negative number. In that case, it is all right to simply solve this term by the forward-in-time method.

The turbulence closure scheme is applicable not only to the surface mixed layer but also to the bottom boundary layer. However, its application should be accompanied by fine vertical resolution. Otherwise, shear-induced TKE production is not properly represented. Since COCO is a  $z$  coordinate OGCM, where fine vertical resolution near the ocean floor of changing depths means fine vertical resolution all the way from top to bottom, the bottom boundary layer is separately dealt with by a different parameterization. Therefore, it is reasonable to limit the application of the turbulence closure scheme to upper several hundred meters and reduce computational cost.

## 4.6 Background Vertical Diffusivity

Vertical diffusivity in the ocean interior, where its value is not controlled by boundary layer processes, is often called background vertical diffusivity<sup>5</sup>. It is one of the most crucial parameters in OGCMs, controlling thermocline depth and deep meridional overturning circulation, for example. The source of background vertical diffusivity is considered to be breaking of internal waves. Internal waves are, on the other hand, generated by wind-induced turbulence at the sea surface, internal tides on the ocean floor (especially for rough bottom), and various kinds of dynamical instability (e.g., Kelvin-Helmholtz instability). Therefore,

<sup>5</sup>Strictly speaking, the word ‘‘vertical’’ should be replaced by ‘‘diapycnal,’’ as what really affect thermocline or deep meridional overturning circulation is diapycnal buoyancy flux.

vertical diffusivity is expected to be spatially (and also temporally) inhomogeneous, and observations have actually shown that it is the case. However, its actual distribution is still largely unknown. Note that a region of strong internal wave generation does not necessarily coincide with that of high vertical diffusivity, as internal waves could propagate a long distance before breaking. Since wave breaking is highly associated with vertical stratification, background vertical diffusivity is sometimes parameterized as a function of the buoyancy frequency (inversely proportional to it, for example).

In the standard setup of COCO, a vertical profile is prescribed for background vertical diffusivity, and its horizontal variation is not taken into account. For global ocean modeling, an empirical vertical profile of *Tsujino et al. [2000]* is usually used. The profile is given by

$$\begin{aligned} 0.1 + 0.9 \times \left( 1 + \tanh \frac{-z - 1500}{750} \right) & \text{ for } z > -1500, \\ -1 + 2 \times \left( 1 + \tanh \frac{-z - 1500}{2000} \right) & \text{ for } z < -1500, \end{aligned} \quad (4.126)$$

where the depth  $z$  (negative) is measured in meters, and the unit of the resulting vertical diffusivity is  $10^{-4} \text{ m}^2 \text{ s}^{-1}$ . Between  $30^\circ\text{N}$  and  $30^\circ\text{S}$ , this background diffusivity is multiplied by the factor of

$$\frac{|f| \cosh^{-1}(N/|f|)}{f_{30} \cosh^{-1}(N_0/f_{30})}, \quad (4.127)$$

following the finding by *Gregg et al. [2003]* that the dissipation rate is reduced in this manner at low latitudes. Here,  $f$  is the Coriolis parameter and  $f_{30}$  is its value at  $30^\circ\text{N}$ ; and  $N$  is the buoyancy frequency and  $N_0 = 5.24 \times 10^{-3} \text{ s}^{-1}$  is its value for the reference stratification assumed in the internal wave model of *Garret and Munk [1975]*. Although the above described function is for the dissipation rate, it is applied directly to vertical diffusivity in COCO. Furthermore,  $N$  is replaced by  $N_0$ , thus making this multiplied factor known *a priori*.

## 4.7 Bottom Boundary Layer

COCO incorporates the bottom boundary layer (BBL) parameterization of *Nakano and Suginozono [2002]*. It assumes a layer of constant depth at the bottom of each water column, and horizontal transfer of momentum and tracers are realized between those BBL grids. Since the bottom boundary layer exists along the ocean floor, its formulation should be based on a terrain-following coordinate system.

Let us consider a  $\sigma$  coordinate system with its base chosen as the ocean floor. Variables and symbols are defined in section 1.1, except for the definition of  $\sigma$ . It is now defined by

$$\sigma = \frac{z^* + H}{\eta + H}. \quad (4.128)$$

Spatial partial derivatives are converted as

$$\frac{\partial \psi^*}{\partial x^*} = \frac{\partial \psi}{\partial x} + \frac{1}{\eta + H} \frac{\partial \psi}{\partial \sigma} \left[ (1 - \sigma) \frac{\partial H}{\partial x} - \sigma \frac{\partial \eta}{\partial x} \right], \quad (4.129)$$

$$\frac{\partial \psi^*}{\partial y^*} = \frac{\partial \psi}{\partial y} + \frac{1}{\eta + H} \frac{\partial \psi}{\partial \sigma} \left[ (1 - \sigma) \frac{\partial H}{\partial y} - \sigma \frac{\partial \eta}{\partial y} \right], \quad (4.130)$$

$$\frac{\partial \psi^*}{\partial z^*} = \frac{1}{\eta + H} \frac{\partial \psi}{\partial \sigma}, \quad (4.131)$$

so the hydrostatic equation is represented by

$$0 = -\frac{1}{\eta + H} \frac{\partial P}{\partial \sigma} - \rho g. \quad (4.132)$$

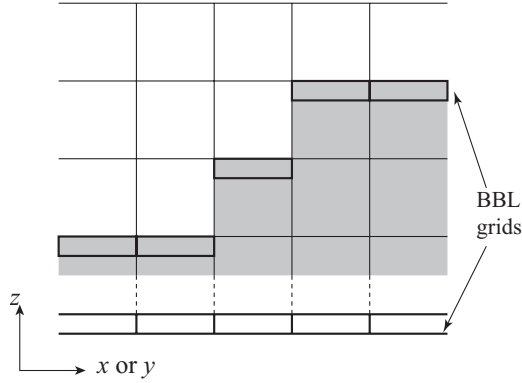


Figure 4.4: Grid configuration for the bottom boundary layer parameterization.

Thus, the horizontal pressure gradient is converted as

$$\frac{\partial P}{\partial x} \rightarrow \frac{\partial P}{\partial x} + \rho g \left[ \sigma \frac{\partial \eta}{\partial x} + (\sigma - 1) \frac{\partial H}{\partial x} \right], \quad (4.133)$$

$$\frac{\partial P}{\partial y} \rightarrow \frac{\partial P}{\partial y} + \rho g \left[ \sigma \frac{\partial \eta}{\partial y} + (\sigma - 1) \frac{\partial H}{\partial y} \right]. \quad (4.134)$$

The ocean floor is represented by  $\sigma = 0$ . For the bottom boundary layer calculation, therefore, the right hand sides of the momentum equations (1.1) and (1.2) are replaced by

$$-\frac{1}{\rho_0 h_x} \left[ \frac{\partial P}{\partial x} - \rho g \frac{\partial H}{\partial x} \right] + \mathcal{V}_u, \quad (4.135)$$

$$-\frac{1}{\rho_0 h_y} \left[ \frac{\partial P}{\partial y} - \rho g \frac{\partial H}{\partial y} \right] + \mathcal{V}_v, \quad (4.136)$$

respectively. Note that the terms  $\partial P/\partial x$  and  $\partial P/\partial y$  are calculated in the  $\sigma$  coordinate system. So, in their discretized representations, the four grid point values of pressure used in (3.114) and (3.115) are estimated at different levels when the bottom level is different among them. Newtonian drag terms,  $-\alpha u$  and  $-\alpha v$ , are also added to these right hand sides. These Newtonian drag terms represent the effect of baroclinic eddies which allows flows on a slope to deviate from geostrophic contours (lines of constant  $f/H$ ). The coefficient  $\alpha$  is chosen to be identical to  $f$ , as numerical and laboratory experiments indicate that the direction of down-sloping flows is inclined by the angle of  $45^\circ$  against geostrophic contours.

Vertical diffusion and viscosity coefficients at the top of the BBL grids are specified independently of their background values. Larger values are specified for them to represent the effect of entrainment taking place at the top of the boundary layer.

In COCO the BBL variables are stored in two ways, as illustrated in Figure 4.4. The bottom-most grids of the three-dimensional arrays for the velocity components and tracers are used exclusively for the BBL parameterization. The BBL variables are stored in those bottom-most grids and also just below the bottom of the regular (non-BBL) grids. Horizontal transfer of momentum and tracers is calculated by using the values stored in the former, and vertical transfer is done by using the latter. Diagnostic calculation of vertical velocity is started from the bottom-most BBL grids and proceeds upward irrespective of whether the grid is above or below the ocean floor. In this calculation, the horizontal velocity components of the BBL grids just below the regular grids are set to zero. Since the horizontal velocity components of land grid points are zero, this procedure gives the correct BBL vertical velocity for both of the BBL storages. Note that the BBL grids are not necessarily defined at all the horizontal points.

## 4.8 Isopycnal Diffusion

The diffusion term appearing in the tracer equations does not represent the molecular diffusion but effects of unresolved-scale motions. Such unresolved-scale motions are often called symbolically as eddies. Owing to the large aspect ratio of the ocean and the existence of stratification, motions of such eddies occur primarily on horizontal planes. When the diffusion term is represented by (1.33), therefore, horizontal diffusivity is chosen to be much larger than vertical diffusivity. Tracers in the ocean are actually well mixed in the horizontal direction as compared with the vertical direction. A closer look of eddy-induced mixing of tracers reveals that eddies mix tracers along isopycnal surfaces rather than horizontal planes. When an isopycnal surface is significantly<sup>6</sup> inclined against the horizontal direction, large horizontal diffusivity could induce diapycnal diffusivity larger than a background value. Such a situation is not favorable in using OGCMs. Large diffusivity should be applied selectively to isopycnal directions.

Since COCO is formulated under the  $z$  vertical coordinate system, diffusive tracer fluxes along isopycnal surfaces should be remapped to fluxes in the  $x$ ,  $y$  and  $z$  directions, which is realized by coordinate system rotation. In its formulation, COCO adopts the method (and approximation) of *Cox [1987]*. Slope of isopycnal surface in the  $x$  and  $y$  directions is given by

$$s_x = -\frac{1}{h_x} \frac{\partial \rho}{\partial x} \bigg/ \frac{\partial \rho}{\partial z}, \quad s_y = -\frac{1}{h_y} \frac{\partial \rho}{\partial y} \bigg/ \frac{\partial \rho}{\partial z}, \quad (4.137)$$

respectively, and the rotation matrix becomes

$$\begin{pmatrix} 1 & 0 & s_x \\ 0 & 1 & s_y \\ s_x & s_y & s_x^2 + s_y^2 \end{pmatrix}. \quad (4.138)$$

Let  $K_I$  be a coefficient for isopycnal diffusion. Diffusive fluxes of tracer  $T$  in the  $x$ ,  $y$  and  $z$  directions are represented by

$$x : \quad K_I \left( \frac{1}{h_x} \frac{\partial T}{\partial x} + s_x \frac{\partial T}{\partial z} \right), \quad (4.139)$$

$$y : \quad K_I \left( \frac{1}{h_y} \frac{\partial T}{\partial y} + s_y \frac{\partial T}{\partial z} \right), \quad (4.140)$$

$$z : \quad K_I \left[ \frac{s_x}{h_x} \frac{\partial T}{\partial x} + \frac{s_y}{h_y} \frac{\partial T}{\partial y} + (s_x^2 + s_y^2) \frac{\partial T}{\partial z} \right] \quad (4.141)$$

instead of (1.32), so the diffusion term becomes

$$\begin{aligned} \mathcal{D}_T = & \frac{1}{h_x h_y} \left\{ \frac{\partial}{\partial x} \left[ h_y K_I \left( \frac{1}{h_x} \frac{\partial T}{\partial x} + s_x \frac{\partial T}{\partial z} \right) \right] + \frac{\partial}{\partial y} \left[ h_x K_I \left( \frac{1}{h_y} \frac{\partial T}{\partial y} + s_y \frac{\partial T}{\partial z} \right) \right] \right\} \\ & + \frac{\partial}{\partial z} \left\{ K_I \left[ \frac{s_x}{h_x} \frac{\partial T}{\partial x} + \frac{s_y}{h_y} \frac{\partial T}{\partial y} + (s_x^2 + s_y^2) \frac{\partial T}{\partial z} \right] \right\} \end{aligned} \quad (4.142)$$

instead of (1.33). The background vertical diffusion term is added to it. Regular horizontal diffusion could also be added to it.

A large isopycnal slope means large effective vertical diffusivity. Although the vertical diffusion is implicitly solved, excessively large vertical diffusivity could induce a numerical problem. To avoid it, isopycnal slope is bounded by a prescribed value, which is typically chosen as 0.01.

<sup>6</sup>The ‘‘significance’’ may be judged, for example, against the aspect ratio of the ocean, which is of the order of  $10^4$  or larger. By this standard, an angle  $\theta$  is significantly large when  $\tan \theta > 10^{-4}$ .

## 4.9 Isopycnal Layer Thickness Diffusion

Under horizontal resolution of  $\sim 1^\circ$  or coarser, mesoscale eddies are the primary contributor to isopycnal mixing. However, isopycnal diffusion of tracers described in section 4.8 is not sufficient for representing the effects of mesoscale eddies on tracer distribution. Mesoscale eddies are generated principally by baroclinic instability, which occurs where isopycnal surfaces are steeply sloping. As a result of tracer transport induced by those eddies, slope of the isopycnal surfaces is reduced. One possible way to parameterize such an effect of mesoscale eddies is to consider diffusion of isopycnal layer thickness (vertical distance between two isopycnal surfaces) in the direction of isopycnal surfaces [Gent and McWilliams, 1990].

In the  $z$  vertical coordinate system, isopycnal diffusion of isopycnal layer thickness is represented either by bolus velocity [Gent and McWilliams, 1990] or by a skew component of the diffusion coefficient tensor [Griffies, 1998]. COCO adopts the latter method, which is very easily implemented once the isopycnal diffusion scheme is introduced. The diffusion coefficient tensor of the isopycnal diffusion scheme is the product of  $K_I$  and (4.138). Let  $K_G$  be the diffusion coefficient for the layer thickness diffusion. The combined coefficient tensor of the isopycnal diffusion and layer thickness diffusion becomes

$$\begin{pmatrix} K_I & 0 & (K_I - K_G)s_x \\ 0 & K_I & (K_I - K_G)s_y \\ (K_I + K_G)s_x & (K_I + K_G)s_y & K_I(s_x^2 + s_y^2) \end{pmatrix}. \quad (4.143)$$

In the bolus velocity method, on the other hand, tracers are advected by the sum of large scale velocity (represented by the regular velocity components appearing in the primitive equations) and bolus velocity. Let  $u^*$ ,  $v^*$  and  $w^*$  denote  $x$ ,  $y$  and  $z$ , respectively, components of the bolus velocity. They are defined by

$$u^* = -\frac{\partial}{\partial z}(K_G s_x), \quad (4.144)$$

$$v^* = -\frac{\partial}{\partial z}(K_G s_y), \quad (4.145)$$

$$w^* = \frac{1}{h_x h_y} \left[ \frac{\partial}{\partial x}(h_y K_G s_x) + \frac{\partial}{\partial y}(h_x K_G s_y) \right]. \quad (4.146)$$

It is easy to see that the bolus velocity satisfies the continuity equation:

$$\frac{1}{h_x h_y} \left[ \frac{\partial}{\partial x}(h_y u^*) + \frac{\partial}{\partial y}(h_x v^*) \right] + \frac{\partial w^*}{\partial z} = 0, \quad (4.147)$$

and it is also easy to see that the two methods give the same result:

$$\text{div} \begin{pmatrix} 0 & 0 & -K_G s_x \\ 0 & 0 & -K_G s_y \\ K_G s_x & K_G s_y & 0 \end{pmatrix} \begin{pmatrix} \frac{1}{h_x} \frac{\partial \psi}{\partial x} \\ \frac{1}{h_y} \frac{\partial \psi}{\partial y} \\ \frac{\partial \psi}{\partial z} \end{pmatrix} = -\frac{1}{h_x h_y} \left[ \frac{\partial}{\partial x}(h_y u^* \psi) + \frac{\partial}{\partial y}(h_x v^* \psi) \right] - \frac{\partial}{\partial z}(w^* \psi), \quad (4.148)$$

where  $\psi$  stands for a tracer quantity.



# Appendix A

## Sea Surface Forcing

OGCMs are driven by fluxes of momentum ( $\tau_x$  and  $\tau_y$ ), heat ( $F_H$ ) and freshwater ( $F_W$ ) at the sea surface, as described in section 1.3. There are several possible methods to impose these fluxes, and the ways adopted in COCO are described below. These fluxes are closely linked to sea ice where it exists, and their formulation is heavily dependent on how sea ice is dealt with. Issues related to sea ice is not mentioned here but in appendix B.

### A.1 Heat Flux

#### A.1.1 Sea Surface Temperature Restore

A classical and one of the easiest way to specify sea surface heat flux is Newtonian damping of model sea surface temperature to observed values. Let  $T_1$  be temperature of the model's top level and  $T_*$  be observed sea surface temperature to which  $T_1$  is restored. Sea surface heat flux  $F_H$  is estimated by

$$\frac{F_H}{\rho_0 C_p} = \frac{(T_1 - T_*) \Delta z_1}{\tau_R}, \quad (\text{A.1})$$

where  $\Delta z_1$  is the thickness of the model's top level, and  $\tau_R$  is a time constant for restoring. An actual value for  $\tau_R$  should depend on  $\Delta z_1$ , and a typical choice is to make them satisfy  $\Delta z_1 / \tau_R = 1 \text{ m dy}^{-1}$ . Time discretization for the heat flux term is done by the forward-in-time method, which means that  $T_1^{n-1}$  is used when temperature is predicted from the  $(n-1)$ -th time level to the  $(n+1)$ -th time level. Use of the leap-frog method ( $T_1^n$ ) would lead to numerical instability.

There are some fundamental problems in this method. First and foremost, although it is intended to reproduce the specified sea surface temperature  $T_*$ , the model sea surface temperature  $T_1$  never realize it. If  $T_1$  exactly coincides with  $T_*$ ,  $F_H$  becomes zero everywhere, which means that the model ocean is not thermally forced. Related to this problem, there is no experimental or observational way to determine a *physically valid* value for  $\tau_R$ .

As described later, however, the same procedure is also applicable to a more physically plausible representation of sea surface heat flux. In COCO, the default setup for the sea surface heat flux calculation is this restoring method, where horizontal distributions (and their temporal variations) of  $T_*$  and  $\tau_R$  are prescribed. When a sea ice model is coupled, the next method is used normally.

### A.1.2 Using Surface Air Properties and Bulk Formulae

Sea surface heat flux  $Q$  is decomposed into four parts as

$$Q = Q_{SW} + Q_{LW} + Q_{SH} + Q_{LH}, \quad (\text{A.2})$$

where the terms in the right hand side stand for shortwave radiative flux, longwave radiative flux, sensible heat flux, and latent heat flux, respectively<sup>1</sup>. Shortwave and longwave radiative fluxes are further decomposed into upward (denoted by the superscript  $u$ ) and downward (denoted by the superscript  $d$ ) parts:

$$Q_{SW} = Q_{SW}^u + Q_{SW}^d, \quad (\text{A.3})$$

$$Q_{LW} = Q_{LW}^u + Q_{LW}^d. \quad (\text{A.4})$$

Note that the sign for all of these flux components is defined as upward positive, thus the downward radiative fluxes are always negative and the upward radiative fluxes are always positive.

Downward radiative fluxes are not directly dependent on the condition of the sea surface, and their observed values are simply specified to drive the model. Shortwave emission from the sea surface is negligible, so the upward part of the shortwave radiative flux is accounted for solely by reflection of the incoming downward flux. Let  $\alpha_S$  be the sea surface albedo for shortwave radiation. The upward shortwave radiative flux is represented by

$$Q_{SW}^u = -\alpha_S Q_{SW}^d. \quad (\text{A.5})$$

On the other hand, the upward longwave radiative flux has both reflection of the incoming flux and emission from the sea surface. Let  $\alpha_L$  be the sea surface albedo for longwave radiation and  $\varepsilon_L$  be emissivity of the sea surface relative to the black body radiation. The upward longwave radiative flux is represented by

$$Q_{LW}^u = -\alpha_L Q_{LW}^d + \varepsilon_L \sigma T_S^4, \quad (\text{A.6})$$

where  $\sigma$  is the Stefan-Boltzmann constant and  $T_S$  is sea surface temperature.  $T_S$  is given by  $T_1$  when there is no sea ice, and by snow or sea ice surface temperature when it exists. When radiative equilibrium is assumed, emissivity becomes identical to coalbedo:

$$\varepsilon_L = 1 - \alpha_L. \quad (\text{A.7})$$

By use of a bulk formula, sensible heat flux is calculated from sea surface temperature and surface air temperature. It is generally represented by

$$Q_{SH} = \rho_A C_A C_S (T_S - T_A), \quad (\text{A.8})$$

where  $\rho_A$  and  $T_A$  are surface air density and temperature, respectively, measured at several meters above the sea surface, for example, and  $C_A$  is the heat capacity of air. The coefficient  $C_S$  is a function of surface air conditions and has the dimension of length per time. Latent heat flux is also calculated by using a bulk formula as

$$Q_{LH} = \rho_A L C_L (q_S - q_A), \quad (\text{A.9})$$

where  $q_A$  is surface air specific humidity and  $q_S$  is sea surface specific humidity.  $L$  stands for the latent heat of evaporation when the surface is liquid, and for the latent heat of sublimation when the surface is solid.

---

<sup>1</sup>The symbol  $Q$  is employed here instead of  $F_H$  to avoid confusion in appendix B.  $Q$  calculated here is given as  $F_H$  in (1.58) when there is no sea ice.

The coefficient  $C_L$  also depends on surface air conditions and has the dimension of length per time. Sea surface specific humidity is estimated as saturation specific humidity of air at sea surface temperature:

$$q_S = q_{\text{sat}}(T_S), \quad (\text{A.10})$$

where  $q_{\text{sat}}$  represents saturation specific humidity as a function of temperature<sup>2</sup>. It is sometimes multiplied by a factor slightly smaller than unity.

As a whole, sea surface heat flux  $Q$  is obtained as follows when  $Q_{SW}^d$ ,  $Q_{LW}^d$ ,  $T_A$ ,  $q_A$  and  $T_S$  are specified:

$$Q = (1 - \alpha_S)Q_{SW}^d + \varepsilon_L(Q_{LW}^d + \sigma T_S^4) + \rho_A C_A C_S (T_S - T_A) + \rho_A L C_L (q_{\text{sat}}(T_S) - q_A). \quad (\text{A.11})$$

Note that surface wind velocity is usually required to estimate  $C_S$  and  $C_L$ . As in the case of the Newtonian damping, time level for  $T_S$  should be chosen so that the forward-in-time method is realized.

Representation of  $C_S$  and  $C_L$  as functions of surface air conditions is not unique. Several datasets are provided to force OGCMs, and each dataset has its own relevant set of bulk formulae. For example, a climatological dataset compiled by *Röske [2001]* requires the bulk formulae of *Kara et al. [2000]*, while another dataset by *Large and Yeager [2004]* does a different one (described therein).

While incoming downward longwave radiation is completely absorbed within a very thin surface layer, shortwave radiation can penetrate significantly into depths. In order to take account of its effect, shortwave radiative flux at an arbitrary depth in the ocean is parameterized by

$$I(z) = I(0) \left[ R e^{z/\zeta_1} + (1 - R) e^{z/\zeta_2} \right], \quad (\text{A.12})$$

as done by *Rosati and Miyakoda [1988]*, where  $I(0) = (1 - \alpha_S)Q_{SW}^d$  is its value at  $z = 0$ . Here, shortwave radiation is split into two portions: one is a fast-attenuating spectral portion and the other is a deeply penetrating spectral portion, and these two portions attenuate with length scales of  $\zeta_1$  and  $\zeta_2$ , respectively. The fraction of the fast-attenuating portion is represented by  $R$ . These parameters depend on turbidity of seawater (such as phytoplankton concentration) and also on a spectrum of shortwave radiation.

### A.1.3 Bulk Formula-Based Sea Surface Temperature Restore

Sea surface heat flux is nonlinearly dependent on sea surface temperature in (A.11). When it is linearized around  $T_S$ , it can be written in the form of

$$F_H = \gamma(T_S - T_A^*), \quad (\text{A.13})$$

as described by *Haney [1971]*. When a dataset required for (A.11) is specified,  $\gamma$  and  $T_A^*$  are uniquely determined. This representation is formally identical to (A.1): just replacing  $\tau_R$  and  $T_*$  by  $\rho_0 C_p \Delta z_1 / \gamma$  and  $T_A^*$ , respectively, results in (A.13).

## A.2 Freshwater Flux

### A.2.1 Sea Surface Salinity Restore

OGCMs in early times are formulated under the rigid lid approximation, where sea level is not allowed to change. Volume of seawater is not allowed to change in such OGCMs, so sea surface salinity is directly modified by taking account of virtual salt flux. The easiest and most widely used way to specify virtual salt

<sup>2</sup>Saturation specific humidity depends also on pressure.

flux is Newtonian damping of sea surface salinity to observed values, as in the case of heat flux. Let  $S_1$  be salinity of the model's top level and  $S_*$  be observed sea surface salinity to which  $S_1$  is restored. Virtual sea surface salinity flux  $F_S$  is estimated by

$$F_S = \frac{(S_1 - S_*)\Delta z_1}{\tau_R}, \quad (\text{A.14})$$

and it is applied as a surface boundary condition for salinity equation:

$$\left. \frac{\partial S}{\partial z} \right|_{\text{surface}} = -F_S. \quad (\text{A.15})$$

The time constant is usually chosen to be the same as in heat flux. The time discretization method should also follow that of heat flux.

This sea surface salinity restore method can also be applied to free surface OGCMs, either as virtual salinity flux or as equivalent freshwater flux, the latter of which is the default method adopted in COCO when sea ice is not coupled. In the former method,  $S_1$  is directly changed with setting sea surface freshwater flux to zero. For the latter method, equivalent freshwater flux  $F_W$  is obtained by

$$F_W = -\frac{F_S}{S_1}, \quad (\text{A.16})$$

and sea level and sea surface salinity are modified at the same time in a consistent way. The sign of  $F_W$  is so defined that sea level is lowered when  $F_W > 0$ , as in section 3.2.3. There is no guarantee that long-term mean of globally averaged  $F_W$  becomes zero, so mean sea level of model ocean could increase or decrease unboundedly in the course of model integration. In order to avoid this drift,  $F_W$  should be adjusted so that its global average becomes zero at every time step, for example.

The problems noted above for the sea surface temperature restore are also true for the sea surface salinity restore. Furthermore, the actual sea surface freshwater flux does not directly depend on sea surface salinity, while the restoring method makes them directly related.

### A.2.2 Drive Directly by Freshwater Flux

The actual sea surface freshwater flux is made up of evaporation (or sublimation), precipitation, and runoff from land. Evaporation could be either prescribed by observation or calculated in a way consistent with (A.9). In the latter case, the evaporative freshwater flux is represented by  $Q_{LH}/L$ . Precipitation and runoff does not directly depend on sea surface condition, so they should be simply prescribed. In this case, too, long-term mean of globally averaged  $F_W$  does not become zero in general, so it must be adjusted somehow to avoid model drift.

Since sea surface freshwater flux thus specified is not directly related to seawater salinity, its direct application could result in severe drift of simulated salinity. For the purpose of preventing such drift, weak restore of sea surface salinity to observed values is sometimes applied in conjunction with observation-based freshwater flux.

## A.3 Momentum Flux

Sea surface momentum flux is often referred to as surface wind stress. The most widely adopted way to dynamically drive OGCMs is to directly specify a dataset of surface wind stress, and it is the default setup of COCO.

When a dataset of surface winds is specified, on the other hand, surface wind stress is calculated by using a bulk formula, as in the case of sensible and latent heat fluxes. It is generally represented by

$$(\tau_x, \tau_y) = \rho_A C_M(u_A, v_A), \quad (\text{A.17})$$

where  $u_A$  and  $v_A$  are  $x$  and  $y$  components, respectively, of surface winds. The coefficient  $C_M$  has the dimension of length per time, and is usually regarded as proportional to scalar wind speed:

$$C_M = C_{M0} \sqrt{u_A^2 + v_A^2}, \quad (\text{A.18})$$

where  $C_{M0}$  is a nondimensional coefficient, dependent on surface air conditions in usual bulk formulae. The coefficients  $C_S$  and  $C_L$  in (A.8) and (A.9) are usually expressed in such a way, too.



# Appendix B

## Coupling to Sea Ice Model

For the purpose of global ocean modeling, COCO is coupled to a sea ice model in most cases. A relatively simple sea ice model actually used in such cases is described here. It is based on two-category thickness representation, zero-layer thermodynamics [e.g., Semtner, 1976], and dynamics with elastic-viscous-plastic rheology [Hunke and Dukowicz, 1997].

There are five prognostic variables in the sea ice model described herein: sea ice concentration  $A_I$ , which is area fraction of a grid covered by sea ice and takes a value between zero and unity; mean sea ice thickness  $h_I$  over ice-covered part of a grid; mean snow thickness  $h_S$  over sea ice; and  $x$  and  $y$  direction horizontal velocity components of sea ice motion  $u_I$  and  $v_I$ . The model calculates temperature at snow top (sea ice top when there is no snow cover)  $T_I$ , which is a diagnostic variable. Density of sea ice ( $\rho_I$ ) and snow ( $\rho_S$ ) are assumed to be constant. Sea ice is assumed to have nonzero salinity, and its value  $S_I$  is assumed to be a constant parameter.

### B.1 Thermodynamics

Let us consider here a case that the model is integrated from the  $n$ -th time level to the  $(n + 1)$ -th time level.  $A_I$ ,  $h_I$  and  $h_S$  are incrementally modified in the following order. See Figure B.1 for a schematic illustration of related variables and heat fluxes.

#### B.1.1 Heat Flux and Growth Rate

Temperature at sea ice base is taken to be the ocean model's top level temperature  $T_1$ . In this model, sea ice exists only when and where  $T_1$  is at the freezing point  $T_f$ , which is a decreasing function of salinity ( $T_f = -0.0543S$  is used in COCO, where temperature and salinity are measured by  $^{\circ}\text{C}$  and psu, respectively). In heat budget calculation for snow and sea ice, only latent heat of fusion and sublimation is taken into account, and heat content associated with temperature is neglected. Therefore, temperature inside sea ice and snow are not calculated, and  $T_I$  is estimated from surface heat balance.

Nonzero minimum values are prescribed for  $A_I$  and  $h_I$ , which are denoted by  $A_I^{\min}$  and  $h_I^{\min}$ , respectively. These parameters define a minimum possible volume of sea ice in a grid. If a predicted volume  $A_I h_I$  is less than that minimum,  $A_I$  is reset to zero, and  $T_1$  is lowered to compensate the corresponding latent heat. In this case, the ocean model's top level is kept at a supercooled state. Such a state continues until the ocean is further cooled and the temperature becomes low enough to produce more sea ice than that minimum by releasing the latent heat corresponding to the supercooling.

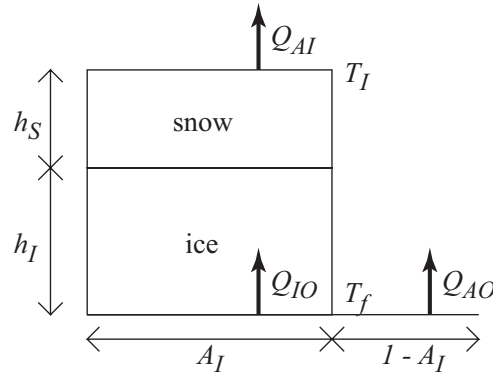


Figure B.1: Sea ice variables and heat fluxes.

Surface heat flux is separately calculated for each of air-sea and air-ice interfaces in one grid. Let us define  $Q_{AI}$  by

$$Q_{AI} = A_I Q, \quad (\text{B.1})$$

i.e., air-ice heat flux multiplied by the factor of sea ice concentration.  $Q$  is calculated by (A.11) by setting  $T_S = T_I$  and using relevant values for the parameters therein. Penetration of shortwave radiation is not taken into account for ice-covered region. Assuming constant heat conductivity, vertical temperature profile in sea ice and snow is linear, so vertical heat flux through sea ice and snow, multiplied by the factor of sea ice concentration, is

$$Q_{IO} = A_I \frac{k_I k_S (T_1 - T_I)}{k_I h_S + k_S h_I}, \quad (\text{B.2})$$

where  $k_I$  and  $k_S$  are heat conductivity for sea ice and snow, respectively.  $T_I$  is determined such that

$$Q_{AI} = Q_{IO} \quad (\text{B.3})$$

is satisfied. However, when the estimated  $T_I$  exceeds the melting point of sea ice  $T_m$  (which is set to  $0^\circ\text{C}$  for convenience),  $T_I$  is reset to  $T_m$ , and  $Q_{AI}$  and  $Q_{IO}$  are re-estimated by using it. The heat imbalance between  $Q_{AI}$  and  $Q_{IO}$  is consumed to melt snow (sea ice when there is no snow cover). Snow growth rate due to this heat imbalance is estimated by

$$W_{AS} = \frac{Q_{AI} - Q_{IO}}{\rho_O L_f}, \quad (\text{B.4})$$

where  $\rho_O$  is density of seawater and  $L_f$  is the latent heat of fusion (the same value is applied to snow and sea ice). This growth rate is expressed as a change of equivalent liquid water depth per unit time. It is zero when  $T_I < T_m$  and negative when  $T_I = T_m$ . Note that  $W_{AS}$  is weighted by sea ice concentration.

Although it is assumed that  $T_1 = T_f$  when sea ice exists,  $T_1$  could deviated from  $T_f$  due to a change of salinity or other factors. Such deviation should be adjusted by forming or melting sea ice. Under a temperature deviation

$$\Delta T = T_1 - T_f, \quad (\text{B.5})$$

sea ice growth rate necessary to compensate it in a single time step is given by

$$W_{FZ} = -\frac{C_p \Delta T \Delta z_1}{L_f \Delta t}, \quad (\text{B.6})$$

where  $C_p$  is the heat capacity of seawater and  $\Delta z_1$  is the thickness of the ocean model's top level. This growth rate is estimated at all grids, irrespective of sea ice existence, for a technical reason. As described below,

this growth rate first estimates negative ice volume for ice-free grids, but the same heat flux calculation procedure as for ice-covered grids finally results in the correct heat flux to force the ocean. Basal growth rate of sea ice is given by

$$W_{IO} = A_I W_{FZ} + \frac{Q_{IO}}{\rho_O L_f}, \quad (\text{B.7})$$

where, again,  $W_{IO}$  is weighted by sea ice concentration.

Sea ice formation could also occur in ice-free area. Let us define  $Q_{AO}$  by

$$Q_{AO} = (1 - A_I) [Q - (1 - \alpha_S) Q_{SW}^d], \quad (\text{B.8})$$

i.e., air-sea heat flux except for shortwave, multiplied by the factor of the fraction of ice-free area. Here,  $Q$  is calculated by (A.11) by setting  $T_S = T_1$ . Shortwave radiation absorbed at ice-free sea surface, with the factor of ice-free area multiplied, is represented by

$$Q_{SW}^A = (1 - A_I)(1 - \alpha_S) Q_{SW}^d. \quad (\text{B.9})$$

Sea ice growth rate in ice-free area is calculated by

$$W_{AO} = (1 - A_I) W_{FZ} + \frac{Q_{AO} + c_1 Q_{SW}^A}{\rho_O L_f}, \quad (\text{B.10})$$

where  $c_1$  denotes the fraction of  $Q_{SW}^A$  absorbed by the ocean model's top level, which is calculated from (A.12) as

$$c_1 = \frac{I(0) - I(-\Delta z_1)}{I(0)}. \quad (\text{B.11})$$

The growth rate  $W_{AO}$  is weighted by the fraction of ice-free area.

### B.1.2 Sublimation of Sea Ice

Sublimation (freshwater) flux  $F_W^{SB}$  is calculated or prescribed over ice cover. In the model, it is also weighted by sea ice concentration. For example, when it is calculated in a way consistent with surface latent heat flux  $Q_{LH}$ , it is given by

$$F_W^{SB} = \frac{A_I Q_{LH}}{\rho_O L_s}, \quad (\text{B.12})$$

where  $L_s$  is the latent heat of sublimation, which is the sum of the latent heat of fusion and evaporation. Its sign is defined such that snow or ice is reduced when  $F_W^{SB} > 0$ . Evaporation (freshwater) flux  $F_W^{EV}$  is also weighted by the fraction of ice-free area. For the same example as the above, it is given by

$$F_W^{EV} = \frac{(1 - A_I) Q_{LH}}{\rho_O L_e}, \quad (\text{B.13})$$

where  $L_e$  is the latent heat of evaporation.

Sublimation flux is first consumed to reduce snow thickness:

$$h'_S = h_S^n - \frac{\rho_O F_W^{SB} \Delta t}{\rho_S A_I^n}. \quad (\text{B.14})$$

If  $h'_S$  becomes less than zero, it is reset to zero. Then,  $F_W^{SB}$  is redefined by

$$F_W^{SB'} = F_W^{SB} + \frac{\rho_S A_I^n (h'_S - h_S^n)}{\rho_O \Delta t}. \quad (\text{B.15})$$

When there remains snow,  $F_W^{SB'} = 0$ . Nonzero  $F_W^{SB'}$  is then consumed to reduce sea ice thickness:

$$h'_I = h_I^n - \frac{\rho_O F_W^{SB'} \Delta t}{\rho_I A_I^n}. \quad (\text{B.16})$$

If  $h'_I$  becomes less than  $h_I^{\min}$ , it is reset to  $h_I^{\min}$ . Then,  $F_W^{SB}$  is redefined by

$$F_W^{SB''} = F_W^{SB'} + \frac{\rho_I A_I^n (h'_I - h_I^n)}{\rho_O \Delta t}. \quad (\text{B.17})$$

Finally, nonzero  $F_W^{SB''}$  is consumed to reduce sea ice concentration:

$$A'_I = A_I^n - \frac{\rho_O F_W^{SB''} \Delta t}{\rho_I h_I^{\min}}. \quad (\text{B.18})$$

If  $A'_I$  becomes less than zero, it is reset to zero. Even if  $A'_I$  becomes less than  $A_I^{\min}$ , on the other hand, it is not adjusted here. If  $A'_I$  is adjusted to zero, it means that the sublimation flux is not used up by eliminating snow and sea ice. The remaining part is consumed to reduce seawater, so the evaporation flux is modified as

$$F_W^{EV'} = F_W^{EV} + F_W^{SB''} + \frac{\rho_I (A'_I - A_I^n) h_I^{\min}}{\rho_O \Delta t}. \quad (\text{B.19})$$

The last two terms cancel out if the adjustment does not take place.

When sublimation flux is consumed to reduce sea ice amount, salt contained in sea ice has to be added to the remaining sea ice or the underlying water. Otherwise, total salt of the ice-ocean system is not conserved. Here, it is added to the underlying water, and the way of this adjustment is described later. Note that sea ice tends to gradually drain high salinity water contained in brine pockets in reality. Thus, such an adjustment is not very unreasonable. When  $A'_I$  is adjusted to zero, on the other hand, the remaining sublimation flux is consumed to reduce seawater. In this case, difference between the latent heat of sublimation and evaporation has to be adjusted, which is also described later.

### B.1.3 Dynamical Redistribution

$A_I$ ,  $h_I$  and  $h_S$  are modified due to horizontal motion and freezing of ice-free surface, whose formulation is described in section B.2.1. First,  $A'_I$  is modified to  $A_I^*$  by using (B.40), with an adjustment that  $A_I^*$  is reset to zero if it becomes less than  $A_I^{\min}$  and is bounded by unity. Changes of sea ice volume  $V_I$  and snow volume  $V_S$ , which are defined by

$$V_I = A_I h_I, \quad V_S = A_I h_S, \quad (\text{B.20})$$

are then estimated by using (B.41). The prediction is initiated by

$$V'_I = A'_I h'_I, \quad V'_S = A'_I h'_S, \quad (\text{B.21})$$

and their predicted values are denoted by  $V_I^*$  and  $V_S^*$ . Note that  $V_I$  and  $V_S$  are conserved quantities, while  $A_I$ ,  $h_I$  and  $h_S$  are not.

### B.1.4 Growth and Melting

Changes of snow thickness due to snowfall (freshwater) flux  $F_W^{SN}$  (expressed by negative values to be consistent with other freshwater flux components) is first taken into account.  $F_W^{SN}$  is not weighted by sea ice concentration or ice-free area fraction, as snowfall takes place for both regions. If the newly predicted sea

ice concentration  $A_I^*$  is zero, the amount of snow existed before the dynamical redistribution is added to the snowfall flux, and snow thickness is set to zero:

$$F_W^{SN'} = F_W^{SN} - \frac{\rho_S V_S'}{\rho_O \Delta t}, \quad (\text{B.22})$$

$$V_S^{**} = 0. \quad (\text{B.23})$$

Otherwise, snowfall accumulates over the ice covered region, and the snowfall flux is reduced by that amount:

$$F_W^{SN'} = (1 - A_I^*) F_W^{SN}, \quad (\text{B.24})$$

$$V_S^{**} = V_S^* - \frac{A_I^* \rho_O F_W^{SN} \Delta t}{\rho_S}. \quad (\text{B.25})$$

Next,  $W_{AS}$  is used to reduce snow. Snow thickness is modified by

$$h_S^{**} = \frac{V_S^{**}}{A_I^*} + \frac{\rho_O W_{AS} \Delta t}{\rho_S A_I^*}. \quad (\text{B.26})$$

If  $A_I^* = 0$  or  $h_S^{**} < 0$ ,  $h_S^{**}$  is reset to zero. Then,  $W_{AI}$  is estimated by

$$W_{AI} = W_{AS} - \frac{\rho_S (A_I^* h_S^{**} - V_S^{**})}{\rho_O \Delta t}. \quad (\text{B.27})$$

It is zero when  $h_S^{**}$  is not reset to zero.

Then,  $W_{AI}$  is used to reduce sea ice:

$$V_I^{**} = V_I^* + \frac{\rho_O W_{AI} \Delta t}{\rho_I}. \quad (\text{B.28})$$

If  $V_I^{**}$  becomes less than zero, it is reset to zero, and the imbalance is added to  $W_{IO}$ :

$$W_{IO}^* = W_{IO} + W_{AI} - \frac{\rho_I (V_I^{**} - V_I^*)}{\rho_O \Delta t}, \quad (\text{B.29})$$

which is equal to  $W_{IO}$  when  $V_I^{**}$  is not reset to zero.

Finally, basal ice growth  $W_{IO}$  and freezing of ice-free surface  $W_{AO}$  is taken into account:

$$V_I^{n+1} = V_I^{**} + \frac{\rho_O (W_{IO}^* + W_{AO}) \Delta t}{\rho_I}. \quad (\text{B.30})$$

If  $V_I^{n+1}$  becomes less than zero, define

$$A_I^{n+1} = 0, \quad h_I^{n+1} = h_I^{\min}, \quad h_S^{n+1} = 0. \quad (\text{B.31})$$

Otherwise,

$$A_I^{n+1} = A_I^*, \quad h_I^{n+1} = \frac{V_I^{n+1}}{A_I^{n+1}}, \quad h_S^{n+1} = h_S^{**}. \quad (\text{B.32})$$

However, if  $h_I^{n+1}$  becomes less than  $h_I^{\min}$ , they are redefined by

$$A_I^{n+1} = \frac{V_I^{n+1}}{h_I^{\min}}, \quad h_I^{n+1} = h_I^{\min}. \quad (\text{B.33})$$

Here,  $h_S^{n+1}$  is not modified, so snow on the disappearing ice is regarded as falling onto the created ice-free sea surface.  $A_I^{n+1}$  is further adjusted to be zero when it is less than  $A_I^{\min}$ .

### B.1.5 Heat and Freshwater Fluxes Passed to the Ocean

Sea surface heat flux  $F_H$  applied to (1.58) is given by

$$F_H = -L_f \rho_O W_{FZ} - \frac{L_f \rho_I (A_I^{n+1} h_I^{n+1} - V_I^{n+1})}{\Delta t} - \frac{L_f \rho_S (A_I^{n+1} h_S^{n+1} - A_I^* h_S^{**})}{\Delta t} - L_f \rho_O F_W^{SN'} - L_f \left[ \rho_O F_W^{SB''} + \frac{\rho_I (A_I' - A_I^n) h_I^{\min}}{\Delta t} \right]. \quad (\text{B.34})$$

The second term is nonzero only when  $A_I^{n+1}$  is zero, including the case that it is so adjusted because of the constraint of  $A_I^{\min}$ . Sea ice formation and melting does not affect temperature of the underlying water as long as its temperature is at the freezing point, so it does not contribute to  $F_H$ . In the case of sea ice formation in an originally ice-free grid, the heat flux needed to lower  $T_1$  to  $T_f$  is accounted for by the first term. When sea ice disappears over the considered time interval,  $V_I^{n+1}$  becomes negative, while the final  $A_I^{n+1}$  becomes zero. So, the second term represents heating (negatively contributing to  $F_H$ ) of the underlying water in this case. In the case that an ice-free grid remains to be so, the sum of the first two terms represents  $Q_{AO} + c_1 Q_{SW}^A$ . In this case, too, the estimated ice volume  $V_I^{n+1}$  is negative. The third term becomes nonzero only when snow cover on sea ice is judged to fall onto the underlying water. The fourth term represents the latent heat of fusion of the snowfall onto ice-free surface. The last term represent the necessary adjustment noted in section B.1.2. Note that the portion of the shortwave radiative flux absorbed by the ocean model's top level is included in this  $F_H$ . The remaining part of the shortwave radiation should separately be applied to lower levels.

Sea surface freshwater flux  $F_W$  is

$$F_W = F_W^{EV'} + F_W^{SN'} + F_W^{RN} + F_W^{RO} + \frac{\rho_S (A_I^{n+1} h_S^{n+1} - V_S^*)}{\rho_O \Delta t} + \frac{\rho_I (A_I^{n+1} h_I^{n+1} - V_I^*)}{\rho_O \Delta t}, \quad (\text{B.35})$$

where  $F_W^{RN}$  and  $F_W^{RO}$  are rainfall and continental runoff (freshwater) fluxes, respectively. These fluxes also take negative values in the current definition. Neither sublimation nor dynamical redistribution of snow and sea ice yields freshwater flux at the sea surface. Therefore, the freshwater flux due to changes in snow and sea ice is estimated by comparing the final amounts of sea ice and snow with those right after the dynamical redistribution.

Sea surface salinity flux  $F_S$  is

$$F_S = S_I \left[ \frac{\rho_I (A_I^{n+1} h_I^{n+1} - V_I^*)}{\rho_O \Delta t} + \frac{\rho_I A_I^n (h_I' - h_I^n)}{\rho_O \Delta t} + \frac{\rho_I (A_I' - A_I^n) h_I^{\min}}{\rho_O \Delta t} \right]. \quad (\text{B.36})$$

Its first term accounts for contribution of melting or formation of sea ice, and the second and third terms for the adjustment due to sublimation of sea ice. Modification of salinity due to this salinity flux is represented by

$$\frac{\Delta S_1}{\Delta t} = -\frac{F_S}{\Delta z_1}, \quad (\text{B.37})$$

where  $\Delta S_1$  represents a change of salinity for the ocean model's top level over one time step. Note that  $F_S$  does not (directly) represent the effect of brine rejection under sea ice formation, but rather represents moderation of brine rejection due to salt trapped in sea ice. The salinity-raising effect of sea ice formation is accounted for by salinity condensation associated with  $F_W$ , and nonzero  $F_S$  works to moderate the effect of  $F_W$ .

### B.1.6 Empirical Parameterization

A large part of sea ice exist below sea level in reality. If snow thickness is large enough, ice-snow interface could come below sea level. Snow-ice is formed in such a case in reality. To mimic it in the model, excessive snow cover is removed and dumped into the ocean. The depth of ice bottom measured from the sea surface is

$$\frac{\rho_S h_S + \rho_I h_I}{\rho_O}, \quad (\text{B.38})$$

so the maximum snow thickness  $h_S^{\max}$  which does not cause submersion of ice-snow interface is

$$h_S^{\max} = \frac{\rho_O - \rho_I}{\rho_S} h_I. \quad (\text{B.39})$$

After the prediction of snow thickness by the procedure described in section B.1.4,  $h_S^{n+1}$  is adjusted by this constraint. The reduced amount of snow is taken into account in the heat and freshwater fluxes described in section B.1.5. The latent heat of fusion lowers  $T_1$ , which results in a supercooled state, and it eventually cause sea ice formation compensating that latent heat at the next time level.

Coarse resolution sea ice models tend to underestimate leads, especially when high-frequency forcing variations are neglected. In order to parameterize existence of leads, sea ice concentration is kept under a prescribed maximum value  $A_I^{\max}$ . It is realized simply by limiting  $A_I$  by  $A_I^{\max}$  at the timing when the adjustment of  $A_I$  by  $A_I^{\min}$  is considered in the above.

## B.2 Dynamics

### B.2.1 Horizontal Ice Transport

Sea ice horizontal velocity does not satisfy the two-dimensional continuity equation. Its divergence means opening of ice cover, and its convergence in a compactly packed region means ridging. Convergent flow is suppressed in a compactly packed region due to mechanical resistance, especially when ice is thick. Such an effect is taken into account by the internal stress term of the momentum equations described later.

Prognostic equations for sea ice concentration and thickness are

$$\frac{\partial A_I}{\partial t} + \frac{1}{h_x h_y} \left[ \frac{\partial}{\partial x} (h_y u_I A_I) + \frac{\partial}{\partial y} (h_x v_I A_I) \right] = \frac{\Phi \rho_O W_{AO}}{\rho_I h_I}, \quad (\text{B.40})$$

$$\frac{\partial V_I}{\partial t} + \frac{1}{h_x h_y} \left[ \frac{\partial}{\partial x} (h_y u_I V_I) + \frac{\partial}{\partial y} (h_x v_I V_I) \right] = 0, \quad (\text{B.41})$$

following *Mellor and Kantha [1989]*. Harmonic and biharmonic diffusion terms are added to the right hand sides for numerical stability. Snow thickness is predicted by the same form of equation as (B.41). Thermodynamic change of sea ice is not included here, which is taken into account by the procedure described in section B.1, except for the change in concentration due to freezing of ice-free surface.

The factor  $\Phi$  multiplied to the sea ice growth rate over ice-free surface is an empirical parameter relating heating/cooling of ice-free surface to change in concentration. When it is unity, heating/cooling of ice-free surface does not affect thickness, which means that it adds or removes sea ice of the same thickness as the already existing one. When it is zero, on the other hand, heating/cooling of ice-free surface does not affect concentration but only changes thickness. For the case of new ice formation over ice-free surface ( $W_{AO} > 0$ ), thin new ice is expected to be formed there. Then, it is reasonable to think that mean thickness is reduced because newly added sea ice is thinner than the already existing one. In this case, therefore,  $\Phi$  should be larger than unity. For the case of heating of ice-free surface ( $W_{AO} < 0$ ), on the other hand, it is expected

that some of the absorbed heat is used to warm seawater well below the surface, and it induces basal melting of the already existing sea ice. In this case,  $\Phi$  should be smaller than unity.

## B.2.2 Momentum Equation

The momentum equations are represented by

$$\begin{aligned} \frac{\partial}{\partial t}(V_I u_I) + \frac{1}{h_x h_y} \left[ \frac{\partial}{\partial x}(h_y u_I V_I u_I) + \frac{\partial}{\partial y}(h_x v_I V_I u_I) \right] + h_{xy} V_I u_I v_I - h_{yx} V_I v_I v_I - f V_I v_I \\ = -\frac{V_I g}{h_x} \frac{\partial \eta}{\partial x} + \frac{A_I(\tau_{AIx} - \tau_{IOx})}{\rho_I} + \frac{F_x}{\rho_I}, \end{aligned} \quad (\text{B.42})$$

$$\begin{aligned} \frac{\partial}{\partial t}(V_I v_I) + \frac{1}{h_x h_y} \left[ \frac{\partial}{\partial x}(h_y u_I V_I v_I) + \frac{\partial}{\partial y}(h_x v_I V_I v_I) \right] + h_{yx} V_I u_I v_I - h_{xy} V_I u_I u_I + f V_I u_I \\ = -\frac{V_I g}{h_y} \frac{\partial \eta}{\partial y} + \frac{A_I(\tau_{AIy} - \tau_{IOy})}{\rho_I} + \frac{F_y}{\rho_I}, \end{aligned} \quad (\text{B.43})$$

where  $\tau_{AIx}$  and  $\tau_{AIy}$  are  $x$  and  $y$  components, respectively, of wind stress over sea ice, which are given as described in section A.3. On the other hand,  $\tau_{IOx}$  and  $\tau_{IOy}$  are stress components at ice-ocean interface. They are calculated by

$$\tau_{IOx} = \rho_O C_W \sqrt{(u_I - u_O)^2 + (v_I - v_O)^2} [(u_I - u_O) \cos \theta - (v_I - v_O) \sin \theta], \quad (\text{B.44})$$

$$\tau_{IOy} = \rho_O C_W \sqrt{(u_I - u_O)^2 + (v_I - v_O)^2} [(v_I - v_O) \cos \theta + (u_I - u_O) \sin \theta], \quad (\text{B.45})$$

where  $C_W$  is a nondimensional drag coefficient,  $u_O$  and  $v_O$  are  $x$  and  $y$ , respectively, components of oceanic horizontal velocity at a referenced level, and  $\theta$  is a rotation angle of the effective ocean flow direction interacting with sea ice. The level of reference should be selected as the depth where geostrophic flow is realized (i.e., base of the surface Ekman layer). Since ice keel interacts with ocean flows at various depths, the rotation angle is not easily determined from theory but given as an empirical/experimental parameter [McPhee, 1978]. Since the rotation angle is associated with the surface Ekman flow, the sign of  $\theta$  is opposite between the Northern and Southern Hemispheres.

The ice-ocean drag term works as damping of sea ice velocity toward the referenced ocean velocity, and its time scale is estimated by

$$\frac{\rho_I h_I}{\rho_O C_W \sqrt{(u_I - u_O)^2 + (v_I - v_O)^2}}. \quad (\text{B.46})$$

If its value is larger than the time step of model integration  $\Delta t$ , the ice-ocean drag term must be integrated by the backward-in-time method. Since sea ice motion is strongly coupled to upper ocean currents, which means that velocity difference between sea ice and upper ocean is small, this damping time scale could easily exceed  $\Delta t$  for most applications.

The last terms of the right hand sides of (B.42) and (B.43) represent the force related to mechanical deformation of sea ice, and are often referred to as internal stress terms. They are represented by divergence of internal stress  $\sigma$  as

$$F_x = \frac{1}{h_x h_y} \left[ \frac{\partial}{\partial x}(h_y \sigma_{xx}) + \frac{\partial}{\partial y}(h_x \sigma_{xy}) \right] + h_{xy} \sigma_{yx} - h_{yx} \sigma_{yy}, \quad (\text{B.47})$$

$$F_y = \frac{1}{h_x h_y} \left[ \frac{\partial}{\partial x}(h_y \sigma_{yx}) + \frac{\partial}{\partial y}(h_x \sigma_{yy}) \right] + h_{yx} \sigma_{xy} - h_{xy} \sigma_{xx}. \quad (\text{B.48})$$

Under the elastic-viscous-plastic sea ice rheology, the constitutive equation is represented by

$$\frac{1}{E} \frac{\partial \sigma_{xx}}{\partial t} + \frac{1}{2\eta} \sigma_{xx} + \frac{\eta - \zeta}{4\eta\zeta} (\sigma_{xx} + \sigma_{yy}) + \frac{P}{4\zeta} = \varepsilon_{xx}, \quad (\text{B.49})$$

$$\frac{1}{E} \frac{\partial \sigma_{yy}}{\partial t} + \frac{1}{2\eta} \sigma_{yy} + \frac{\eta - \zeta}{4\eta\zeta} (\sigma_{xx} + \sigma_{yy}) + \frac{P}{4\zeta} = \varepsilon_{yy}, \quad (\text{B.50})$$

$$\frac{1}{E} \frac{\partial \sigma_{xy}}{\partial t} + \frac{1}{2\eta} \sigma_{xy} = \varepsilon_{xy}, \quad (\text{B.51})$$

where  $\varepsilon$  is strain rate tensor. Here,  $\sigma_{xy} = \sigma_{yx}$  holds, as strain rate tensor is symmetric (see below). In numerically solving these equations, the regular time step  $\Delta t$  is split into a number of shorter intervals, and time integration with a shorter time step  $\Delta t_s$  is repeated. In their time integration, the backward-in-time method is used. The components of strain rate tensor are represented by

$$\varepsilon_{xx} = \frac{1}{h_x} \frac{\partial u_I}{\partial x} + h_{xy} v_I, \quad (\text{B.52})$$

$$\varepsilon_{yy} = \frac{1}{h_y} \frac{\partial v_I}{\partial y} + h_{yx} u_I, \quad (\text{B.53})$$

$$\varepsilon_{xy} = \varepsilon_{yx} = \frac{1}{2} \left[ \frac{h_x}{h_y} \frac{\partial}{\partial y} \left( \frac{u_I}{h_x} \right) + \frac{h_y}{h_x} \frac{\partial}{\partial x} \left( \frac{v_I}{h_y} \right) \right]. \quad (\text{B.54})$$

The parameters for plasticity are given by

$$P = P_0 V_I \exp[-C(1 - A_I)], \quad (\text{B.55})$$

$$\zeta = \frac{P}{2\Delta}, \quad (\text{B.56})$$

$$\eta = \frac{\zeta}{e^2}, \quad (\text{B.57})$$

$$\Delta = \sqrt{\left(1 + \frac{1}{e^2}\right) (\varepsilon_{xx}^2 + \varepsilon_{yy}^2) + 2 \left(1 - \frac{1}{e^2}\right) \varepsilon_{xx} \varepsilon_{yy} + \frac{4}{e^2} \varepsilon_{xy} \varepsilon_{yx}}, \quad (\text{B.58})$$

where  $P_0$  and  $C$  are the parameters governing resistance of ice against deformation, and  $e$  is the eccentricity of an assumed elliptic yield curve. The plastic rheology is expressed by the form of two-dimensional nonlinear viscosity, with  $\zeta$  and  $\eta$  standing for bulk and shear viscosity, respectively. A minimum value is prescribed for  $\Delta$  to avoid numerical difficulty. When that minimum value is applied, this formulation results in linear viscosity. Thus, it is called the viscous-plastic rheology. See *Hibler [1979]* for its detail.

The parameter for elasticity (Young's modulus)  $E$ , on the other hand, is selected as

$$E = \frac{2V_I E_0 \rho_I}{\Delta t_s^2} \times \min(h_x^2 \Delta x^2, h_y^2 \Delta y^2), \quad (\text{B.59})$$

where  $E_0$  is a nondimensional parameter, and its value should be between zero and unity. Elasticity is added to the viscous-plastic rheology for a technical reason. Thick and compactly packed sea ice is hard, which results in large values for  $\zeta$  and  $\eta$ . Large viscosity makes it necessary to solve the internal stress terms by the backward-in-time method<sup>1</sup>. Since the internal stress terms are nonlinearly dependent on velocity, the backward-in-time method requires an iterative procedure. Introduction of elasticity relaxes this constraint and makes it possible to explicitly solve the internal stress term, though it still has to be dealt with by the time-splitting method. See *Hunke and Dukowicz [1997]* for its detail.

Momentum flux passed to the ocean model is calculated by

$$\tau_x = A_I \tau_{IOx} + (1 - A_I) \tau_{AOx}, \quad (\text{B.60})$$

$$\tau_y = A_I \tau_{IOy} + (1 - A_I) \tau_{AOy}, \quad (\text{B.61})$$

where  $\tau_{AOx}$  and  $\tau_{AOy}$  are components of wind stress over ice-free surface.

<sup>1</sup>A time step required for solving it by the forward-in-time method is as small as several seconds for typical ice thickness and velocity.



# Appendix C

## The Equation of State for Seawater

### C.1 International Equation of State for Seawater

#### C.1.1 IES80 Formula

The equation of state for seawater described here is the one determined by UNESCO Joint Panel on Oceanographic Tables in 1980 [*UNESCO, 1981*], which is often referred to as IES80. Here, temperature  $t$  is measured in °C, salinity  $S$  in practical salinity unit, pressure  $p$  in bars, and density in kilograms per cubic meter.

The density of pure water  $\rho_w$  at one standard atmosphere is given as a function of temperature  $t$  by

$$\begin{aligned}\rho_w(t) = & 999.842594 + 6.793952 \times 10^{-2}t - 9.095290 \times 10^{-3}t^2 \\ & + 1.001685 \times 10^{-4}t^3 - 1.120083 \times 10^{-6}t^4 + 6.536332 \times 10^{-9}t^5.\end{aligned}\quad (\text{C.1})$$

The density of seawater at one standard atmosphere, which is indicated by  $p = 0$ , is given by

$$\begin{aligned}\rho(S, t, 0) = & \rho_w + S(0.824493 - 4.0899 \times 10^{-3}t + 7.6438 \times 10^{-5}t^2 \\ & - 8.2467 \times 10^{-7}t^3 + 5.3875 \times 10^{-9}t^4) \\ & + S^{3/2}(-5.72466 \times 10^{-3} + 1.0227 \times 10^{-4}t - 1.6546 \times 10^{-6}t^2) \\ & + 4.8314 \times 10^{-4}S^2.\end{aligned}\quad (\text{C.2})$$

The density at pressure  $p$  is given by

$$\rho(S, t, p) = \frac{\rho(S, t, 0)}{1 - p/K(S, t, p)},\quad (\text{C.3})$$

where  $K$  is the secant bulk modulus. The secant bulk modulus for pure water at one standard atmosphere is given by

$$\begin{aligned}K_w = & 19652.21 + 148.4206t - 2.327105t^2 \\ & + 1.360477 \times 10^{-2}t^3 - 5.155288 \times 10^{-5}t^4.\end{aligned}\quad (\text{C.4})$$

The secant bulk modulus for seawater at one standard atmosphere is given by

$$\begin{aligned}K(S, t, 0) = & K_w + S(54.6746 - 0.603459t + 1.09987 \times 10^{-2}t^2 \\ & - 6.1670 \times 10^{-5}t^3) \\ & - S^{3/2}(7.944 \times 10^{-2} + 1.6483 \times 10^{-2}t - 5.3009 \times 10^{-4}t^2).\end{aligned}\quad (\text{C.5})$$

Finally, the secant bulk modulus at pressure  $p$  is given by

$$\begin{aligned}
K(S, t, p) = & K(S, t, 0) \\
& + p(3.239908 + 1.43713 \times 10^{-3}t + 1.16092 \times 10^{-4}t^2 \\
& \quad - 5.77905 \times 10^{-7}t^3) \\
& + pS(2.2838 \times 10^{-3} - 1.0981 \times 10^{-5}t - 1.6078 \times 10^{-6}t^2) \\
& + 1.91075 \times 10^{-4}pS^{3/2} \\
& + p^2(8.50935 \times 10^{-5} - 6.12293 \times 10^{-6}t + 5.2787 \times 10^{-8}t^2) \\
& + p^2S(-9.9348 \times 10^{-7} + 2.0816 \times 10^{-8}t + 9.1697 \times 10^{-10}t^2). \tag{C.6}
\end{aligned}$$

### C.1.2 Relationship Between Temperature and Potential Temperature

The temperature equation (1.5) is not for *in situ* temperature  $t$  but for potential temperature  $T$ , so it is necessary to specify the relationship between the two quantities. According to *Bryden [1973]*, it is given by

$$\begin{aligned}
T = & t \\
& - p(3.6504 \times 10^{-4} + 8.3198 \times 10^{-5}t - 5.4065 \times 10^{-7}t^2 \\
& \quad + 4.0274 \times 10^{-9}t^3) \\
& - p(S - 35)(1.7439 \times 10^{-5} - 2.99778 \times 10^{-7}t) \\
& - p^2(8.9309 \times 10^{-7} - 3.1628 \times 10^{-8}t + 2.1987 \times 10^{-10}t^2) \\
& + 4.1057 \times 10^{-9}(S - 35)p^2 \\
& - p^3(-1.6056 \times 10^{-10} + 5.0484 \times 10^{-12}t). \tag{C.7}
\end{aligned}$$

### C.1.3 Polynomial Approximation of the Equation of State

The IES80 formula guarantees the precision of less than  $0.009 \text{ kg/m}^3$  for the range  $-2 < t < 40$ ,  $0 < S < 42$ , and  $0 < p < 1000$ . However, the formula is a bit too complicated, nor is it directly applicable to the potential temperature. For practical application of the equation of state in the model, it often suffices to considerably limit the range of the variations of the variables, especially for  $S$ . For that case, some simpler expression for the equation of state is accurate enough.

In COCO, the equation of state is represented by a polynomial approximation:

$$\begin{aligned}
\rho = & \rho_0 \\
& + C_1(T - T_0) + C_2(S - S_0) \\
& + C_3(T - T_0)^2 + C_4(T - T_0)(S - S_0) + C_5(S - S_0)^2 \\
& + C_6(T - T_0)^3 + C_8(T - T_0)^2(S - S_0) \\
& \quad + C_7(T - T_0)(S - S_0)^2 + C_9(S - S_0)^3, \tag{C.8}
\end{aligned}$$

where  $T_0$  and  $S_0$  are some prescribed values of temperature and salinity defined at each vertical level, and  $\rho_0$  is the density of seawater at  $T = T_0$ ,  $S = S_0$ , and the corresponding pressure. The coefficients (subscripted  $C$ s) are calculated for each vertical level. In their determination, some tens of sample values for  $T$  and  $S$  are chosen from the typical range of variation, and the density for those samples are calculated by use of the IES80 formula and the relationship between  $t$  and  $T$ . Then the least squares fitting is applied.

## C.2 Simpler Expressions for the Equation of State

Several computationally efficient, still accurate enough over a wide range of dependent variables, expressions have been suggested. The following formula represent density as an explicit function of potential temperature, so they can be directly used in OGCMs without further approximation. Beware that  $p$  in the following formulae is measured by decibar.

### C.2.1 Mellor [1991]

Density is expressed as a sum of potential density  $\rho_\theta$  and a correction to it:

$$\rho(S, T, p) = \rho_\theta(S, T) + \rho_p(S, T, p), \quad (\text{C.9})$$

where the expression for potential density

$$\begin{aligned} \rho_\theta = & 999.842594 \\ & + 6.793952 \times 10^{-2}T - 9.095290 \times 10^{-3}T^2 \\ & + 1.001685 \times 10^{-4}T^3 - 1.120083 \times 10^{-6}T^4 + 6.536332 \times 10^{-9}T^5. \\ & + S(0.824493 - 4.0899 \times 10^{-3}T + 7.6438 \times 10^{-5}T^2 \\ & \quad - 8.2467 \times 10^{-7}T^3 + 5.3875 \times 10^{-9}T^4) \\ & + S^{3/2}(-5.72466 \times 10^{-3} + 1.0227 \times 10^{-4}T - 1.6546 \times 10^{-6}T^2) \\ & + 4.8314 \times 10^{-4}S^2 \end{aligned} \quad (\text{C.10})$$

is the same as the IES80 formula. However, the correction term is much simplified:

$$\rho_p = \frac{10^4 p}{c^2} \left( 1 - \frac{0.2p}{c^2} \right), \quad (\text{C.11})$$

where

$$c = 1449.2 + 1.34(S - 35) + 4.55T - 0.045T^2 + 0.00821p + 15 \times 10^{-9}p^2. \quad (\text{C.12})$$

### C.2.2 McDougall et al., [2003]

Density is expressed by two polynomials

$$\rho(S, T, p) = \frac{P_1(S, T, p)}{P_2(S, T, p)}, \quad (\text{C.13})$$

where

$$\begin{aligned} P_1 = & 9.99843699 \times 10^2 \\ & + 7.3521284T - 5.45928211 \times 10^{-2}T^2 + 3.98476704 \times 10^{-4}T^3 \\ & + 2.96938239S - 7.23268813 \times 10^{-3}ST + 2.12382341 \times 10^{-3}S^2 \\ & + 1.04004591 \times 10^{-2}p + 1.03970529 \times 10^{-7}pT^2 + 5.18761880 \times 10^{-6}pS \\ & - 3.24041825 \times 10^{-8}p^2 - 1.2386936 \times 10^{-11}p^2T^2, \\ P_2 = & 1 \\ & + 7.28606739 \times 10^{-3}T - 4.60835542 \times 10^{-5}T^2 \\ & + 3.68390573 \times 10^{-7}T^3 + 1.80809186 \times 10^{-10}T^4 \end{aligned} \quad (\text{C.14})$$

$$\begin{aligned} &+2.14691708 \times 10^{-3}S - 9.27062484 \times 10^{-6}ST \\ &-1.78343643 \times 10^{-10}ST^3 + 4.76534122 \times 10^{-6}S^{3/2} + 1.63410736 \times 10^{-9}S^{3/2}T^2 \\ &+5.30848875 \times 10^{-6}p - 3.03175128 \times 10^{-16}p^2T^3 - 1.27934137 \times 10^{-17}p^3T. \end{aligned} \quad (\text{C.15})$$

# Appendix D

## Basics of Tensor Analysis and Its Physical Application

### D.1 Definition of Tensor

#### D.1.1 Coordinate Transformation

Let  $x^h$  ( $h = 1, \dots, n$ ) denote coordinates of an  $n$ -dimensional space<sup>1</sup>. Throughout this appendix,  $n$  always denotes the total dimension of the considered space. Coordinate transformation in this space is defined by a set of  $n$  functions of  $x^h$ :

$$\bar{x}^j = \bar{x}^j(x^1, \dots, x^n) \quad (j = 1, \dots, n), \quad (\text{D.1})$$

where  $\bar{x}^j$  ( $j = 1, \dots, n$ ) denote the new coordinates. Coordinate transformation (D.1) is hereafter represented briefly by  $\bar{x}^j = \bar{x}^j(x^h)$ . Its inverse transformation consists of  $n$  functions of  $\bar{x}^j$ :  $x^h = x^h(\bar{x}^j)$ .

In order for this coordinate transformation not to degenerate the dimension of the space, the nonsingularity condition

$$\frac{\partial(\bar{x}^1, \dots, \bar{x}^n)}{\partial(x^1, \dots, x^n)} \neq 0 \quad (\text{D.2})$$

is required. Furthermore, the functions for coordinate transformation must satisfy

$$\delta_k^h = \frac{\partial x^h}{\partial \bar{x}^j} \frac{\partial \bar{x}^j}{\partial x^k} \quad (\text{D.3})$$

or, equivalently,

$$\delta_l^j = \frac{\partial \bar{x}^j}{\partial x^h} \frac{\partial x^h}{\partial \bar{x}^l}, \quad (\text{D.4})$$

where

$$\delta_k^h = \begin{cases} 1 & \text{for } h = k \\ 0 & \text{otherwise} \end{cases} \quad (\text{D.5})$$

and the sum rule<sup>2</sup> is applied.

#### D.1.2 Tensor

A set of  $(r+s)$ -index symbols  $T_{k_1 \dots k_s}^{h_1 \dots h_r}$  (each of super- and subscripts varies from 1 to  $n$ ), which represent a set of  $n^{r+s}$  values, constitutes components of an  $(r, s)$  tensor when they are transformed under the coordinate

<sup>1</sup>It should be described as “an  $n$ -dimensional manifold” for the sake of mathematical exactness.

<sup>2</sup>When an index  $j$  appears twice in a single term, it means a sum over  $j = 1, \dots, n$  ( $\sum_{j=1}^n$ ).

transformation (D.1) as

$$\bar{T}_{l_1 \dots l_s}^{j_1 \dots j_r} = \frac{\partial \bar{x}^{j_1}}{\partial x^{h_1}} \dots \frac{\partial \bar{x}^{j_r}}{\partial x^{h_r}} \frac{\partial x^{k_1}}{\partial \bar{x}^{l_1}} \dots \frac{\partial x^{k_s}}{\partial \bar{x}^{l_s}} T_{k_1 \dots k_s}^{h_1 \dots h_r}. \quad (\text{D.6})$$

It is also called a tensor of rank  $(r, s)$ .  $(0, 0)$  tensor is called scalar,  $(1, 0)$  tensor is called contravariant vector, and  $(0, 1)$  tensor is called covariant vector. Scalar is invariant under any coordinate transformation. The quantity  $\delta_k^h$  defined above, which is usually called Kronecker delta, is a  $(1, 1)$  tensor.

For two  $(r, s)$  tensors  $T_{k_1 \dots k_s}^{h_1 \dots h_r}$  and  $S_{k_1 \dots k_s}^{h_1 \dots h_r}$ , a set of the sums of two corresponding components  $T_{k_1 \dots k_s}^{h_1 \dots h_r} + S_{k_1 \dots k_s}^{h_1 \dots h_r}$  also constitutes components of an  $(r, s)$  tensor. For an  $(r, s)$  tensor  $T_{k_1 \dots k_s}^{h_1 \dots h_r}$  and a  $(p, q)$  tensor  $S_{l_1 \dots l_q}^{j_1 \dots j_p}$ , on the other hand, a set of the products of components

$$R_{k_1 \dots k_s l_1 \dots l_q}^{h_1 \dots h_r j_1 \dots j_p} = T_{k_1 \dots k_s}^{h_1 \dots h_r} S_{l_1 \dots l_q}^{j_1 \dots j_p} \quad (\text{D.7})$$

constitutes components of an  $(r + p, s + q)$  tensor.

For an  $(r, s)$  tensor  $T_{k_1 \dots k_s}^{h_1 \dots h_r}$  ( $r, s \geq 1$ ), a set of sums of the components with varying two indices, one from each of the superscripts and the subscripts, simultaneously from 1 to  $n$  (i.e., set  $h_\alpha = k_\beta = l$  for any  $\alpha$  and  $\beta$  satisfying  $1 \leq \alpha \leq r$  and  $1 \leq \beta \leq s$ , and apply the sum rule) constitutes components of an  $(r - 1, s - 1)$  tensor. This procedure of obtaining a tensor of a lower rank is called contraction (of indices).

### D.1.3 Relative Tensor and Levi-Civita Symbols

A set of  $(r + s)$ -index symbols  $\Lambda_{k_1 \dots k_s}^{h_1 \dots h_r}$  constitutes components of an  $(r, s)$  relative tensor of weight  $w$  when they are transformed under the coordinate transformation (D.1) as

$$\bar{\Lambda}_{l_1 \dots l_s}^{j_1 \dots j_r} = J^w \frac{\partial \bar{x}^{j_1}}{\partial x^{h_1}} \dots \frac{\partial \bar{x}^{j_r}}{\partial x^{h_r}} \frac{\partial x^{k_1}}{\partial \bar{x}^{l_1}} \dots \frac{\partial x^{k_s}}{\partial \bar{x}^{l_s}} \Lambda_{k_1 \dots k_s}^{h_1 \dots h_r}, \quad (\text{D.8})$$

where  $J$  is the Jacobian of the coordinate transformation defined by

$$J = \frac{\partial(x^1, \dots, x^n)}{\partial(\bar{x}^1, \dots, \bar{x}^n)}. \quad (\text{D.9})$$

For its special case, a quantity  $\psi$  is called a scalar density if it is transformed under the coordinate transformation (D.1) as

$$\bar{\psi} = J\psi. \quad (\text{D.10})$$

An  $n$ -fold integral of a scalar density  $\psi$  is invariant under coordinate transformations (thus it is a scalar), since

$$\int \bar{\psi} d\bar{x}^1 \dots d\bar{x}^n = \int J\psi d\bar{x}^1 \dots d\bar{x}^n = \int \psi dx^1 \dots dx^n. \quad (\text{D.11})$$

Conversely, a spatial integral of a scalar (tensor) is not a scalar (tensor) quantity.

Let us define  $n$ -index symbols  $\epsilon_{h_1 \dots h_n}$  and  $\epsilon^{h_1 \dots h_n}$  which satisfy

$$\epsilon_{h_1 \dots h_n} = \epsilon^{h_1 \dots h_n} = \begin{cases} 1 & \text{when } (h_1, \dots, h_n) \text{ is an even permutation of } (1, \dots, n) \\ -1 & \text{when } (h_1, \dots, h_n) \text{ is an odd permutation of } (1, \dots, n) \\ 0 & \text{when any two of } (h_1, \dots, h_n) \text{ are identical} \end{cases}. \quad (\text{D.12})$$

They are called the Levi-Civita symbols (or the permutation symbols). The subscripted symbols  $\epsilon_{h_1 \dots h_n}$  constitute components of a  $(0, n)$  relative tensor of weight  $-1$ , while the superscripted symbols  $\epsilon^{h_1 \dots h_n}$  constitute components of an  $(n, 0)$  relative tensor of weight  $+1$ . Using the Levi-Civita symbols, determinant of a matrix  $(a_{jh})$  is calculated by

$$\det(a_{jh}) = \epsilon^{j_1 \dots j_n} a_{1j_1} \dots a_{nj_n}. \quad (\text{D.13})$$

## D.2 Riemannian Geometry

### D.2.1 Riemannian Metric

A  $(0, 2)$  tensor  $g_{jh}$  defines a Riemannian metric in an  $n$ -dimensional space if it is symmetric

$$g_{jh} = g_{hj} \quad (\text{D.14})$$

and nonsingular

$$g = \det(g_{jh}) \neq 0. \quad (\text{D.15})$$

In this case, the tensor  $g_{jh}$  is called a metric tensor. Values of its components are, of course, dependent on a selected coordinate system. A space endowed with a Riemannian metric is called a Riemannian space. Riemannian metric defines a measure of length. Line element  $ds$  is defined by

$$ds^2 = g_{jh} dx^j dx^h, \quad (\text{D.16})$$

and the length of a contravariant vector  $X^j$  is defined by

$$|X| = \sqrt{g_{jh} X^j X^h}. \quad (\text{D.17})$$

Riemannian metric uniquely defines a covariant vector  $Z_j$  from a contravariant vector  $X^h$  by

$$Z_j = g_{jh} X^h. \quad (\text{D.18})$$

When the length of  $Z_j$  is defined by

$$|Z| = \sqrt{g^{jh} Z_j Z_h}, \quad (\text{D.19})$$

it is identical to  $|X|$  because

$$g_{lk} X^l X^k = g_{lk} g^{lh} Z_h g^{jk} Z_j = \delta_k^h Z_h g^{jk} Z_j = g^{jk} Z_h Z_j, \quad (\text{D.20})$$

where  $g^{jh}$  is a  $(2, 0)$  tensor uniquely defined from the metric tensor by

$$g_{jh} g^{jk} = \delta_h^k. \quad (\text{D.21})$$

Components of  $g^{jk}$  are calculated as components of the inverse of the matrix  $(g_{jk})$ . Conversely,  $g^{jh}$  uniquely defines a contravariant vector from a covariant vector. Therefore,  $X^j$  and  $Z_j$  so defined are considered to be different expressions for the same quantity in the space under the Riemannian metric  $g_{jh}$ . This procedure of transformation between contravariant and covariant vectors is called raising/lowering of an index. Index raising/lowering is also applicable to any super- or subscript of a tensor of any rank. Index raising/lowering for relative tensors are differently defined. For example, the two kinds of Levi-Civita symbols are related to each other by

$$\epsilon_{j_1 \dots j_n} = g g_{j_1 h_1} \dots g_{j_n h_n} \epsilon^{h_1 \dots h_n}. \quad (\text{D.22})$$

### D.2.2 Christoffel Symbols and Covariant Differentiation

Three-index symbols  $\gamma_{h \ k}^j$  defined by

$$\gamma_{h \ k}^j = g^{jl} \frac{1}{2} \left( \frac{\partial g_{lk}}{\partial x^h} + \frac{\partial g_{hl}}{\partial x^k} - \frac{\partial g_{hk}}{\partial x^l} \right) \quad (\text{D.23})$$

are called Christoffel symbols of the Riemannian space under consideration. They are symmetric in terms of interchange of the two subscripts, and its contraction of indices yields

$$\gamma_j^k = \frac{1}{\sqrt{g}} \frac{\partial \sqrt{g}}{\partial x^j}. \quad (\text{D.24})$$

Christoffel symbols do not constitute components of a tensor, as they do not follow the transformation rule of a tensor (D.6). For an  $(r, s)$  tensor field  $T_{l_1 \dots l_s}^{j_1 \dots j_r}$ , on the other hand, a quantity defined by

$$T_{l_1 \dots l_s | k}^{j_1 \dots j_r} = \frac{\partial T_{l_1 \dots l_s}^{j_1 \dots j_r}}{\partial x^k} + \sum_{\alpha=1}^r \gamma_m^{\alpha j_\alpha} T_{l_1 \dots l_s}^{j_1 \dots m \dots j_r} - \sum_{\beta=1}^s \gamma_{l_\beta}^m T_{l_1 \dots m \dots l_s}^{j_1 \dots j_r}, \quad (\text{D.25})$$

where the index  $m$  in  $T_{l_1 \dots l_s}^{j_1 \dots m \dots j_r}$  ( $T_{l_1 \dots m \dots l_s}^{j_1 \dots j_r}$ ) is for the  $\alpha$ -th superscript ( $\beta$ -th subscript), constitutes a component of an  $(r, s + 1)$  tensor field. This quantity is called a covariant derivative<sup>3</sup> of  $T_{l_1 \dots l_s}^{j_1 \dots j_r}$ . Note that a simple partial derivative  $\partial T_{l_1 \dots l_s}^{j_1 \dots j_r} / \partial x^k$  does not constitute a component of a tensor.

Covariant differentiation of an  $(r, s)$  relative tensor field of weight  $w$ , whose components are denoted by  $\Lambda_{l_1 \dots l_s}^{j_1 \dots j_r}$ , is defined by

$$\Lambda_{l_1 \dots l_s | k}^{j_1 \dots j_r} = \frac{\partial \Lambda_{l_1 \dots l_s}^{j_1 \dots j_r}}{\partial x^k} + \sum_{\alpha=1}^r \gamma_m^{\alpha j_\alpha} \Lambda_{l_1 \dots l_s}^{j_1 \dots m \dots j_r} - \sum_{\beta=1}^s \gamma_{l_\beta}^m \Lambda_{l_1 \dots m \dots l_s}^{j_1 \dots j_r} - w \gamma_k^h \Lambda_{l_1 \dots l_s}^{j_1 \dots j_r}, \quad (\text{D.26})$$

which yields an  $(r, s + 1)$  relative tensor field of weight  $w$ .

Covariant differentiation of a metric tensor field is identically zero:

$$g_{jh|k} = 0, \quad g_{|k}^{jh} = 0. \quad (\text{D.27})$$

It is known as the Ricci's identity. In successive covariant differentiation, the order of differentiation cannot be swapped in general. For a contravariant vector field  $X^j$ , for example,

$$X_{|h|k}^j - X_{|k|h}^j = R_{l^j}^j{}_{hk} X^l, \quad (\text{D.28})$$

where

$$R_{l^j}^j{}_{hk} = \frac{\partial \gamma_{l^j}^j{}_{hk}}{\partial x^k} - \frac{\partial \gamma_{l^j}^j{}_{kh}}{\partial x^h} + \gamma_m^j{}_k \gamma_l^m{}_h - \gamma_m^j{}_h \gamma_l^m{}_k \quad (\text{D.29})$$

is called a curvature tensor. If and only if the curvature tensor is the zero tensor (all of its components are zero, and thus it is the zero tensor under any coordinate system), the order of covariant differentiation can freely be swapped. When the curvature tensor is the zero tensor, the space is called a flat space.

### D.2.3 Descartes Coordinate System

When the components of the metric tensor are

$$g_{jh} = \begin{cases} 1 & \text{for } j = h \\ 0 & \text{otherwise} \end{cases}, \quad (\text{D.30})$$

*everywhere* under the selected coordinate system, the coordinate system is called the Descartes coordinate system. Under the Descartes coordinate system, length of a contravariant vector  $X^j$  is given simply by

$$|X|^2 = (X^1)^2 + \dots + (X^n)^2. \quad (\text{D.31})$$

<sup>3</sup>Covariant derivative is denoted by different symbols in different literature, such as  $T_{l_1 \dots l_s, k}^{j_1 \dots j_r}$  or  $\partial_k T_{l_1 \dots l_s}^{j_1 \dots j_r}$ .

Furthermore, components of the covariant vector

$$Z_h = g_{jh} X^j \quad (\text{D.32})$$

are identical to the corresponding components of the original contravariant vector:

$$Z_j = X^j. \quad (\text{D.33})$$

Therefore, there is no distinction between covariance and contravariance in the Descartes coordinate system.

There is no guarantee that the Descartes coordinate system can be defined for any space. At any point in a Riemannian space, however, there is always a linear coordinate transformation which yields

$$\bar{g}_{jh} = \begin{cases} 1 & \text{for } j = h \\ 0 & \text{otherwise} \end{cases}, \quad (\text{D.34})$$

at the selected point<sup>4</sup>. Such a transformation does not guarantee that the metric tensor is diagonalized at other points. The coordinate system where (D.34) is realized at a point  $P$  is called a local Descartes coordinate system at  $P$ . When there is a coordinate system in which (D.34) is satisfied everywhere (non-local Descartes coordinate system), the space is flat and is also called Euclidean.

### D.3 Orthogonal Curvilinear Coordinate System

A coordinate system where

$$g_{jh} \begin{cases} \neq 0 & \text{for } j = h \\ = 0 & \text{otherwise} \end{cases} \quad (\text{D.35})$$

holds is called an orthogonal curvilinear coordinate system (or simply a curvilinear coordinate system). A local Descartes coordinate system is easily obtained at each point from an orthogonal curvilinear coordinate system by just rescaling each coordinate. Let  $g_{\alpha\alpha}$  be an  $\alpha$ -th diagonal component of the metric tensor of an orthogonal curvilinear coordinate system, and let  $x^\alpha$  denote its coordinate. Note that the sum rule is not applied to Greek symbols here and hereafter. In this case, a so-called metric of the  $\alpha$ -th coordinate  $h_\alpha$  is defined by

$$(h_\alpha)^2 = g_{\alpha\alpha}. \quad (\text{D.36})$$

Let  $\hat{x}^\alpha$  denote the local Descartes coordinate system generated from the orthogonal curvilinear coordinate system  $x^\alpha$ . The coordinate transformation is described by

$$\hat{x}^\alpha = h_\alpha x^\alpha, \quad (\text{D.37})$$

infinitesimal displacement to a direction of one of the local Descartes coordinates is given by

$$d\hat{x}^\alpha = h_\alpha dx^\alpha, \quad (\text{D.38})$$

and the line element of the space is expressed by

$$ds^2 = \sum_{\alpha=1}^n g_{\alpha\alpha} (dx^\alpha)^2 = \sum_{\alpha=1}^n (h_\alpha dx^\alpha)^2 = \sum_{\alpha=1}^n (d\hat{x}^\alpha)^2. \quad (\text{D.39})$$

For a contravariant vector whose components in the  $x^\alpha$  coordinate system are represented by  $X^\alpha$ , its corresponding components  $\hat{X}_\alpha$  in the local Descartes coordinate system are

$$\hat{X}_\alpha = h_\alpha X^\alpha, \quad (\text{D.40})$$

---

<sup>4</sup>It is realized by rotation of the coordinate system which diagonalize the matrix  $(g_{jh})$ .

while components of a covariant vector whose components in the  $x^\alpha$  coordinate system are  $Z_\alpha$  are represented by

$$\hat{Z}_\alpha = \frac{Z_\alpha}{h_\alpha} \quad (\text{D.41})$$

in the local Descartes coordinate system. If  $X^\alpha$  and  $Z_\alpha$  are related to each other by raising/lowering of the index (D.18), it is guaranteed that  $\hat{X}_\alpha$  and  $\hat{Z}_\alpha$  are identical. As stated before, there is no distinction between covariance and contravariance in the Descartes coordinate system, whether it is defined globally or locally.

For a (2, 0) tensor whose components are expressed by  $T^{\alpha\beta}$  in an orthogonal curvilinear coordinate system and related (1, 1) and (0, 2) tensors obtained by lowering the indices

$$T_\beta^\alpha = g_{j\beta} T^{\alpha j}, \quad T_{\alpha\beta} = g_{h\alpha} T_\beta^h, \quad (\text{D.42})$$

the corresponding components in the local Descartes coordinate system are obtained by

$$\hat{T}_{\alpha\beta} = h_\alpha h_\beta T^{\alpha\beta} = \frac{h_\alpha}{h_\beta} T_\beta^\alpha = \frac{T_{\alpha\beta}}{h_\alpha h_\beta}. \quad (\text{D.43})$$

Likewise, for an  $(r, s)$  tensor whose components in an orthogonal curvilinear coordinate system are denoted by  $T_{\beta_1 \dots \beta_s}^{\alpha_1 \dots \alpha_r}$ , its corresponding components in the local Descartes coordinate system are obtained by

$$\hat{T}_{\alpha_1 \dots \alpha_r \beta_1 \dots \beta_s} = \frac{h_{\alpha_1} \dots h_{\alpha_r}}{h_{\beta_1} \dots h_{\beta_s}} T_{\beta_1 \dots \beta_s}^{\alpha_1 \dots \alpha_r}. \quad (\text{D.44})$$

Hereafter, local Descartes coordinates and components of tensors under a local Descartes coordinate system are denoted by symbols with a hat, and their indices are always denoted by subscripts.

A covariant derivative of a scalar  $\phi$  constitutes a component of a covariant vector:

$$X_j = \phi_{|j} = \frac{\partial \phi}{\partial x^j}. \quad (\text{D.45})$$

The corresponding expression for this operation in the local Descartes coordinate system is

$$\hat{X}_\alpha = \frac{X_\alpha}{h_\alpha} = \frac{1}{h_\alpha} \frac{\partial \hat{\phi}}{\partial x^\alpha}, \quad (\text{D.46})$$

where  $\hat{\phi} = \phi$ . Note that the partial differentiation in the right hand side is in terms of the original curvilinear coordinate, while the components of the tensors are expressed in the local Descartes coordinate system. That is the very reason why the metric appears in this expression. When the differentiation is performed in terms of the local Descartes coordinate, it simply yields an expression identical to (D.45):

$$\hat{X}_\alpha = \frac{\partial \hat{\phi}}{\partial \hat{x}^\alpha}. \quad (\text{D.47})$$

Covariant differentiation of a contravariant vector yields a (1, 1) tensor:

$$T_h^j = X^j_{|h} = \frac{\partial X^j}{\partial x^h} + \gamma_k^j{}^h X^k. \quad (\text{D.48})$$

The corresponding expression for this operation in the local Descartes coordinate system is

$$\hat{T}_{\alpha\beta} = \frac{h_\alpha}{h_\beta} T_\beta^\alpha = \frac{h_\alpha}{h_\beta} \left( \frac{\partial X^\alpha}{\partial x^\beta} + \gamma_k^\alpha{}_\beta X^k \right) = \frac{h_\alpha}{h_\beta} \left[ \frac{\partial}{\partial x^\beta} \left( \frac{\hat{X}_\alpha}{h_\alpha} \right) + \sum_{\delta=1}^n \frac{\gamma_\delta^\alpha{}_\beta}{h_\delta} \hat{X}_\delta \right]. \quad (\text{D.49})$$

A successive operation of covariant differentiation and contraction in terms of that index is called divergence. Divergence of a contravariant vector is represented by

$$\operatorname{div} X = X^j_{|j} = \frac{1}{\sqrt{g}} \frac{\partial}{\partial x^j} (\sqrt{g} X^j) = \sum_{\alpha=1}^n \frac{1}{\sqrt{g}} \frac{\partial}{\partial x^\alpha} \left( \frac{\sqrt{g}}{h_\alpha} \hat{X}_\alpha \right), \quad (\text{D.50})$$

where

$$\sqrt{g} = \prod_{\alpha=1}^n h_\alpha. \quad (\text{D.51})$$

Christoffel symbols are expressed by coordinate metrics as

$$\gamma_\alpha^\alpha{}_\alpha = \frac{1}{h_\alpha} \frac{\partial h_\alpha}{\partial x^\alpha} \quad (\text{D.52})$$

$$\gamma_\beta^\alpha{}_\alpha = \gamma_\alpha^\alpha{}_\beta = \frac{g^{\alpha\alpha}}{2} \frac{\partial g_{\alpha\alpha}}{\partial x^\beta} = \frac{1}{h_\alpha} \frac{\partial h_\alpha}{\partial x^\beta} \quad (\text{D.53})$$

$$\gamma_\beta^\alpha{}_\beta = -\frac{g^{\alpha\alpha}}{2} \frac{\partial g_{\beta\beta}}{\partial x^\alpha} = -\frac{h_\beta}{h_\alpha^2} \frac{\partial h_\beta}{\partial x^\alpha} \quad (\text{D.54})$$

$$\gamma_\beta^\alpha{}_\delta = 0 \quad (\text{D.55})$$

where  $\alpha \neq \beta \neq \delta$ .

## D.4 Tensoric Representation of Physical Quantities

### D.4.1 How should physical quantities be defined as tensors?

If mass  $m$  of a substance does not depend on a selected coordinate system,  $m$  is a scalar quantity. Density  $\rho$  is defined as a quantity whose spatial integral represents mass. So,  $\rho$  is a scalar density.

Though coordinates  $x^k$  are represented by superscripted quantities, they do not constitute components of a tensor, as they do not follow the transformation rule (D.6). On the other hand, infinitesimal displacement  $dx^k$  constitutes a component of a contravariant vector, as it is transformed as

$$d\bar{x}^k = \frac{\partial \bar{x}^k}{\partial x^h} dx^h. \quad (\text{D.56})$$

When coordinate values of a moving point are represented by  $x^k = x^k(t)$ , where  $t$  is a parameter representing time, velocity of the moving point defined by

$$v^k = \dot{x}^k = \frac{dx^k}{dt} \quad (\text{D.57})$$

constitutes a component of a contravariant vector.

Time evolution of a moving point, whose mass is  $m$  and velocity is  $v^k$ , under an influence of force  $f^k$  is described in the Descartes coordinate system as

$$\frac{d}{dt}(mv^k) = f^k. \quad (\text{D.58})$$

If the form of this equation is invariant under any coordinate transformation,  $f^k$  in this expression must be a contravariant vector. In this case, the equation is said to be described in a covariant form.

Note that you can freely exchange covariance and contravariance by raising or lowering indices with a help of the metric tensor. Then, it is free to represent velocity of a moving point as a covariant vector (or to transform between covariance and contravariance for any tensoric quantity). However, values of components

differ depending on whether the velocity is represented as contravariant or covariant, unless the selected coordinate system is Cartesian.

The continuity equation of incompressible fluid in the Descartes coordinate system is

$$\frac{\partial v^k}{\partial x^k} = 0. \quad (\text{D.59})$$

If it is required (or proven by observations) that this equation is written in a covariant form, the differentiation must be replaced by covariant differentiation:

$$v_{|k}^k = 0. \quad (\text{D.60})$$

It is written down as

$$\frac{\partial v^k}{\partial x^k} + \gamma_m^k v^m = 0, \quad (\text{D.61})$$

and its representation in the local Descartes coordinate system is

$$\sum_{\alpha=1}^n \frac{1}{\sqrt{g}} \frac{\partial}{\partial x^\alpha} \left( \frac{\sqrt{g}}{h_\alpha} \hat{v}_\alpha \right) = 0. \quad (\text{D.62})$$

For the case of  $n = 3$ ,

$$\frac{1}{h_1 h_2 h_3} \left[ \frac{\partial}{\partial x^1} (h_2 h_3 \hat{v}_1) + \frac{\partial}{\partial x^2} (h_3 h_1 \hat{v}_2) + \frac{\partial}{\partial x^3} (h_1 h_2 \hat{v}_3) \right] = 0. \quad (\text{D.63})$$

#### D.4.2 External Product and Curl Operation

Here, only the case of  $n = 3$  is considered. For two contravariant vectors  $X^k$  and  $Y^l$ , the contraction of the products of the Levi-Civita symbols  $\epsilon_{jkl}$  and them  $(\epsilon_{jkl} X^k Y^l)$  yields a relative covariant vector of weight  $-1$ . Likewise, for two covariant vectors  $X_k$  and  $Y_l$ , the contraction of the products of the Levi-Civita symbols  $\epsilon^{jkl}$  and them  $(\epsilon^{jkl} X_k Y_l)$  yields a relative contravariant vector of weight  $+1$ . Then, quantities

$$Z_j = \sqrt{g} \epsilon_{jkl} X^k Y^l, \quad (\text{D.64})$$

$$Z^j = \frac{1}{\sqrt{g}} \epsilon^{jkl} X_k Y_l \quad (\text{D.65})$$

define the external product of the two vectors. The latter (former) is obtained by raising (lowering) the index of the former (latter) by using the metric tensor when  $X^k$  and  $X_k$  ( $Y^l$  and  $Y_l$ ) are so related. However, these quantities are slightly different from (relative) tensors defined hereabove. Under a coordinate transformation, their components are transformed like (D.6), but a factor of the sign of the Jacobian of the transformation is multiplied. Their components are written down as

$$(Z_1, Z_2, Z_3) = \sqrt{g} (X^2 Y^3 - X^3 Y^2, X^3 Y^1 - X^1 Y^3, X^1 Y^2 - X^2 Y^1), \quad (\text{D.66})$$

$$(Z^1, Z^2, Z^3) = \frac{1}{\sqrt{g}} (X_2 Y_3 - X_3 Y_2, X_3 Y_1 - X_1 Y_3, X_1 Y_2 - X_2 Y_1), \quad (\text{D.67})$$

and both of them result in the same expression in the local Descartes coordinate system:

$$(\hat{Z}_1, \hat{Z}_2, \hat{Z}_3) = (\hat{X}_2 \hat{Y}_3 - \hat{X}_3 \hat{Y}_2, \hat{X}_3 \hat{Y}_1 - \hat{X}_1 \hat{Y}_3, \hat{X}_1 \hat{Y}_2 - \hat{X}_2 \hat{Y}_1). \quad (\text{D.68})$$

Length of  $Z_j$  and  $Z^j$  defined above is given by

$$\begin{aligned} |Z|^2 &= g^{jh} Z_j Z_h = g^{jh} Z^j Z^h = Z_j Z^j \\ &= \epsilon_{jkl} \epsilon^{jpk} X^k Y^l X_p Y_q. \end{aligned} \quad (\text{D.69})$$

Here, the relationship

$$\epsilon_{jkl}\epsilon^{j pq} = \delta_k^p \delta_l^q - \delta_l^p \delta_k^q \quad (\text{D.70})$$

identically holds, so

$$|Z|^2 = X^k X_k Y^l Y_l - X^k Y_k X_l Y^l = |X|^2 |Y|^2 - (X^k Y_k)^2. \quad (\text{D.71})$$

The second term of its final expression is the square of the inner product of the vectors  $X$  and  $Y$ . The inner product is also represented as

$$(X \cdot Y) = g_{jh} X^j Y^h = g^{jh} X_j Y_h. \quad (\text{D.72})$$

For a covariant vector field  $X_l$ , its product with the Levi-Civita symbols and contraction of indices

$$H^{jk} = \epsilon^{jkl} X_l \quad (\text{D.73})$$

yields a  $(2, 0)$  relative tensor field of weight  $+1$ , and its covariant differentiation and successive contraction of the index

$$H_{|k}^{jk} = \frac{\partial H^{jk}}{\partial x_k} + \gamma_m^j{}^k H^{mk} + \gamma_m^k{}^j H^{jm} - \gamma_k^m{}^j H^{jm} \quad (\text{D.74})$$

yields a relative contravariant vector field of weight  $+1$ . The last two terms of the right hand side of (D.74) are identical to each other, and its second term is identically zero because  $\gamma_m^j{}^k = \gamma_k^j{}^m$  and  $H^{mk} = -H^{km}$  ( $H^{mk} = 0$  for  $m = k$ ). Curl of the covariant vector field  $X_l$  is defined by

$$R^j = (\text{curl } X)^j = \frac{1}{\sqrt{g}} \frac{\partial H^{jk}}{\partial x^k}. \quad (\text{D.75})$$

It has the same tensoric characteristics as (D.65). Their actual expressions are

$$(R^1, R^2, R^3) = \frac{1}{\sqrt{g}} \left( \frac{\partial X_3}{\partial x^2} - \frac{\partial X_2}{\partial x^3}, \frac{\partial X_1}{\partial x^3} - \frac{\partial X_3}{\partial x^1}, \frac{\partial X_2}{\partial x^1} - \frac{\partial X_1}{\partial x^2} \right), \quad (\text{D.76})$$

and their representation in the Descartes coordinate system is

$$\hat{R}_1 = \frac{1}{h_2 h_3} \left[ \frac{\partial}{\partial x^2} (h_3 \hat{X}_3) - \frac{\partial}{\partial x^3} (h_2 \hat{X}_2) \right], \quad (\text{D.77})$$

$$\hat{R}_2 = \frac{1}{h_3 h_1} \left[ \frac{\partial}{\partial x^3} (h_1 \hat{X}_1) - \frac{\partial}{\partial x^1} (h_3 \hat{X}_3) \right], \quad (\text{D.78})$$

$$\hat{R}_3 = \frac{1}{h_1 h_2} \left[ \frac{\partial}{\partial x^1} (h_2 \hat{X}_2) - \frac{\partial}{\partial x^2} (h_1 \hat{X}_1) \right]. \quad (\text{D.79})$$

### D.4.3 Tensoric Representation of Viscosity

Stress tensor  $\sigma^{jk}$  is defined as a  $(2, 0)$  tensor whose divergence represents force:

$$f^j = \sigma_{|k}^{jk}. \quad (\text{D.80})$$

Strain rate tensor  $\varepsilon^{jk}$  is a  $(2, 0)$  tensor defined by

$$\varepsilon^{jk} = \frac{1}{2} \left( g^{jl} v_{|l}^k + g^{lk} v_{|l}^j \right), \quad (\text{D.81})$$

or, equivalently, a  $(0, 2)$  tensor defined by

$$\varepsilon_{jk} = \frac{1}{2} \left( g_{jl} v_{|k}^l + g_{lk} v_{|j}^l \right). \quad (\text{D.82})$$

Stress tensor and strain rate tensor are related to each other by a constitutive equation

$$\sigma^{jk} = c^{jklm} \varepsilon_{lm}, \quad (\text{D.83})$$

where  $c^{jklm}$  is a  $(4, 0)$  tensor.

For isotropic viscosity of an incompressible fluid, the constitutive equation is given by

$$\tau^{jk} = 2\eta \varepsilon^{jk}, \quad (\text{D.84})$$

where  $\eta$  is a constant of proportionality, and

$$\tau^{jk} = \sigma^{jk} + P g^{jk} \quad (\text{D.85})$$

is deviatoric stress tensor, where  $P$  is mechanical pressure (isotropic component of the stress tensor) defined by

$$P = -\frac{\text{tr } \sigma}{n}. \quad (\text{D.86})$$

By definition, trace of the deviatoric stress tensor is identically zero. Divergence of  $\tau^{jk}$  is expressed as

$$\tau_{|k}^{jk} = (2\eta \varepsilon^{jk})_{|k} = 2\eta_{|k} \varepsilon^{jk} + 2\eta \varepsilon_{|k}^{jk}. \quad (\text{D.87})$$

For the second term of its last expression,

$$\varepsilon_{|k}^{jk} = \frac{1}{2} \left( g^{jl} v_{|l|k}^k + g^{lk} v_{|l|k}^j \right) \quad (\text{D.88})$$

using the Ricci's identity (D.27). In a flat space, furthermore,

$$v_{|l|k}^k = v_{|k|l}^k = 0, \quad (\text{D.89})$$

due to the facts that the curvature tensor is the zero tensor and the continuity equation holds, so

$$\varepsilon_{|k}^{jk} = \frac{1}{2} g^{lk} v_{|l|k}^j. \quad (\text{D.90})$$

The covariant form of the Navier-Stokes equation is expressed as

$$\frac{\partial v^j}{\partial t} + v^k v_{|k}^j = -\frac{1}{\rho} g^{jk} \frac{\partial P}{\partial x^k} + \frac{1}{\rho} \tau_{|k}^{jk}. \quad (\text{D.91})$$

Its advection term is written down as

$$a^j = v^k v_{|k}^j = v^k \left( \frac{\partial v^j}{\partial x^k} + \gamma_m^j{}^k v^m \right), \quad (\text{D.92})$$

and its representation in the local Descartes coordinate system is

$$\frac{\hat{a}_\alpha}{h_\alpha} = a^\alpha = \sum_\beta \frac{\hat{v}_\beta}{h_\beta} \frac{\partial}{\partial x^\beta} \left( \frac{\hat{v}_\alpha}{h_\alpha} \right) + \sum_\beta \sum_\delta \frac{\gamma_\beta^\alpha{}_\delta}{h_\beta h_\delta} \hat{v}_\beta \hat{v}_\delta. \quad (\text{D.93})$$

Viscous force is calculated by

$$f^j = \tau_{|k}^{jk} = \frac{\partial \tau^{jk}}{\partial x^k} + \gamma_m^j{}^k \tau^{mk} + \gamma_m^k{}^j \tau^{jm}. \quad (\text{D.94})$$

For the local Descartes coordinate system,

$$\hat{f}_\alpha = h_\alpha f^\alpha, \quad \hat{\tau}_{\alpha\beta} = h_\alpha h_\beta \tau^{\alpha\beta}, \quad (\text{D.95})$$

and

$$\frac{\hat{f}_\alpha}{h_\alpha} = \sum_\beta \frac{\partial}{\partial x^\beta} \left( \frac{\hat{\tau}_{\alpha\beta}}{h_\alpha h_\beta} \right) + \sum_\beta \sum_\delta \frac{\gamma_{\beta\delta}^\alpha}{h_\beta h_\delta} \hat{\tau}_{\beta\delta} + \sum_\beta \frac{1}{\sqrt{g}} \frac{\partial \sqrt{g}}{\partial x^\beta} \frac{\hat{\tau}_{\alpha\beta}}{h_\alpha h_\beta}. \quad (\text{D.96})$$

Components of strain rate tensor are represented as

$$\begin{aligned} \hat{\varepsilon}_{\alpha\beta} &= h_\alpha h_\beta \varepsilon^{\alpha\beta} \\ &= \frac{h_\alpha h_\beta}{2} \left( g^{\alpha\alpha} v_{|\alpha}^\beta + g^{\beta\beta} v_{|\beta}^\alpha \right) \\ &= \frac{1}{2} \frac{h_\beta}{h_\alpha} \left[ \frac{\partial}{\partial x^\alpha} \left( \frac{\hat{v}_\beta}{h_\beta} \right) + \sum_\delta \frac{\gamma_{\delta\alpha}^\beta}{h_\delta} \hat{v}_\delta \right] + \frac{1}{2} \frac{h_\alpha}{h_\beta} \left[ \frac{\partial}{\partial x^\beta} \left( \frac{\hat{v}_\alpha}{h_\alpha} \right) + \sum_\delta \frac{\gamma_{\delta\beta}^\alpha}{h_\delta} \hat{v}_\delta \right]. \end{aligned} \quad (\text{D.97})$$

#### D.4.4 Anisotropic viscosity for three-dimensional fluid

A constitutive equation for viscosity is usually described as a relation between deviatoric stress tensor and strain rate tensor:

$$\tau^{jk} = c^{jklm} \varepsilon^{lm}. \quad (\text{D.98})$$

For the three dimensional case,  $c^{jklm}$  consists of 81 components. Because of the symmetry of  $\tau$  and  $\varepsilon$ , the coefficient has symmetries

$$c^{jklm} = c^{kjlm} = c^{jkm}, \quad (\text{D.99})$$

which reduces the number of independent parameters from 81 to 36. The general form for the constitutive equation can now be described as

$$\begin{pmatrix} \tau_{11} \\ \tau_{22} \\ \tau_{33} \\ \tau_{12} \\ \tau_{13} \\ \tau_{23} \end{pmatrix} = \begin{pmatrix} c^{1111} & c^{1122} & c^{1133} & c^{1112} & c^{1113} & c^{1123} \\ c^{2211} & c^{2222} & c^{2233} & c^{2212} & c^{2213} & c^{2223} \\ c^{3311} & c^{3322} & c^{3333} & c^{3312} & c^{3313} & c^{3323} \\ c^{1211} & c^{1222} & c^{1233} & c^{1212} & c^{1213} & c^{1223} \\ c^{1311} & c^{1322} & c^{1333} & c^{1312} & c^{1313} & c^{1323} \\ c^{2311} & c^{2322} & c^{2333} & c^{2312} & c^{2313} & c^{2323} \end{pmatrix} \begin{pmatrix} \varepsilon_{11} \\ \varepsilon_{22} \\ \varepsilon_{33} \\ 2\varepsilon_{12} \\ 2\varepsilon_{13} \\ 2\varepsilon_{23} \end{pmatrix}. \quad (\text{D.100})$$

Note that the factor of 2 multiplied to  $\varepsilon_{12}$ ,  $\varepsilon_{13}$  and  $\varepsilon_{23}$  comes from the symmetry such as:

$$\begin{aligned} \tau_{12} &= c^{1211} \varepsilon_{11} + c^{1222} \varepsilon_{22} + c^{1233} \varepsilon_{33} + c^{1212} \varepsilon_{12} + c^{1221} \varepsilon_{21} + c^{1213} \varepsilon_{13} + c^{1231} \varepsilon_{31} + c^{1223} \varepsilon_{23} + c^{1232} \varepsilon_{32} \\ &= c^{1211} \varepsilon_{11} + c^{1222} \varepsilon_{22} + c^{1233} \varepsilon_{33} + 2c^{1212} \varepsilon_{12} + 2c^{1213} \varepsilon_{13} + 2c^{1223} \varepsilon_{23} \end{aligned} \quad (\text{D.101})$$

In order for energy dissipation rate, defined by

$$\tau^{jk} \varepsilon_{jk} = c^{jklm} \varepsilon_{jk} \varepsilon_{lm}, \quad (\text{D.102})$$

to be well-defined, another symmetry arises:

$$c^{jklm} = c^{lmjk}, \quad (\text{D.103})$$

which makes the coefficient matrix symmetric, and reduces the number of independent parameters to 21. This is the most general representation for three-dimensional anisotropic viscosity.

When the fluid is isotropic about an axis directing to  $x^3$ , the coefficient matrix reduces to

$$\begin{pmatrix} c_1 & c_2 & c_3 & 0 & 0 & 0 \\ c_2 & c_1 & c_3 & 0 & 0 & 0 \\ c_3 & c_3 & c_4 & 0 & 0 & 0 \\ 0 & 0 & 0 & (c_1 - c_2)/2 & 0 & 0 \\ 0 & 0 & 0 & 0 & c_5 & 0 \\ 0 & 0 & 0 & 0 & 0 & c_5 \end{pmatrix}. \quad (\text{D.104})$$

See, for example, *Love [1927]*. Furthermore, when the fluid is incompressible, the zero-trace requirement for the deviatoric stress tensor yields

$$\begin{aligned} 0 &= \tau_{11} + \tau_{22} + \tau_{33} \\ &= (c_1 + c_2 + c_3)(\varepsilon_{11} + \varepsilon_{22}) + (2c_3 + c_4)\varepsilon_{33} \\ &= -(c_1 + c_2 + c_3)\varepsilon_{33} + (2c_3 + c_4)\varepsilon_{33}, \end{aligned} \quad (\text{D.105})$$

and thus

$$c_4 = c_1 + c_2 - c_3. \quad (\text{D.106})$$

The constitutive equation is now described as

$$\tau_{11} = (c_1 - c_3)\varepsilon_{11} + (c_2 - c_3)\varepsilon_{22}, \quad (\text{D.107})$$

$$\tau_{22} = (c_2 - c_3)\varepsilon_{11} + (c_1 - c_3)\varepsilon_{22}, \quad (\text{D.108})$$

$$\tau_{33} = (c_1 + c_2 - 2c_3)\varepsilon_{33}, \quad (\text{D.109})$$

$$\tau_{12} = (c_1 - c_2)\varepsilon_{12}, \quad (\text{D.110})$$

$$\tau_{13} = 2c_5\varepsilon_{13}, \quad (\text{D.111})$$

$$\tau_{23} = 2c_5\varepsilon_{23}. \quad (\text{D.112})$$

## D.5 Three-Dimensional Polar Coordinate Example

To illustrate what are an orthogonal curvilinear coordinate system and its local Descartes coordinate system, a well-known example of the polar coordinate system of the three-dimensional Euclidean space is considered here. Let  $r$ ,  $\varphi$  and  $\lambda$  denote radial distance, latitude and longitude, respectively, of the polar coordinate system (latitude is used here instead of polar zenith angle). The metric tensor of the polar coordinate system is diagonal, and those diagonal components are written as

$$g_{rr} = 1, \quad g_{\varphi\varphi} = r^2, \quad g_{\lambda\lambda} = r^2 \cos^2 \varphi. \quad (\text{D.113})$$

Velocity components of a moving point defined by

$$v^r = \frac{dr}{dt}, \quad v^\varphi = \frac{d\varphi}{dt}, \quad v^\lambda = \frac{d\lambda}{dt} \quad (\text{D.114})$$

constitute components of a contravariant vector, where  $t$  is time, and the scalar magnitude of this velocity is given by

$$|\mathbf{v}|^2 = (v^r)^2 + r^2(v^\varphi)^2 + r^2 \cos^2 \varphi (v^\lambda)^2. \quad (\text{D.115})$$

The components of this velocity vector in the local Descartes coordinate system are

$$w = \hat{v}^r = h_r v^r = v^r, \quad v = \hat{v}^\varphi = h_\varphi v^\varphi = r v^\varphi, \quad u = \hat{v}^\lambda = h_\lambda v^\lambda = r \cos \varphi v^\lambda, \quad (\text{D.116})$$

and its scalar magnitude is represented by

$$|\mathbf{v}|^2 = u^2 + v^2 + w^2. \quad (\text{D.117})$$

Nonzero components of the Christoffel symbols are

$$\gamma_{\varphi}^r{}_{\varphi} = -r, \quad (\text{D.118})$$

$$\gamma_{\lambda}^r = -r \cos^2 \varphi, \quad (D.119)$$

$$\gamma_r^\varphi = \gamma_\varphi^r = \gamma_r^\lambda = \gamma_\lambda^r = \frac{1}{r}, \quad (D.120)$$

$$\gamma_\lambda^\varphi = \sin \varphi \cos \varphi, \quad (D.121)$$

$$\gamma_\varphi^\lambda = \gamma_\lambda^\varphi = -\tan \varphi, \quad (D.122)$$

so the local Descartes coordinate expressions for the Navier-Stokes equations are

$$\frac{\partial u}{\partial t} + \frac{u}{r \cos \varphi} \frac{\partial u}{\partial \lambda} + \frac{v}{r} \frac{\partial u}{\partial \varphi} + w \frac{\partial u}{\partial r} - \frac{uv \tan \varphi}{r} + \frac{uw}{r} = -\frac{1}{\rho r \cos \varphi} \frac{\partial P}{\partial \lambda} + \frac{1}{\rho} \hat{f}_\lambda, \quad (D.123)$$

$$\frac{\partial v}{\partial t} + \frac{u}{r \cos \varphi} \frac{\partial v}{\partial \lambda} + \frac{v}{r} \frac{\partial v}{\partial \varphi} + w \frac{\partial v}{\partial r} + \frac{u^2 \tan \varphi}{r} + \frac{vw}{r} = -\frac{1}{\rho r} \frac{\partial P}{\partial \varphi} + \frac{1}{\rho} \hat{f}_\varphi, \quad (D.124)$$

$$\frac{\partial w}{\partial t} + \frac{u}{r \cos \varphi} \frac{\partial w}{\partial \lambda} + \frac{v}{r} \frac{\partial w}{\partial \varphi} + w \frac{\partial w}{\partial r} - \frac{u^2 + v^2}{r} = -\frac{1}{\rho} \frac{\partial P}{\partial r} + \frac{1}{\rho} \hat{f}_r, \quad (D.125)$$

where

$$\begin{aligned} \frac{\hat{f}_\lambda}{\eta} &= \frac{1}{r^2 \cos^2 \varphi} \frac{\partial^2 u}{\partial \lambda^2} + \frac{1}{r^2 \cos \varphi} \frac{\partial}{\partial \varphi} \left( \cos \varphi \frac{\partial u}{\partial \varphi} \right) + \frac{1}{r^2} \frac{\partial}{\partial r} \left( r^2 \frac{\partial u}{\partial r} \right) \\ &\quad + \frac{2}{r^2 \cos \varphi} \frac{\partial w}{\partial \lambda} - \frac{2 \sin \varphi}{r^2 \cos^2 \varphi} \frac{\partial v}{\partial \lambda} - \frac{u}{r^2 \cos^2 \varphi}, \end{aligned} \quad (D.126)$$

$$\begin{aligned} \frac{\hat{f}_\varphi}{\eta} &= \frac{1}{r^2 \cos^2 \varphi} \frac{\partial^2 v}{\partial \lambda^2} + \frac{1}{r^2 \cos \varphi} \frac{\partial}{\partial \varphi} \left( \cos \varphi \frac{\partial v}{\partial \varphi} \right) + \frac{1}{r^2} \frac{\partial}{\partial r} \left( r^2 \frac{\partial v}{\partial r} \right) \\ &\quad + \frac{2 \sin \varphi}{r^2 \cos^2 \varphi} \frac{\partial u}{\partial \lambda} + \frac{2}{r^2} \frac{\partial w}{\partial \varphi} - \frac{v}{r^2 \cos^2 \varphi}, \end{aligned} \quad (D.127)$$

$$\begin{aligned} \frac{\hat{f}_r}{\eta} &= \frac{1}{r^2 \cos^2 \varphi} \frac{\partial^2 w}{\partial \lambda^2} + \frac{1}{r^2 \cos \varphi} \frac{\partial}{\partial \varphi} \left( \cos \varphi \frac{\partial w}{\partial \varphi} \right) + \frac{1}{r^2} \frac{\partial}{\partial r} \left( r^2 \frac{\partial w}{\partial r} \right) \\ &\quad - \frac{2}{r^2 \cos^2 \varphi} \frac{\partial u}{\partial \lambda} - \frac{2}{r^2 \cos^2 \varphi} \frac{\partial (v \cos \varphi)}{\partial \varphi} - \frac{2w}{r^2}, \end{aligned} \quad (D.128)$$

for homogeneous, isotropic viscosity.

## D.6 Application to COCO

Let  $x$  and  $y$  be two horizontal coordinates and  $r$  be radial distance from the earth's center. The metric in the radial direction is

$$h_r = 1, \quad (D.129)$$

and the metrics for the horizontal coordinates are represented by a product of  $r$  and a function independent of  $r$ :

$$h_x = r h'_x(x, y), \quad h_y = r h'_y(x, y). \quad (D.130)$$

Given the metrics  $h_x$  and  $h_y$ , nonzero components of the Christoffel symbols are calculated as

$$\gamma_x^x = \frac{1}{h_x} \frac{\partial h_x}{\partial x}, \quad (D.131)$$

$$\gamma_y^y = \frac{1}{h_y} \frac{\partial h_y}{\partial y}, \quad (D.132)$$

$$\gamma_y^x = \gamma_x^y = \frac{1}{h_x} \frac{\partial h_x}{\partial y}, \quad (D.133)$$

$$\gamma_x^y = \gamma_y^x = \frac{1}{h_y} \frac{\partial h_y}{\partial x}, \quad (D.134)$$

$$\gamma_r^x = \gamma_x^r = \gamma_r^y = \gamma_y^r = \frac{1}{r}, \quad (\text{D.135})$$

$$\gamma_y^x = -\frac{h_y}{h_x^2} \frac{\partial h_y}{\partial x}, \quad (\text{D.136})$$

$$\gamma_x^y = -\frac{h_x}{h_y^2} \frac{\partial h_x}{\partial y}, \quad (\text{D.137})$$

$$\gamma_x^r = -h_x \frac{\partial h_x}{\partial r} = -\frac{h_x^2}{r}, \quad (\text{D.138})$$

$$\gamma_y^r = -h_y \frac{\partial h_y}{\partial r} = -\frac{h_y^2}{r}. \quad (\text{D.139})$$

The geopotential vertical coordinate  $z$  is defined as

$$r = a + z, \quad (\text{D.140})$$

where  $a$  is the earth's radius (the distance between the earth's center and the mean sea surface). Infinitesimal displacement in the  $z$  direction is identical to that in the  $r$  direction:

$$dr = dz, \quad (\text{D.141})$$

and the shallowness approximation

$$\frac{1}{r} \simeq \frac{1}{a} \quad (\text{D.142})$$

is employed, as  $|z| \ll a$ .

The continuity equation of incompressible fluid is represented by

$$\frac{1}{h_x h_y} \left[ \frac{\partial}{\partial x} (h_y u) + \frac{\partial}{\partial y} (h_x v) + \frac{\partial}{\partial r} (h_x h_y w) \right] = 0, \quad (\text{D.143})$$

where  $u$ ,  $v$  and  $w$  are velocity components for  $x$ ,  $y$  and  $r$  directions, respectively. It is rewritten as

$$\frac{1}{h_x h_y} \left[ \frac{\partial}{\partial x} (h_y u) + \frac{\partial}{\partial y} (h_x v) \right] + \frac{1}{r^2} \frac{\partial}{\partial r} (r^2 w) = 0. \quad (\text{D.144})$$

Under the shallowness approximation,  $r$  and  $dr$  in its last term of the left hand side are replaced by  $a$  and  $dz$ , respectively, thus yielding

$$\frac{1}{h_x h_y} \left[ \frac{\partial}{\partial x} (h_y u) + \frac{\partial}{\partial y} (h_x v) \right] + \frac{\partial w}{\partial z} = 0. \quad (\text{D.145})$$

The general representation of the frictional force in the current  $(x, y, r)$  coordinate system is:

$$f_x = \frac{1}{h_x h_y} \left[ \frac{\partial}{\partial x} (h_y \tau_{xx}) + \frac{\partial}{\partial y} (h_x \tau_{xy}) + \frac{\partial h_x}{\partial y} \tau_{xy} - \frac{\partial h_y}{\partial x} \tau_{yy} \right] + \frac{1}{r^2} \frac{\partial}{\partial r} (r^2 \tau_{xr}) + \frac{\tau_{xr}}{r}, \quad (\text{D.146})$$

$$f_y = \frac{1}{h_x h_y} \left[ \frac{\partial}{\partial x} (h_y \tau_{xy}) + \frac{\partial}{\partial y} (h_x \tau_{yy}) + \frac{\partial h_y}{\partial x} \tau_{xy} - \frac{\partial h_x}{\partial y} \tau_{xx} \right] + \frac{1}{r^2} \frac{\partial}{\partial r} (r^2 \tau_{yr}) + \frac{\tau_{yr}}{r}, \quad (\text{D.147})$$

$$f_r = \frac{1}{h_x h_y} \left[ \frac{\partial}{\partial x} (h_y \tau_{xr}) + \frac{\partial}{\partial y} (h_x \tau_{yr}) \right] + \frac{1}{r^2} \frac{\partial}{\partial r} (r^2 \tau_{rr}) - \frac{\tau_{xx}}{r} - \frac{\tau_{yy}}{r}. \quad (\text{D.148})$$

The terms inside the square bracket of (D.146) can be rewritten as

$$\frac{\partial}{\partial x} \left[ h_y \left( \frac{\tau_{xx} - \tau_{yy}}{2} + \frac{\tau_{xx} + \tau_{yy}}{2} \right) \right] + \frac{1}{h_x} \frac{\partial}{\partial y} (h_x^2 \tau_{xy}) + \frac{\partial h_y}{\partial x} \left( \frac{\tau_{xx} - \tau_{yy}}{2} - \frac{\tau_{xx} + \tau_{yy}}{2} \right). \quad (\text{D.149})$$

Using the fact that trace of deviatoric tensor is identically zero:

$$\tau_{xx} + \tau_{yy} + \tau_{rr} = 0, \quad (\text{D.150})$$

it reduces to

$$\frac{1}{h_y} \frac{\partial}{\partial x} \left( h_y^2 \frac{\tau_{xx} - \tau_{yy}}{2} \right) + \frac{1}{h_x} \frac{\partial}{\partial y} (h_x^2 \tau_{xy}) - \frac{h_y}{2} \frac{\partial \tau_{rr}}{\partial x}. \quad (\text{D.151})$$

Therefore, (D.146) becomes

$$f_x = \frac{1}{h_x h_y} \left[ \frac{1}{h_y} \frac{\partial}{\partial x} \left( h_y^2 \frac{\tau_{xx} - \tau_{yy}}{2} \right) + \frac{1}{h_x} \frac{\partial}{\partial y} (h_x^2 \tau_{xy}) \right] + \frac{1}{r^2} \frac{\partial}{\partial r} (r^2 \tau_{xr}) + \frac{\tau_{xr}}{r} - \frac{1}{2h_x} \frac{\partial \tau_{rr}}{\partial x}. \quad (\text{D.152})$$

Likewise, (D.147) becomes

$$f_y = \frac{1}{h_x h_y} \left[ \frac{1}{h_y} \frac{\partial}{\partial x} (h_y^2 \tau_{xy}) + \frac{1}{h_x} \frac{\partial}{\partial y} \left( h_x^2 \frac{\tau_{yy} - \tau_{xx}}{2} \right) \right] + \frac{1}{r^2} \frac{\partial}{\partial r} (r^2 \tau_{yr}) + \frac{\tau_{yr}}{r} - \frac{1}{2h_y} \frac{\partial \tau_{rr}}{\partial y}. \quad (\text{D.153})$$

Components of strain rate tensor are defined by

$$\varepsilon_{xx} = \frac{1}{h_x} \frac{\partial u}{\partial x} + h_{xy} v + \frac{w}{r}, \quad (\text{D.154})$$

$$\varepsilon_{yy} = \frac{1}{h_y} \frac{\partial v}{\partial y} + h_{yx} u + \frac{w}{r}, \quad (\text{D.155})$$

$$\varepsilon_{rr} = \frac{\partial w}{\partial r}, \quad (\text{D.156})$$

$$\varepsilon_{xy} = \varepsilon_{yx} = \frac{1}{2} \left[ \frac{h_x}{h_y} \frac{\partial}{\partial y} \left( \frac{u}{h_x} \right) + \frac{h_y}{h_x} \frac{\partial}{\partial x} \left( \frac{v}{h_y} \right) \right], \quad (\text{D.157})$$

$$\varepsilon_{xr} = \varepsilon_{rx} = \frac{1}{2} \left( \frac{\partial u}{\partial r} + \frac{1}{h_x} \frac{\partial w}{\partial x} - \frac{u}{r} \right), \quad (\text{D.158})$$

$$\varepsilon_{yr} = \varepsilon_{ry} = \frac{1}{2} \left( \frac{\partial v}{\partial r} + \frac{1}{h_y} \frac{\partial w}{\partial y} - \frac{v}{r} \right). \quad (\text{D.159})$$

For the case of horizontal-vertical transverse anisotropic viscosity (i.e., isotropy about the axis of symmetry which coincides with the vertical direction), the constitutive equation is represented by using three parameters  $A_H$ ,  $A_V$  and  $\nu$ :

$$\tau_{xx} = (A_H + \nu) \varepsilon_{xx} + (\nu - A_H) \varepsilon_{yy}, \quad (\text{D.160})$$

$$\tau_{yy} = (\nu - A_H) \varepsilon_{xx} + (A_H + \nu) \varepsilon_{yy}, \quad (\text{D.161})$$

$$\tau_{rr} = 2\nu \varepsilon_{rr}, \quad (\text{D.162})$$

$$\tau_{xy} = 2A_H \varepsilon_{xy}, \quad (\text{D.163})$$

$$\tau_{xr} = 2A_V \varepsilon_{xr}, \quad (\text{D.164})$$

$$\tau_{yr} = 2A_V \varepsilon_{yr}, \quad (\text{D.165})$$

by setting

$$A_H = \frac{c_1 - c_2}{2}, \quad A_V = c_5, \quad \nu = \frac{c_1 + c_2 - 2c_3}{2} \quad (\text{D.166})$$

in (D.107)–(D.112). See *Wajsovicz [1993]* for detail. In (D.152) and (D.153),  $\tau_{xx}$  and  $\tau_{yy}$  appear only as their subtraction,  $\tau_{xx} - \tau_{yy}$ , for which the constitutive equation reduces simply to

$$\tau_{xx} - \tau_{yy} = 2A_H (\varepsilon_{xx} - \varepsilon_{yy}). \quad (\text{D.167})$$

In this representation, the last term of the right hand sides of (D.154) and (D.155) cancels each other out. With the shallowness approximation and consistency with the hydrostatic approximation (the latter leads

to  $\nu = 0$  and means that the terms including  $w$  should be neglected), therefore, the frictional force terms are represented by

$$f_x = \frac{1}{h_x h_y} \left[ \frac{1}{h_y} \frac{\partial}{\partial x} \left( h_y^2 \frac{\tau_{xx} - \tau_{yy}}{2} \right) + \frac{1}{h_x} \frac{\partial}{\partial y} (h_x^2 \tau_{xy}) \right] + \frac{\partial \tau_{xz}}{\partial z} + \frac{\tau_{xz}}{a}, \quad (\text{D.168})$$

$$f_y = \frac{1}{h_x h_y} \left[ \frac{1}{h_y} \frac{\partial}{\partial x} (h_y^2 \tau_{xy}) + \frac{1}{h_x} \frac{\partial}{\partial y} \left( h_x^2 \frac{\tau_{yy} - \tau_{xx}}{2} \right) \right] + \frac{\partial \tau_{yz}}{\partial z} + \frac{\tau_{yz}}{a}, \quad (\text{D.169})$$

where

$$\tau_{xx} - \tau_{yy} = 2A_H(\varepsilon_{xx} - \varepsilon_{yy}), \quad (\text{D.170})$$

$$\tau_{xy} = 2A_H \varepsilon_{xy}, \quad (\text{D.171})$$

$$\tau_{xz} = 2A_V \varepsilon_{xz}, \quad (\text{D.172})$$

$$\tau_{yz} = 2A_V \varepsilon_{yz}, \quad (\text{D.173})$$

with the components of strain rate tensor redefined as

$$\varepsilon_{xx} = \frac{1}{h_x} \frac{\partial u}{\partial x} + h_{xy} v, \quad (\text{D.174})$$

$$\varepsilon_{yy} = \frac{1}{h_y} \frac{\partial v}{\partial y} + h_{yx} u, \quad (\text{D.175})$$

$$\varepsilon_{xy} = \varepsilon_{yx} = \frac{1}{2} \left[ \frac{h_x}{h_y} \frac{\partial}{\partial y} \left( \frac{u}{h_x} \right) + \frac{h_y}{h_x} \frac{\partial}{\partial x} \left( \frac{v}{h_y} \right) \right], \quad (\text{D.176})$$

$$\varepsilon_{xz} = \varepsilon_{zx} = \frac{1}{2} \left( \frac{\partial u}{\partial z} - \frac{u}{a} \right), \quad (\text{D.177})$$

$$\varepsilon_{yz} = \varepsilon_{zy} = \frac{1}{2} \left( \frac{\partial v}{\partial z} - \frac{v}{a} \right). \quad (\text{D.178})$$

# References

- Adcroft, A., C. Hill and J. Marshall (1997): Representation of topography by shaved cells in a height coordinate ocean model, *Mon. Wea. Rev.*, *125*, 2293–2315.
- Arakawa, A. (1966): Computational design for long-term numerical integration of the equation of fluid motion: Two-dimensional incompressible flow. Part I, *J. Comput. Phys.*, *1*, 119–143.
- Baum, E., and E. A. Capani (1992): Modeling the effects of buoyancy on the evolution of geophysical boundary layers, *J. Geophys. Res.*, *97*, 15,513–15,527.
- Bentsen, M., G. Evensen, H. Drange and D. Jenkins (1999): Coordinate transformation on a sphere using conformal mapping, *Mon. Wea. Rev.*, *127*, 2733–2740.
- Bryan, K., S. Manabe and R. C. Pacanowski (1975): A global ocean-atmosphere climate model. Part II. The oceanic circulation, *J. Phys. Oceanogr.*, *5*, 30–46.
- Bryan, K. (1984): Accelerating the convergence to equilibrium of ocean climate models, *J. Phys. Oceanogr.*, *14*, 663–673.
- Bryden, H. L. (1973): New polynomials for thermal expansion, adiabatic temperature gradient and potential temperature of sea water, *Deep-Sea Res.*, *20*, 401–408.
- Cox, M. D. (1987): Isopycnal diffusion in a z-coordinate ocean model, *Ocean Modelling*, *74*, 1–5.
- Garret, C. J. R., and W. H. Munk (1975): Space-time scales of internal waves: A progress report, *J. Geophys. Res.*, *80*, 291–297.
- Gent, P. R. and J. C. McWilliams (1990): Isopycnal mixing in ocean circulation models, *J. Phys. Oceanogr.*, *20*, 150–155.
- Gregg, M. C., T. B. Sanford, and D. P. Winkel (2003): Reduced mixing from the breaking of internal waves in equatorial waters, *Nature*, *422*, 513–515.
- Griffies, S. M. (1998): The Gent-McWilliams skew flux, *J. Phys. Oceanogr.*, *28*, 831–841.
- Griffies, S. M., and R. W. Hallberg (2000): Biharmonic friction with a Smagorinsky-like viscosity for use in large-scale eddy-permitting ocean models, *J. Phys. Oceanogr.*, *30*, 2935–2946.
- Haney, R. L. (1971): Surface thermal boundary condition for ocean circulation models, *J. Phys. Oceanogr.*, *1*, 241–248.
- Hibler, W. D., III (1979): A dynamic thermodynamic sea ice model, *J. Phys. Oceanogr.*, *9*, 815–846.

- Hunke, E., and J. K. Dukowicz (1997): An elastic-viscous-plastic model for sea ice dynamics, *J. Phys. Oceanogr.*, *27*, 1849–1867.
- Ishizaki, H., and T. Motoi (1999): Reevaluation of the Takano-Oonishi scheme for momentum advection on bottom relief in ocean models, *J. Atmos. Ocean Tech.*, *16*, 1994–2010.
- Kara, A. B., P. A. Rochford and H. E. Hurlburt (2000): Efficient and accurate bulk parameterizations of air-sea fluxes for use in general circulation models, *J. Atmos. Oceanic Tech.*, *17*, 1421–1438.
- Killworth, P. D., D. Stainforth, D. J. Webb and S. M. Paterson (1991): The development of a free-surface Bryan-Cox-Semtner ocean model, *J. Phys. oceanogr.*, *21*, 1333–1348.
- Kondo, J., O. Kanechika and N. Yasuda (1978): Heat and momentum transfers under strong stability in the atmospheric surface layer, *J. Atmos. Sci.*, *35*, 1012–1021.
- Large, W. G., G. D. Danabasoglu, J. C. McWilliams, P. R. Gent and F. O. Bryan (2001): Equatorial circulation of a global ocean climate model with anisotropic horizontal viscosity, *J. Phys. Oceanogr.*, *31*, 518–536.
- Large, W. G., and S. G. Yeager (2004): Diurnal to decadal global forcing for ocean and sea-ice models: the data sets and flux climatologies, NCAR Technical Note 460, National Center for Atmospheric Research, Boulder, 105pp.
- Leonard, B. P. (1979): A stable and accurate convective modelling procedure based on quadratic upstream interpolation, *Comput. Method Appl. Mech. Eng.*, *19*, 59–98.
- Leonard, B. P. (1991): The ULTIMATE conservative difference scheme applied to unsteady one-dimensional advection, *Comput. Methods Appl. Mech. Eng.*, *88*, 17–74.
- Leonard, B. P., M. K. MacVean and A. P. Lock (1993): Positivity-preserving numerical schemes for multi-dimensional advection, *NASA Tech. Memo.*, *106055*, ICOMP-93-05.
- Leonard, B. P., M. K. MacVean and A. P. Lock (1994): The flux-integral method for multidimensional convection and diffusion, *NASA Tech. Memo.*, *106679*, ICOMP-94-13.
- Leonard, B. P., A. P. Lock and M. K. MacVean (1996): Conservative explicit unrestricted-time-step multi-dimensional constancy-preserving advection schemes, *Mon. Wea. Rev.*, *124*, 2588–2606.
- Love, A. E. (1927): *A Treatise on the Mathematical Theory of Elasticity*, Cambridge University Press, Cambridge.
- McDougall, T. J., D. R. Jackett, D. G. Wright and R. Feistel (2003): Accurate and computationally efficient algorithms for potential temperature and density of seawater, *J. Atmos. Ocean Tech.*, *20*, 730–741.
- McPhee, M. G. (1978): A simulation of inertial oscillation in drifting pack ice, *Dyn. Atmos. Oceans*, *2*, 107–122.
- Mellor, G. L., and T. Yamada (1982): Development of a turbulence closure model for geophysical fluid problems, *Rev. Geophys. Space Phys.*, *20*, 851–875.
- Mellor, G. L., and L. Kantha (1989): An ice-ocean coupled model, *J. Geophys. Res.*, *94*, 10,936–10,954.

- Mellor, G. L. (1991): *An equation of state for numerical models of oceans and estuaries*, J. Atmos. Ocean Tech., 8, 609–611.
- Mesinger, R. and A. Arakawa (1976): *Numerical Methods Used in Atmospheric Models, 1, Vol. 17 of GARP Publication Series, World Meteorological Organization, Geneva.*
- Nakano, H., and N. Sugimoto (2002): *Effects of bottom boundary layer parameterization on reproducing deep and bottom waters in a World Ocean model*, J. Phys. Oceanogr., 32, 1209–1227.
- Noh, Y., and H. J. Kim (1999): *Simulations of temperature and turbulence structure of the oceanic boundary layer with the improved near-surface process*, J. Geophys. Res., 104, 15,621–15,634.
- Peixoto, J. P., and A. H. Oort (1991): *Physics of Climate, American Institute of Physics, New York, 520pp.*
- Röske, F. (2001): *An atlas of surface fluxes based on the ECMWF Re-Analysis – a climatological dataset to force global ocean general circulation models*, Max-Planck-Institut für Meteorologie Rep. 323, Max-Planck-Institut für Meteorologie, Hamburg, 31 pp.
- Rosati, A., and K. Miyakoda (1988): *A general circulation model for upper ocean simulation*, J. Phys. Oceanogr., 18, 1601–1626.
- Semtner, A. J., Jr. (1976): *A model for the thermodynamic growth of sea ice in numerical investigations of climate*, J. Phys. Oceanogr., 6, 379–389.
- Smagorinsky, J. (1963): *General circulation experiments with the primitive equations*, Mon. Wea. Rev., 91, 99–164.
- Tsujino, H., H. Hasumi and N. Sugimoto (2000): *Deep Pacific circulation controlled by vertical diffusivity at the lower thermocline depths*, J. Phys. Oceanogr., 30, 2853–2865.
- UNESCO (1981): *Tenth report of the joint panel on oceanographic tables and standards, Vol. 36 of UNESCO Technical Papers in Marine Science, UNESCO, Paris.*
- Webb, D. J. (1995): *The vertical advection of momentum in Bryan-Cox-Semtner ocean general circulation models*, J. Phys. Oceanogr., 25, 3186–3195.
- Wajsbowicz, R. C. (1993): *A consistent formulation of the anisotropic stress tensor for use in models of the large-scale ocean circulation*, J. Comput. Phys., 105, 333–338.